

The role of plasma membrane transporters in chloride homeostasis of developing auditory brainstem neurons

Dissertation
zur Erlangung des Doktorgrades der
Naturwissenschaften

Fachbereich Biologie
Technische Universität Kaiserslautern

vorgelegt von
Veeramuthu Balakrishnan
April 2004

Vorsizender: Prof. Dr. Ekkehard Neuhaus

Betreuer: Prof. Dr. Eckhard Friauf

Korreferent: Prof. Dr. Joachim W. Deitmer

Tag der Disputation: May 2004

I, Veeramuthu Balakrishnan, do hereby declare that this submission is my own work and that, to the best of my knowledge and belief, it contains no material previously published or written by another person, nor material which to a substantial extent has been accepted for the award of any other degree or diploma of a university or other institute of higher learning.

Kaiserslautern, 18th April 2004.

TABLE OF CONTENTS

| | |
|---|----|
| 1. Introduction | 1 |
| 1.1 Mammalian auditory pathway | 1 |
| 1.2 Circuitry and function of LSO | 3 |
| 1.3 Development of glycinergic neurotransmission in LSO | 3 |
| 1.4 Chloride regulation in neurons | 4 |
| 1.5 Aim of this thesis | 7 |
| 2. Materials and methods | 8 |
| 2.1 Auditory brainstem and hippocampal slice preparation | 8 |
| 2.2 Electrophysiological recordings | 8 |
| 2.3 Data analysis | 11 |
| 2.4 Single cell RT-PCR | 12 |
| 2.5 Multiplex PCR | 15 |
| 2.6 Genotyping | 15 |
| 3. Results | 17 |
| 3.1 Glycine-induced response in LSO neurons | 17 |
| 3.1.1 Stability of $[Cl^-]_i$ during perforated patch recordings | 17 |
| 3.1.2 Glycine-induced responses and determination of E_{Gly} in rat LSO neurons | 18 |
| 3.1.3 Glycine-induced responses change during LSO development in mice | 20 |
| 3.2 Expression analysis of cation chloride cotransporters | 22 |
| 3.2.1 Multiplex RT-PCR expression analysis of NKCC1 and KCC2 in several brain regions | 22 |
| 3.2.2 Single-cell RT-PCR confirms the presence of KCC2 mRNA at P3 and P12 and the absence of NKCC1 mRNA at P3 | 24 |
| 3.3 Characterization of Cl^- homeostasis in KCC2 $-/-$ mice | 26 |
| 3.3.1 LSO neurons of P3 KCC2 $-/-$ mice display normal E_{Gly} | 27 |
| 3.3.2 LSO neurons of P12 KCC2 $-/-$ mice display abnormal E_{Gly} | 27 |

| | | |
|--------|---|----|
| 3.4 | Pharmacological characterization of the role of NKCC1 in Cl ⁻ homeostasis | 29 |
| 3.4.1 | At low (NKCC1-specific) concentration, bumetanide does not influence E _{Gly} of P3-5 and P12 LSO neurons | 29 |
| 3.4.2 | At low (NKCC1-specific) concentration, bumetanide influences E _{GABA} in P3-5 pyramidal LSO neurons | 31 |
| 3.4.3 | At high (non-specific) concentration, bumetanide influences E _{Gly} of P12 LSO neurons | 32 |
| 3.5 | On the role of Na ⁺ involved in Cl ⁻ homeostasis of LSO neurons | 33 |
| 3.5.1 | Lowering [Na ⁺] _o has no effect on E _{Gly} in P3/4 LSO neurons, but shifts E _{GABA} towards negative in P3/4 pyramidal neurons | 33 |
| 3.5.2 | Effects of altering [Na ⁺] _i on E _{Gly} of neonatal LSO neurons | 35 |
| 3.6 | Characterization of Cl ⁻ homeostasis in NKCC1 -/- mice | 36 |
| 3.6.1 | LSO neurons of P3 NKCC1 -/- mice display normal E _{Gly} | 36 |
| 3.6.2 | LSO neurons of P12 NKCC1 -/- mice display normal E _{Gly} | 37 |
| 3.7 | Voltage treatment modulates [Cl ⁻] _i in young LSO neurons | 38 |
| 3.7.1 | Hyperpolarizing voltage treatment induces the Cl ⁻ influx in P3 LSO neurons | 39 |
| 3.7.2 | Depolarizing voltage treatment reduces the Cl ⁻ influx in P3 LSO neurons | 40 |
| 3.7.3 | Depolarizing voltage treatment causes no change in Cl ⁻ regulation of P12 LSO neurons | 41 |
| 3.8 | Pharmacological revealing of GAT1 in Cl ⁻ homeostasis | 42 |
| 3.8.1 | GAT1 specific inhibitor influences [Cl ⁻] _i in LSO neurons at P3/4, but not at P11/12 | 42 |
| 3.8.2 | GAT1 specific inhibitor influences [Cl ⁻] _i in the presence of GABA receptors blockers | 43 |
| 3.8.3 | GAT specific activator influences the [Cl ⁻] _i in LSO neurons at P3/4, but not at P11/12 | 45 |
| 3.9 | Characterization of Cl ⁻ homeostasis in GLYT2 -/- mice | 46 |
| 3.9.1 | At P3/4, LSO neurons of GLYT2 -/- mice display relatively negative E _{Gly} values | 46 |
| 3.10 | Influence of phosphorylation in the regulation of [Cl ⁻] _i | 47 |
| 3.10.1 | In P3 LSO neurons treated with calyculin A, [Cl ⁻] _i is reduced | 48 |

| | | |
|--------|---|----|
| 3.11 | Influence of thyroid hormone in the regulation of $[Cl^-]_i$ | 49 |
| 3.11.1 | Hypothyroid rats lack a developmental shift in E_{Gly} between P5 and P12 | 49 |
| 4. | Discussion | 51 |
| 4.1 | Developmental changes in glycine-induced responses in mice LSO neurons | 51 |
| 4.2 | KCC2 renders glycine hyperpolarizing by setting $E_{Gly} < V_{rest}$ | 52 |
| 4.3 | NKCC1 is not involved in setting $E_{Gly} > V_{rest}$ in immature LSO neurons | 54 |
| 4.4 | GAT1 and GLYT2 - a focus on their role in Cl^- accumulation | 57 |
| 4.5 | Inhibitory circuits in SOC develop through excitation | 59 |
| 4.6 | Possible induction factors underlying the developmental shift in E_{Gly} | 61 |
| 4.7 | Outlook | 62 |
| 5. | Summary | 63 |
| 6. | Bibliography | 67 |
| 7. | Appendix | 81 |
| | Abbreviations | 81 |
| | Curriculum Vitae | 84 |
| | Acknowledgments | 85 |

1 INTRODUCTION

The brain is the most complex part of the human body. It is the seat of intelligence, the interpreter of the senses, the initiator of body movements, and the controller of behaviors. In the adult mammalian brain, there are some 10^{12} neurons, each connected through a plethora of synapses. So, more important are the connections that actually determine the brain's behaviour which are in the order of 10^{15} . That is, a typical neuron in the brain may have something like 1000 synapses on it. Each neuron processes all incoming information and decides how to respond. Thus, the output of a single neuron is controlled by an ensemble of neurons firing in an organized fashion. During ontogenesis, neurons wire themselves into networks by extending cable-like axons that grow towards specific targets and undergo refinement in terms of anatomy and physiology to establish a mature network. This thesis addresses some of the issues regarding the maturation of inhibitory synapse in the auditory brainstem.

1.1 Mammalian auditory pathway

Acoustic signals travel through the air, enter the pinna, and are finally transformed into electrical signals in the cochlea. From the cochlea, information encoded in the timing of action potentials in a tonotopic array of auditory nerve fibres reaches the cochlear nucleus (CN) of the ipsilateral side. From the CN, acoustic information is fed through at least six parallel ascending pathways (Cant, 1991), including several brainstem nuclei that converge upon the inferior colliculus (IC). Neurons of the IC send their axons to the auditory thalamus, the medial geniculate body, which then relays information to different areas of the auditory cortex where a neuronal correlate of sound perception is formed. The integrative roles of these pathways are not completely understood.

The evidence is compelling that the cross correlation of inputs from the two ears through spherical bushy neurons in the CN and through the medial superior olive (MSO) serve to measure interaural time and phase differences that are used to localize sound in the azimuth (Grothe and Park, 1998; Brand et al., 2002). It has been suggested that a pathway through the lateral superior olive (LSO) serves to detect interaural level differences through which animals can localize high frequencies in the azimuth (Goldberg and Brown, 1969). These two nuclei (MSO and LSO) are situated in the superior olivary complex (SOC), the first station in the ascending auditory pathway, where the information from both cochleae converges. The SOC plays a pivotal role in sound localization. It is comprised of four well defined nuclei, surrounded by more diffuse periolivary regions (Irving and Harrison, 1967). The major nuclei are the medial nucleus of the trapezoid body (MNTB), the LSO, the MSO and the superior paraolivary nucleus (SPN; Fig. 1.1).

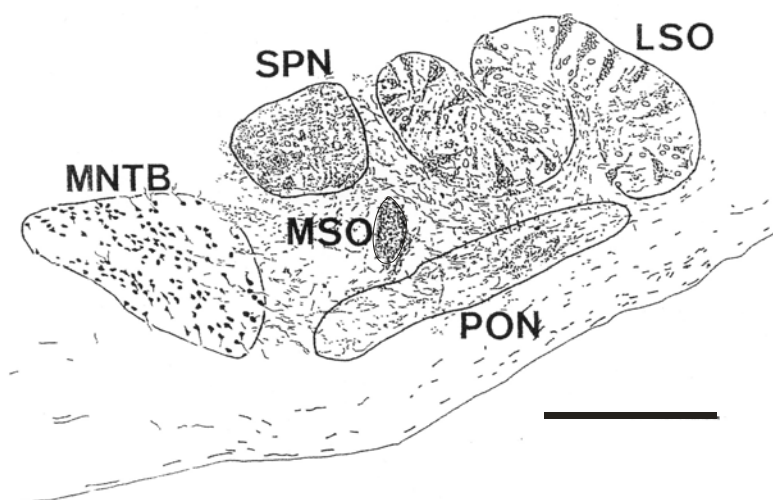


Fig. 1.1: The major nuclei of the superior olivary complex (SOC).

Camera-lucida drawing of a coronal section through the right SOC of a postnatal day (P) 60 rat, showing the nuclei outlined, namely the medial nucleus of the trapezoid body (MNTB), the lateral superior olive (LSO), the medial

superior olive (MSO), the superior paraolivary nucleus (SPN), and the periolivary nucleus (PON). Scale bar = 500 μ m. Modified from Friauf (1993).

1.2 Circuitry and function of the LSO

The LSO is the first auditory center that processes differences in sound level between the two ears (Wu and Kelly, 1992a; Sanes, 1993; Tollin and Yin 2002). In carnivores and rodents, it is located laterally in the SOC and is S-shaped (Schwarz, 1992; Fig 1.1). In the rat, seven classes of neurons have been identified (Rietzel and Friauf, 1998). The two most frequent types are bipolar neurons and multipolar neurons. Less frequent neuron types are small multipolar neurons, banana-like neurons, bushy neurons, unipolar neurons and marginal neurons. The LSO receives glutamatergic inputs from the spherical bushy neurons of the ipsilateral ventral CN in a tonotopic fashion (Cant and Casseday, 1986; Friauf and Ostwald, 1988; Suneja et al., 1995; Cant, 1991; Wu and Kelly, 1995) and glycinergic inputs indirectly from the globular bushy cells in the contralateral CN via the MNTB (Warr, 1972; Tolbert et al., 1982; Wenthold, 1991; Wu and Kelly, 1992b; Vater, 1995). The frequency of sound to which the LSO neurons respond best varies systematically across the LSO (Sanes et al., 1990) i.e., the LSO displays a tonotopic representation.

1.3 Development of glycinergic neurotransmission in LSO

Glycinergic transmission from the MNTB to the LSO starts at embryonic day (E) 18 and is depolarizing until the end of the first postnatal week, after which it becomes hyperpolarizing (Kandler and Friauf, 1995). During the early depolarizing phase, the coexistence of GABAergic and glycinergic inputs to rat LSO neurons was recently reported (Nabekura et al., 2004). Furthermore, a shift from mainly GABAergic to glycinergic neurotransmission has been reported in the gerbil (Kotak et al., 1998) and the rat (Nabekura et al., 2004). There are similar reports demonstrating depolarization upon GABAergic or glycinergic activation in several other systems

during their early postnatal life, e.g., in the hippocampus (Mueller et al., 1984; Janigro and Schwartzkroin, 1988; Ben-Ari et al., 1989; Cherubini et al., 1990; Zhang et al., 1990), cerebral cortex (Luhmann and Prince, 1991; Yuste and Katz, 1991; Lo Turco et al., 1995; Owens et al., 1996), hypothalamus (Chen et al., 1996), spinal cord (Wu et al., 1992; Reichling et al., 1994; Rohrbough and Spitzer, 1996) and retina (Huang and Redburn, 1996; Billups and Attwell, 2002). The depolarization during early development leads to increased cytoplasmic Ca^{2+} levels and action potentials (Reichling et al., 1994; Obrietan and van den Pol, 1995; Leinekugel et al., 1995; Owens et al., 1996; Flint et al., 1998). This link of glycinergic/GABAergic synaptic activity to intracellular calcium signalling during the period of inhibitory synaptic plasticity may be one of the mechanisms by which tonotopic MNTB-LSO connections become established (Lohmann et al., 1998; Kandler et al., 2002). Moreover, it has been elucidated that in the LSO, depolarizing and hyperpolarizing glycine-induced responses are attributable to developmentally regulated high and low intracellular chloride concentration ($[\text{Cl}^-]_i$), respectively (Ehrlich et al., 1999; Kakazu et al., 1999).

1.4 Chloride regulation in neurons

Chloride is an important ion for neurons. It is a dominant diffusible anion inside the neurons, together with bicarbonate, and both exhibit non-equilibrium distribution across the plasma membrane. Chloride serves as a key player in a variety of cellular functions such as intracellular pH regulation (Russell and Boron, 1976), cell volume regulation (Basavappa, 1996), transepithelial salt transport (Mount and Gamba,

2001), synaptic signalling (for review, see Reimer et al., 2001), neuronal growth (Kriegstein and Owens, 2001; Payne et al., 2003), migration and targeting (Barker et al., 1998), membrane potential stabilization (Valverde et al., 1995; Jentsch and Gunther, 1997), regulation of transport systems (Hoffmann, 1986), and K^+ scavenging (Payne, 1997).

In this thesis, I tried to reveal the mechanisms behind chloride homeostasis in LSO neurons. It is well documented that $[Cl^-]_i$ determines the polarity of glycine-induced responses in postnatal animals (Ehrlich et al., 1999; Fig. 1.2). To date, no evidence for a *primary* active transport mechanism for Cl^- exists (Gerencser and Zhang, 2003). In figure 1.2 and table 1.1, some *secondary* active transporters that are involved in Cl^- transport in neurons are shown. Na^+ - and K^+ -dependent Cl^- cotransporter (NKCC1) and K^+ -dependent Cl^- cotransporter (KCC2) were reported to be the principal inward directed and outward directed Cl^- pumps in neurons, respectively (Plotkin et al., 1997; Rivera et al., 1999; Sun and Murali, 1999; Sung et al., 2000; Vardi et al., 2000; Hubner et al., 2001; Jang et al., 2001).

Table 1.1: Chloride cotransporters/exchangers and the direction of Cl^- transport

| | Chloride transporters | Direction of Cl^- transport |
|------|--|---|
| KCC | K^+ -dependent Cl^- transporter | Outward |
| NDAE | Na^+ -dependent Cl^-/HCO_3^- exchanger | Outward |
| AE | Na^+ -independent Cl^-/HCO_3^- exchanger | Inward |
| NCC | Na^+ - Cl^- cotransporter | Inward |
| NKCC | Na^+ - and K^+ -dependent Cl^- cotransporter | Inward |
| GAT | GABA transporter | Inward |
| GLYT | Glycine transporter | Inward |

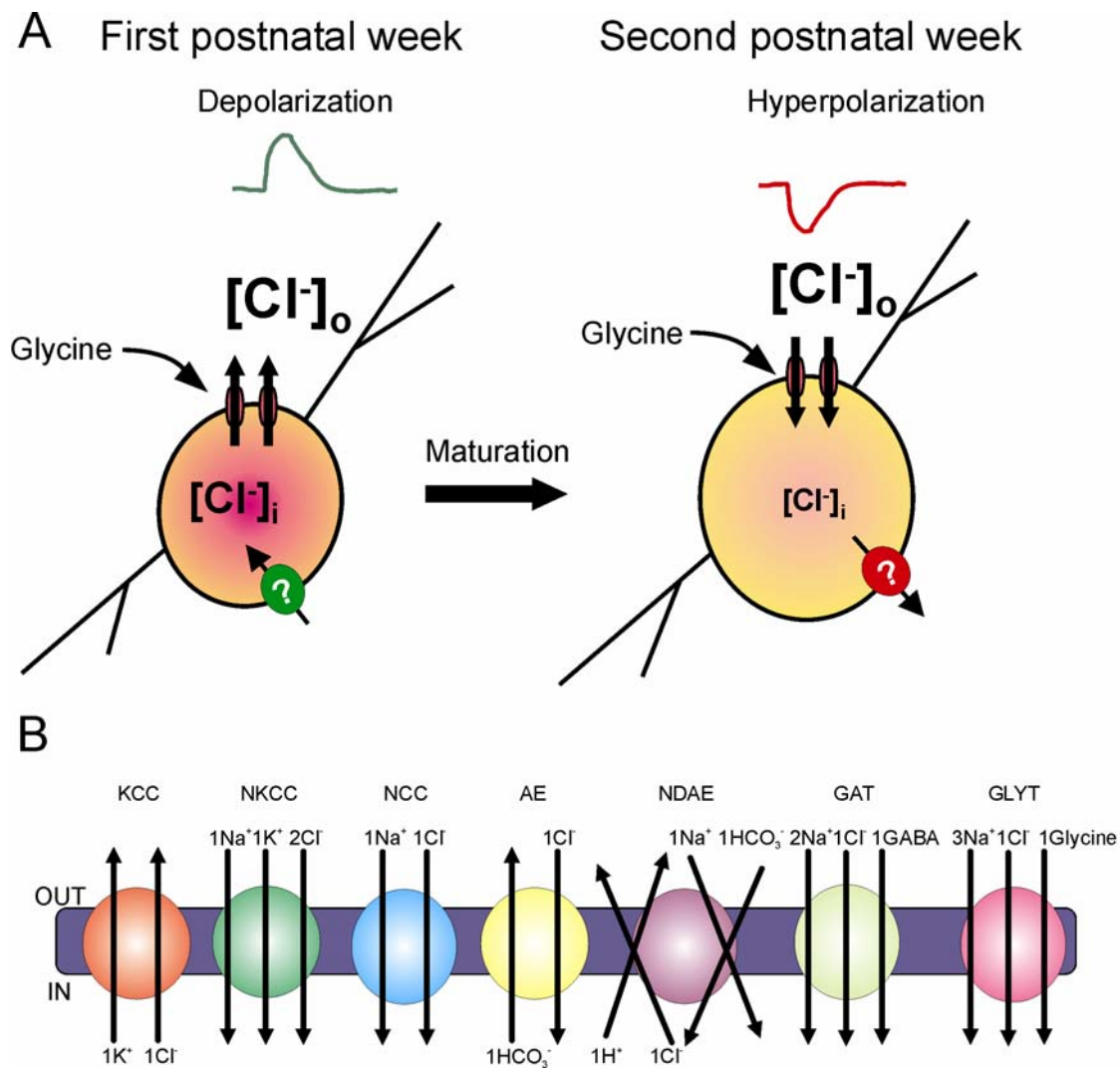


Fig. 1.2: Change in glycine responses is attributable to intracellular chloride regulation during LSO development. (A) During the first postnatal week, neonatal LSO neurons depolarize upon glycine application, whereas they hyperpolarize from the second postnatal week. A depolarizing glycine response is attributable to a high intracellular chloride concentration ($[Cl^-]_i$), whereas a hyperpolarizing response is due to a low $[Cl^-]_i$. Thus, in young cells Cl^- inward transporting mechanisms and in older cells certain Cl^- outward transporting mechanisms are necessary to maintain a high and low $[Cl^-]_i$, respectively. (B) Schematic diagram depicting several transporters possibly involved in Cl^- homeostasis (refer Table 1.1 for abbreviations). Shown are the ions involved and their stoichiometry as well as the direction of flow.

1.5 Aim of this thesis

This doctoral thesis was performed to elucidate the molecular mechanism underlying chloride homeostasis in LSO neurons and to understand the maturation of inhibitory synapses. I investigated the temporal expression and function of brain specific chloride transporters involved in the developmental regulation of $[Cl^-]_i$ in LSO neurons.

More precise, the following two questions were addressed: (1) What are the molecular mechanisms of the accumulation of Cl^- during early postnatal ages? (2) What are the molecular mechanisms of the shift from high to low $[Cl^-]_i$?

2 MATERIALS AND METHODS

All protocols adhered to the German Animal Protection Law, and were approved by the local animal care and use committee.

2.1 Auditory brainstem and hippocampal slice preparation

The following animal strains were used: Sprague–Dawley rats, Wistar rats, C57BL/6J wildtype mice, KCC2 knockout mice (Woo et al., 2002), NKCC1 knockout mice (Delpire et al., 1999), and GLYT2 knockout mice (Gomez et al., 2003), aged between postnatal day (P) 1 and 13. Animals were deeply anaesthetized by a peritoneal injection of ketamine (0.3 g kg^{-1} body weight), decapitated, and their brains were dissected in a chilled ($4 \text{ }^{\circ}\text{C}$) preparation solution (for composition, see Table 2.1). Coronal sections of $300 \text{ }\mu\text{m}$ were cut using a VT-1000 vibratome (Leica, Bensheim, Germany), containing either SOC or the hippocampus. The slices were preincubated in extracellular solution 1 for 1 hr at $36 \text{ }^{\circ}\text{C}$ and stored at room temperature until recording (for composition, see Table 2.1).

2.2 Electrophysiological recordings

Electrophysiological responses were recorded using gramicidin perforated-patch recording technique. For electrophysiological recordings, patch pipettes were pulled from borosilicate glass capillaries with fire polished ends (GP150-8P, Science Products, Hofheim, Germany), which had an outer diameter of 1.5 mm and an inner diameter of 0.86 mm . A vertical puller (PP-83, Narishige, Japan) was employed for pulling the pipettes. Recording electrodes had a resistance of $2\text{--}7 \text{ M}\Omega$ when filled with different pipette solutions (for composition, see Table 2.2). The patch pipettes were front filled with gramicidin-free pipette solution for $2\text{--}3 \text{ min}$ and then backfilled with the same pipette solution, supplemented with $2.5\text{--}10 \text{ }\mu\text{g ml}^{-1}$ gramicidin.

Table 2.1: Composition of bath solutions

| Chemical compounds (mM) | Preparation solution | Extracellular solution 1 | Extracellular solution 2 |
|----------------------------------|----------------------|--------------------------|--------------------------|
| KCl | 2.5 | 2.5 | 2.5 |
| NaCl | - | 125 | - |
| NMDG | - | - | 125 |
| NaHCO ₃ | 25 | 25 | 25 |
| NaH ₂ PO ₄ | 1.25 | 1.25 | 1.25 |
| MgCl ₂ | 1 | 1 | 1 |
| CaCl ₂ | 2 | 2 | 2 |
| Na-pyruvate | 2 | 2 | 2 |
| Myo-inositol | 3 | 3 | 3 |
| Kynurenic acid | 1 | - | - |
| Ascorbic acid | - | 0.4 | 0.4 |
| D-Glucose | 260 | 10 | 10 |

pH 7.4, when gassed with 95% O₂ and 5% CO₂.

Table 2.2: Composition of pipette solutions

| Compound | Solution 1 (mM) | Solution 2 (mM) | Solution 3 (mM) | Solution 4 (mM) |
|---------------------|-----------------|-----------------|-----------------|-----------------|
| KCl | 140 | 110 | 130 | - |
| K-gluconic acid | - | - | | 130 |
| NaCl | - | 20 | | - |
| EGTA | 5 | 5 | 5 | 5 |
| MgCl ₂ | 3 | 1 | 1 | 1 |
| HEPES | 5 | 10 | 10 | 10 |
| Na ₂ ATP | - | 2 | 2 | 2 |
| NA ₂ GTP | - | 0.3 | 0.3 | 0.3 |

pH 7.3 adjusted with KOH

Gramicidin was dissolved in DMSO, such that the final concentration of DMSO in the pipette solution was $\leq 0.1\%$. Most experiments were carried out with pipette solution 1 (for composition, see Table 2.2). The usage of different pipette solutions is mentioned in the appropriate sections. In case of patch-clamp recordings combined

with subsequent single cell RT-PCR, 6 μ l pipette solution 1 with gramicidin was backfilled in the pipette (Fig. 2.1). Electrophysiological responses were recorded with an Axopatch 1D amplifier (Axon Instruments, Foster City, CA) and pClamp 8.0.2 software (Axon Instruments). Slices were transferred to a recording chamber and continually perfused with extracellular solution at room temperature at a rate of 1.5-2.0 ml min⁻¹. LSO neurons were visualized with DIC-infrared optics using a 40X, 0.80 NA water immersion objective on an upright microscope (Eclipse E600-FN, Nikon, Düsseldorf, Germany).

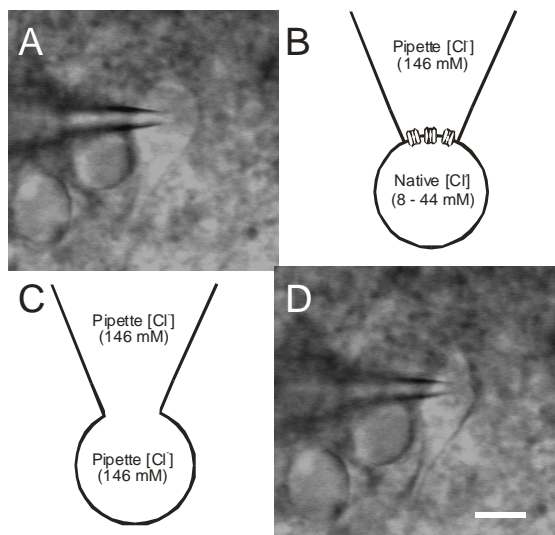


Fig. 2.1: Patch-clamp recordings followed by RT-PCR in a single LSO neuron.

(A) Patch-clamp recordings in the perforated mode were obtained from a P12 neuron with spindle shaped soma. (B) Perforated patch-clamp recordings with gramicidin maintain the native $[Cl]_i$ since the pores are permeable only to monovalent cations. (C) Rupture of patch membrane establishes conventional whole-cell mode where the native $[Cl]_i$ is exchanged by the pipette chloride concentration (pipette $[Cl]_i$). (D) The cell content was harvested into the recording pipette under visual control for performing single cell RT-PCR experiments. Scale bar in D = 20 μ m, holds also for A.

For gramicidin perforated-patch recordings, a gigaohm seal (≥ 1 G Ω) was established and the progress of perforation was controlled by monitoring the decrease in series resistance. Recordings were started when series resistance had stabilized to ~15 to 50 M Ω after 10-30 min. Data were digitized via a Digidata 1322A interface (Axon Instruments) and series resistance compensation was set to 70-80% with a lag of 100 μ s. The voltage-clamp protocol consisted of stepping the membrane potential from a holding potential (V_H) of -70 mV to command potentials (V_C) ranging from -120 mV to 0 mV. Each step lasted 3 s and glycine (1 mM) was

pressure applied (~0.3 bar) for 10 ms with a delay of 500 ms after the step onset, through a wider tip (~1 μm) application pipette (Picospritzer, General Valve Corp., Fairfield, NJ). The application intervals lasted 10 s, which was sufficient to recover from possible changes of $[\text{Cl}^-]_i$, caused by Cl^- loading or depletion at very positive (0 mV) or negative (-120 mV) V_C values, respectively (Ehrlich et al., 1999). The liquid junction potential between the patch pipette solution 1 and the extracellular solution 1 was ~3 mV and was therefore neglected.

2.3 Data analysis

Data analysis was performed with software programs, Clampfit 8.1 (Axon instruments), Excel (Microsoft) and Winstat für Excel (Fitch software). The peak amplitude of glycine-activated currents was calculated by taking the difference between the holding current and the maximum current of the glycine response. Peak current responses were plotted for each V_C and the data were analyzed for best fitting regression functions by the statistics software, Winstat für Excel. The reversal potential of glycine-activated currents (E_{Gly}) was determined as the x-intercept value of the regression line. The $[\text{Cl}^-]_i$ was calculated after the Nernst equation ($E_{\text{Cl}} = \text{RT}/F \ln [\text{Cl}^-]_i / [\text{Cl}^-]_o$) with the measured E_{Gly} , assuming that $E_{\text{Gly}} = E_{\text{Cl}}$ (Ehrlich et al., 1999). The relevant values of RT/F , and $[\text{Cl}^-]_o$ used in the experiment where $\text{RT}/F = 25.69$ mV at 25 °C and $[\text{Cl}^-]_o = 133.5$ mM.

$[\text{Cl}^-]_i$ was calculated as : $[\text{Cl}^-]_i = 10^{2.1254 \left[\frac{E_{\text{Cl}}}{-59.16} \right]}$

Data were expressed as mean \pm SEM, and n is the number of cells tested. Differences between groups were statistically analyzed by carrying out Student's *t*

test by the statistic software Winstat für Excel. The level of significance was set at $p < 0.05$. In the figures, the significant differences are marked with asterisks; *, $p < 0.05$; **, $p < 0.01$; ***, $p < 0.001$.

Table 2.3: Drugs used for pharmacology

| Drug | Concentration (μM) | Action |
|------------------|---------------------------------|---------------------------------------|
| Bumetanide | 30 | Specific NKCC antagonist |
| | 100 | Non-specific CCC antagonist |
| SKF 89976A | 100 | Specific GAT1 antagonist |
| Nipecotinic acid | 100 | Specific GAT agonist (as a substrate) |
| Bicuculline | 30 | GABA _A receptor antagonist |
| SCH50911 | 10 | GABA _B receptor antagonist |
| I4AA | 10 | GABA _C receptor antagonist |
| Calyculin A | 100 | Protein phosphatase inhibitor |

2.4 Single cell RT-PCR

After perforated patch-clamp recordings (see above), whole-cell configuration was established in some cells ($n = 20$) and their cellular content was aspirated into the patch pipette (Fig. 2.1). The complete content of each pipette ($\sim 7 \mu\text{l}$) was expelled into an RNase-free PCR tube containing first strand buffer (Invitrogen, Karlsruhe, Germany), 10 mM dithiothreitol, 0.25 mM deoxynucleotide triphosphates (dNTPs), 2.5 mM random hexamer primers (Invitrogen) and 0.1 μg of yeast tRNA (Roche, Mannheim, Germany) in a total volume of 17 μl . One μl of SUPERase-In ($20 \text{ U } \mu\text{l}^{-1}$; Ambion, Wiesbaden, Germany) and 1 μl RT Enhancer (PepqLab, Erlangen, Germany) were added, and the mixture was incubated at room temperature for 10 min and subsequently at 70°C for 5 min. After adding 1 μl of SuperScript II reverse

transcriptase (200 U μl^{-1} ; Invitrogen), the reverse transcription was carried out for 1 h at 42 °C (Fig. 2.2). The reaction volume was split into two halves; one was analyzed for the presence of KCC2 and the other for NKCC1. First round PCR was performed for 40 cycles with external primers (Table 2.4) and Taq DNA polymerase (Invitrogen) in the presence of 400 nM PCR primers and 0.5 mM dNTPs in a total volume of 50 μl . For the second round PCR, 1 μl of the first round PCR was used as a template and 20 cycles were performed with nested primers. The program for both PCR was as follows: Denaturing at 94 °C for 30 s, annealing at 60 °C for 30 s, and extension at 72 °C for 1 min. Ten μl of each nested PCR was then analyzed in a 1% agarose gel containing ethidium bromide (0.5 $\mu\text{g ml}^{-1}$). After electrophoresis, pictures were captured with a CCD camera (LTF Labortechnik, Wasserburg, Germany).

Table 2.4: Oligonucleotides used for single-cell PCR

| Gene | Round No. | Type | Sequence | Annealing temperature |
|--------------|-----------------|---------|------------------------------------|-----------------------|
| <i>NKCC1</i> | 1 st | forward | 5'-CTGCCGAAAGTAAAGGAGTTGTAAAGTT-3' | 60 ° C |
| | | reverse | 5'-CTTCTTGCTGTCCAGTGAGATAAATGT-3' | |
| | 2 nd | forward | 5'-GGCTGGATCAAGGGTGTTTTAGTAC-3' | 60 ° C |
| | | reverse | 5'-CAGAAGGACGATCTGAGCCTTTGC-3' | |
| <i>KCC2</i> | 1 st | forward | 5'-GCAGCCCCTTCATCAACAGCAC-3' | 60 ° C |
| | | reverse | 5'-CATCGCTGGGAAGAGGTAAGC-3' | |
| | 2 nd | forward | 5'-GCCCTGTTTGAGGAGGAGATGGACAC-3' | 60 ° C |
| | | reverse | 5'-ATTGCGCTCATGGAAATGGCTGTGAG-3' | |

Single cell RT-PCR

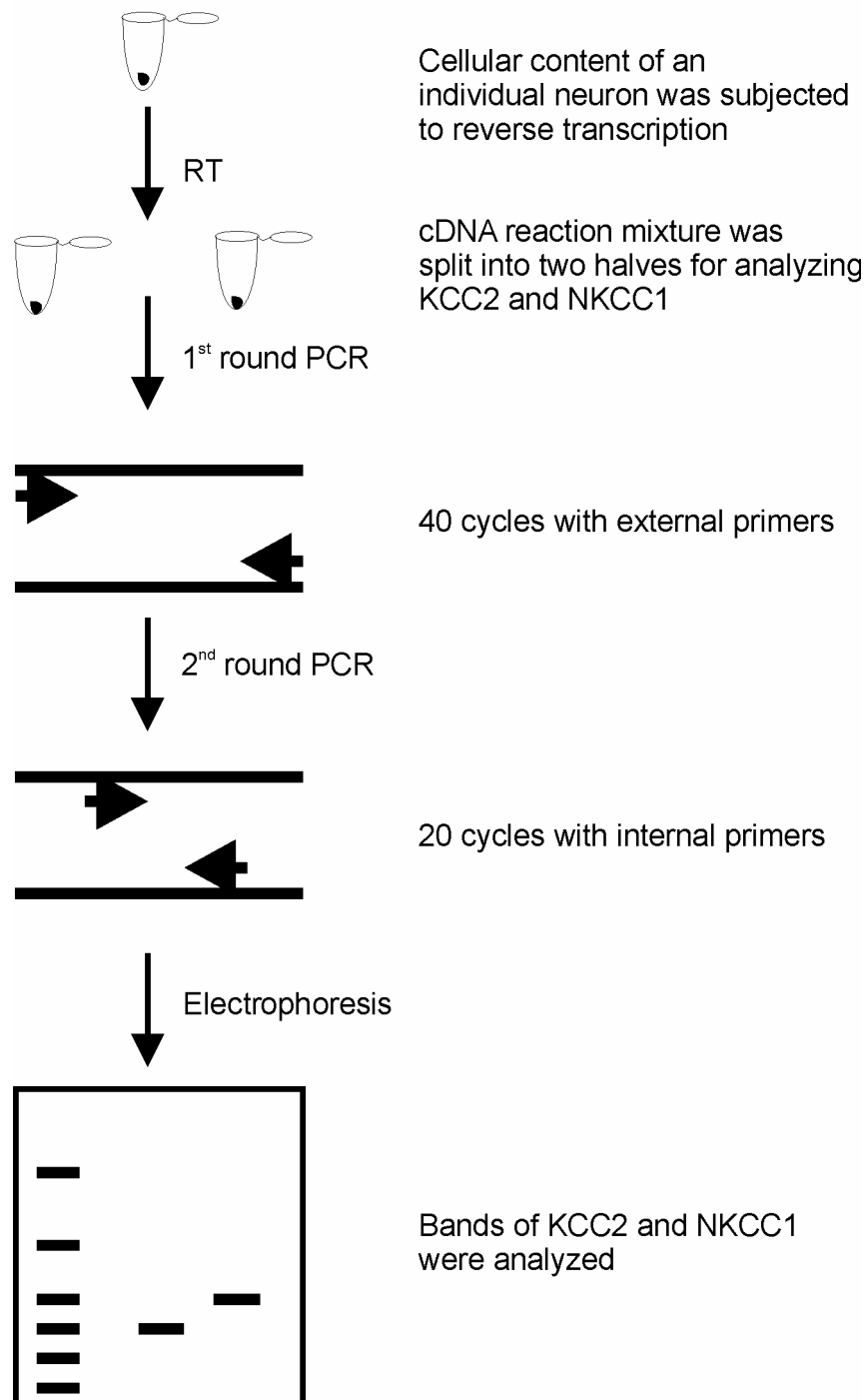


Fig. 2.2: Chart flow of the methodological steps performed for single cell RT-PCR. The content of a single cell was used to investigate the expression profile of KCC2 and NKCC1 mRNAs.

2.5 Multiplex RT-PCR

Reverse transcription of total RNA from different brain regions was performed by using standard protocols with random hexanucleotide priming and SuperScript II as enzyme (Invitrogen). Multiplex RT-PCR was carried out for 35 cycles in a total volume of 50 μ l, using equimolar primers and conditions listed in Table 2.5. Primers for NKCC1 were designed such as to amplify both splice variants (Randall et al., 1997; Vibat et al., 2001). Denaturing was at 94 °C for 30 s, annealing temperature as listed in the table, and elongation at 72 °C for 1-2 min. Ten μ l of each reaction were loaded onto a 2% agarose gel containing ethidium bromide (0.5 μ g ml⁻¹). After electrophoresis, pictures were captured with a CCD camera (LTF Labortechnik).

Table 2.5: Oligonucleotides used for multiplex PCR

| Gene | Type | Sequence | Annealing Temperature |
|---------------------------------|---------|----------------------------|-----------------------|
| <i>β-actin</i> | forward | 5'-CATGGATGACGATATCGCTG-3' | 55 °C |
| | reverse | 5'-CTGTGGTGGTGAAGCTGTAG-3' | |
| NKCC1 | forward | 5'-TCCTAGGAGACATCAACAC -3' | 55 °C |
| | reverse | 5'-ATCCAGTCACTCTGACTAG-3' | |
| KCC2 | forward | 5'-CGGAGGGGATCAAGGACTTC-3' | 55 °C |
| | reverse | 5'-CTCGCCACCTTTATTGCAAC-3' | |

2.6 Genotyping

Tail biopsies (0.5 to 1 cm) from mice were obtained and incubated overnight at 55 °C with 600 μ l TNES buffer (for composition see Table 2.6) and 35 μ l proteinase K (10 mg ml⁻¹) in eppendorf tubes. Thereafter, the tubes were vigorously shaken for 15 min with 166 μ l of 6 M NaCl and centrifuged for 5 minutes at 14,000 g. The supernatant was collected in a new tube and 600 μ l of 95% ethanol were added. Then the DNA was spooled and washed with 500 μ l of 70% ethanol. After that it was centrifuged for 15 min at 14,000 g, and the supernatant was decanted. After air

drying the tubes, the pellet was resuspended in 100 μ l TE buffer (for composition, see Table 2.7) and heated at 65 °C for 10 min to aid dissolution of DNA (Miller et al., 1988). PCR was carried out for 35 cycles in a total volume of 50 μ l, using primers and conditions listed in Table 2.8. Ten μ l of each reaction were loaded onto a 2% agarose gel containing ethidium bromide (0.5 μ g ml⁻¹). After electrophoresis, pictures were captured with a CCD camera (LTF Labortechnik).

Table 2.6: Composition of TNES Buffer

| Compound | Concentration (mM) |
|----------|--------------------|
| Tris | 10 |
| NaCl | 400 |
| EDTA | 100 |
| SDS | 0.6 % |

Table 2.7: Composition of TE Buffer

| Compound | Concentration (mM) |
|----------|--------------------|
| Tris | 10 |
| EDTA | 1 |

pH 7.5, adjusted with HCl

Table 2.8: Oligonucleotides used for genotyping

| Gene | Genotype | Type | Sequence | Annealing temperature |
|--------------|-----------|---------|-------------------------------|-----------------------|
| <i>NKCC1</i> | Wild type | forward | 5'-TATCTCAGGTGATCTTGC-3' | 60 °C |
| | | reverse | 5'-ACACTGCAATTCCTATGTAAACC-3' | |
| | Knockout | forward | 5'-TATCTCAGGTGATCTTGC-3' | 60 °C |
| | | reverse | 5'-ATTCCAAGCTCGAACCCCTCCG-3' | |
| <i>KCC2</i> | Wild type | forward | 5'-AGCGTGTGTCCGTGTGCGAGTG-3' | 62 °C |
| | | reverse | 5'-ATCGCCGTCCTCGCAGTCCGTC-3' | |
| | Knockout | forward | 5'-AGCGTGTGTCCGTGTGCGAGTG-3' | 62 °C |
| | | reverse | 5'-CCAGAGGCCACTTGTGTAGCGC-3' | |

3 RESULTS

3.1 Glycine-induced responses in LSO neurons

Electrophysiological recordings of glycine-induced responses in rats and mice LSO neurons were performed. All recordings were done in perforated patch-clamp mode, using gramicidin as the ionophore to leave the native $[Cl^-]_i$ undisturbed (Fig. 2.1). Gramicidin pores are thought to be impermeable to anions and permeable to monovalent cations (Ebihara et al., 1995; Kyrozis and Reichling, 1995).

3.1.1 Stability of $[Cl^-]_i$ during gramicidin perforated patch recordings

While using pipette solutions with high $[Cl^-]_i$ and without Ca^{2+} buffering, it has been suggested that some caution is needed when attempting gramicidin perforated patch-clamp recordings (Kyrozis and Reichling, 1995). To check if there is any relative permeability of Cl^- through gramicidin pores, E_{Gly} was measured with two different pipette Cl^- concentrations ($[Cl^-]_p$; Fig. 3.1), i.e., with 132 mM and 2 mM Cl^- (Solution 3 and 4, see Table 2.2 for composition). In both cases, the gramicidin concentration was $2.5 \mu g ml^{-1}$ and the animals were aged between P3 and P4. E_{Gly} was determined as the intersection of the regression line of the current-voltage (I-V) relation with the X-axis (Fig. 3.1). With 2 mM $[Cl^-]_p$, E_{Gly} resulted in an average of -38 ± 3 mV ($n = 7$). With 132 mM $[Cl^-]_p$, the average E_{Gly} was -40 ± 3 mV ($n = 7$). The E_{Gly} values determined under high and low $[Cl^-]_p$ displayed no significant difference ($p > 0.05$). Therefore, at a gramicidin concentration of $2.5 \mu g ml^{-1}$, the pores are impermeable to chloride ions. Thus, gramicidin perforated patch-clamp recordings can indeed serve as a tool to investigate the neuron's native Cl^- concentration.

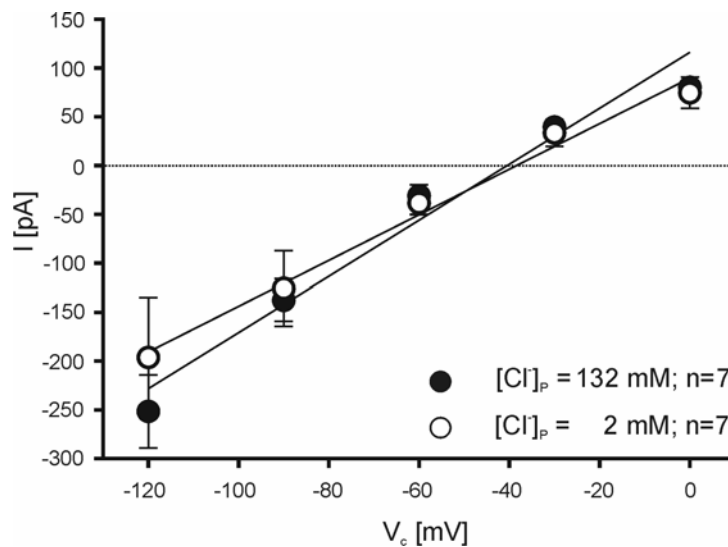


Fig. 3.1: During gramicidin perforated patch-clamp recordings, native $[Cl]_i$ is preserved, irrespective of the used pipette chloride concentration ($[Cl]_p$). I-V plots obtained from P3 and P4 LSO neurons under two different $[Cl]_p$ i.e., 2 mM (open circles) and 132 mM (closed circles). The reversal potential of glycine (E_{Gly}) amounted to -38 ± 3 mV ($n=7$) and -40 ± 3 mV ($n=7$) for 2 mM and 132 mM $[Cl]_p$, respectively, which was not significantly different (p

> 0.05). I = peak amplitude of glycine-induced currents; V_c = command potential; holds for following figures.

3.1.2 Glycine-induced responses and determination of E_{Gly} in rat LSO neurons

During current-clamp recordings, 1 mM glycine was applied focally on the soma of LSO neurons and the change in membrane potential was recorded simultaneously. At P3, focal application of glycine evoked a depolarization in 9 out of 10 neurons and the mean peak amplitude amounted to 8 ± 1 mV (Fig. 3.2A). In order to determine E_{Gly} in voltage-clamp mode, changes in glycine-induced current flow (I) at different command potentials (V_c) were measured (Fig. 3.2B). E_{Gly} was determined as the intersection of the regression line of the I-V relation with the X-axis (Fig. 3.2C). A previous study showed that E_{Gly} is equivalent to E_{Cl} (Ehrlich et al., 1999), thus, Nernst equation can be used for calculating the native $[Cl]_i$. In P3 LSO neurons, the mean E_{Gly} was -32 ± 4 mV ($n = 10$; $p < 0.001$), i.e., less negative than the mean resting membrane potential (V_{rest}) of -59 ± 2 mV ($n = 10$). Usually, after determining E_{Gly} , the membrane under the patch was ruptured, resulting in dialysis of the cell interior by the pipette solution. Due to the $[Cl]_p$ of 132 mM and the increased access

to the cell, large depolarizing glycine responses and concurrent action potentials could be observed in current-clamp mode (Fig. 3.2D).

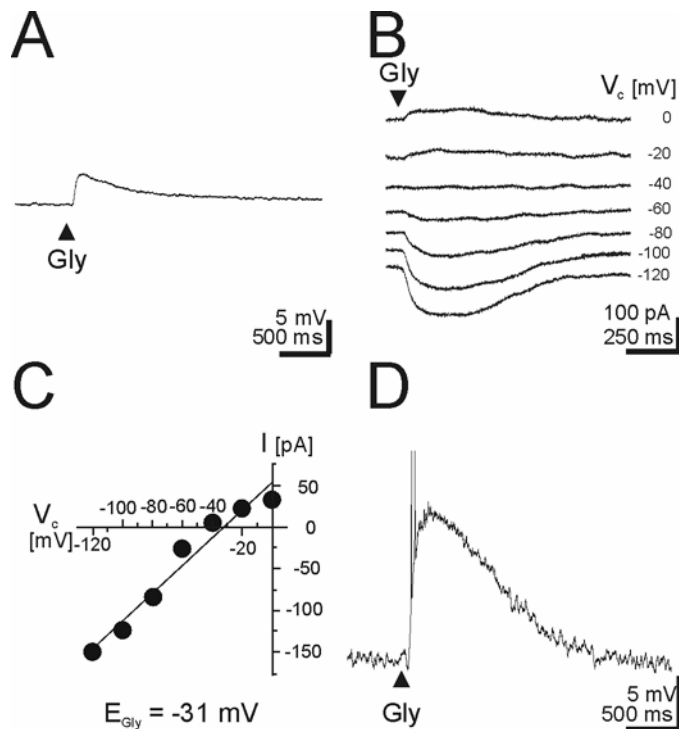


Fig. 3.2: Perforated patch-clamp recordings of a P3 LSO neuron imply high $[Cl^-]_i$. (A) Application of 1 mM glycine (triangle) induced a depolarization of approximately 5 mV when recording in current-clamp configuration. (B) Voltage-clamp recordings at different V_c with regular glycine application show inward and outward currents, revealing movement of chloride ions outward and inward through glycine receptors respectively. (C) The E_{Gly} was determined from the x-intercept value of the regression line in the current voltage (I-V) relationship and found to

be -31 mV which was more positive than the resting membrane potential (V_{rest}) that amounted to -60 mV. (D) After rupture of the patch membrane, glycine elicited a large depolarization due to subsequent dialysis of the cell interior against the pipette solution with high $[Cl^-]_i$. The depolarization caused the cell to fire two action potentials (truncated), demonstrating the excitatory effect of glycine.

At P12, in current-clamp mode, glycine-application induced a hyperpolarization in 9 out of 10 neurons and the mean peak amplitude amounted to 11 ± 2 mV ($n = 10$; Fig. 3.3A). In voltage-clamp mode, E_{Gly} was determined as described above (Fig. 3.3B&C). In P12 neurons, the mean E_{Gly} was -76 ± 4 mV ($n = 10$), i.e., more negative than the mean V_{rest} of -58 ± 1 mV ($n = 10$; $p < 0.01$). In whole cell current-clamp mode, large depolarizing glycine responses and concurrent action potentials could be observed (Fig. 3.3D) due to dialysis of pipette solution.

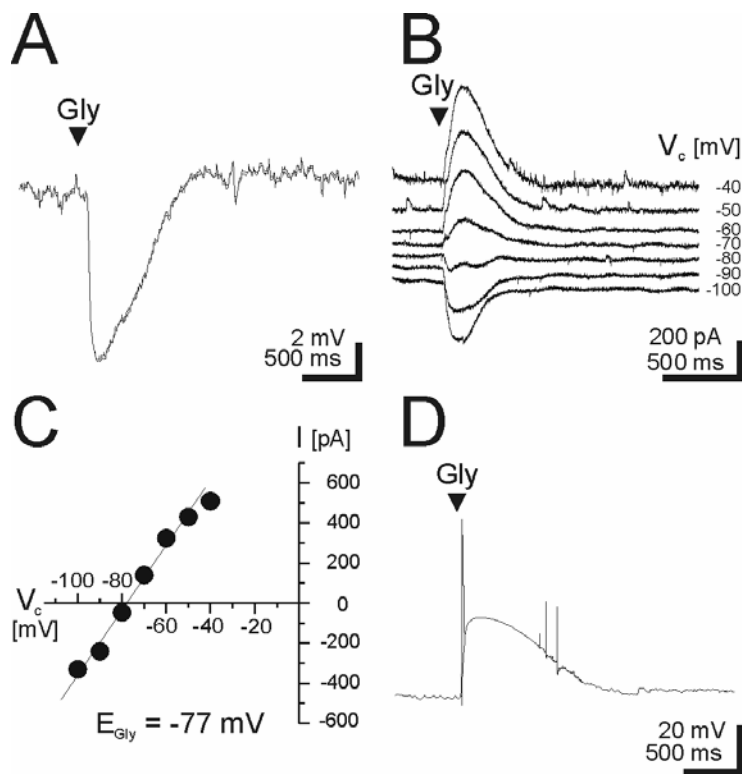


Fig. 3.3: Perforated patch-clamp recordings of a P12 LSO neuron imply low $[Cl]_i$. (A) Application of 1 mM glycine (triangle) induced a hyperpolarization of approximately -8 mV when recording in current-clamp configuration. (B) Voltage-clamp recordings at different V_c with regular glycine application show inward and outward currents, revealing movement of chloride ions outward and inward through glycine receptors respectively. (C) The E_{Gly} was determined as described above and found to be -77 mV which was more negative than V_{rest} that amounted to -57 mV. (D) After

rupture of the patch membrane, glycine elicited a large depolarization due to subsequent dialysis of the cell interior against the pipette solution with high $[Cl]_i$. The depolarization caused the cell to fire few action potentials (partly truncated), demonstrating the excitatory effect of glycine.

3.1.3 Glycine-induced responses change during the LSO development in mice

The development of the MNTB-LSO pathway has been intensively studied in rats and gerbils (Sanes and Friauf, 2000) but less in the case of mice. Mice are preferentially used as genetic models to investigate protein function. In order to make use of mouse knockout models of chloride cotransporters, to examine the functional role of transporters, glycine-induced responses in LSO neurons of wild type mice (C57BL/6J, a common strain used for genetic manipulation) between P2 to P13 ($n = 42$) were characterized. Recordings were done in gramicidin perforated patch-clamp mode. Representative examples of recordings at P3 and P12 are shown in figure 3.4 A and B respectively. E_{Gly} was determined as described above, and amounted to -31 mV at P3 and -77 mV at P12.

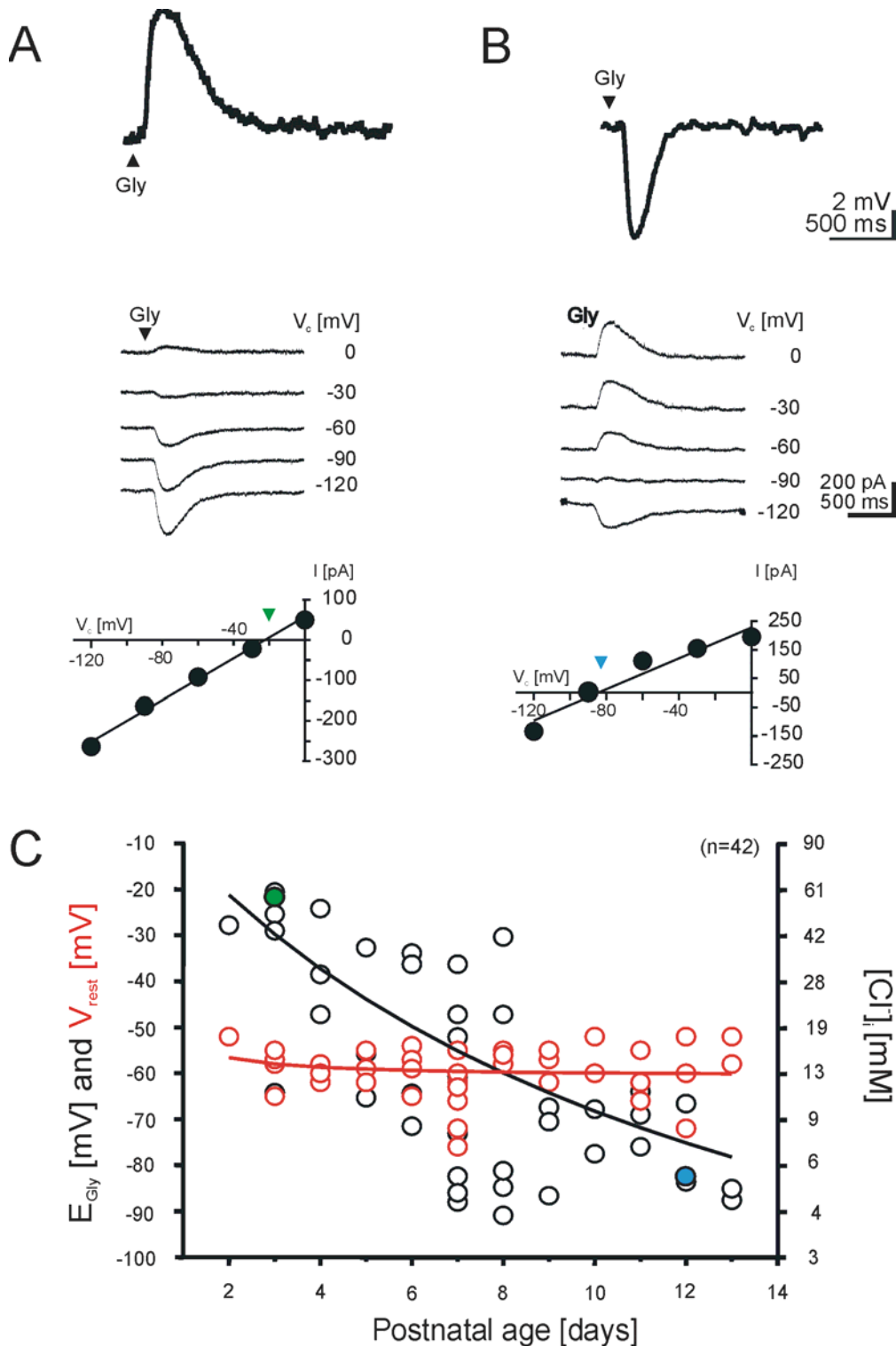


Fig. 3.4: Developmental changes of glycine-induced responses in mouse LSO neurons. Typical examples of glycine-induced responses in mouse LSO neurons at P3 (A) and P12 (B). The upper panels show a glycine-induced depolarization and hyperpolarization at P3 and P12, respectively. Triangles indicate the time of glycine application. The middle panels show glycine-evoked currents at different V_c obtained from the same cells shown in the upper panels. The lower panels depict the corresponding I-V relations, where E_{Gly} (colored triangles) amounted to -21 mV (P3) and -84 mV (P12). (C) E_{Gly} and V_{rest} values from 42 LSO neurons are plotted against age (P2-13). The

corresponding $[Cl^-]_i$ values are given at the right Y-axis. Colored circles mark results from the two cells shown in A and B. At P8, the regression line of E_{Gly} (black) intersects that of V_{rest} (red), demonstrating the time of glycine response shift.

The vast majority of P2-5 neurons (10 out of 12) depolarized upon glycine application, whereas most P8-13 neurons (16 out of 18) hyperpolarized. The switch from glycine-induced depolarization to hyperpolarization takes place at P8, similar to rats, where it happened at P5-7 (Ehrlich et al., 1999). The V_{rest} remains constant irrespective of the age-related negative shift in E_{Gly} , thus revealing an age-dependent positive shift in the driving force ($V_{rest} - E_{Gly}$) of chloride.

3.2 Expression analysis of cation chloride cotransporters

The switch from depolarization to hyperpolarization occurs in several systems due to Cl^- regulation. The role of chloride cotransporters in neuronal chloride homeostasis is well documented (Delpire, 2000; Payne et al., 2003; Vale et al., 2003). Evidence in favor of a pivotal role of Na^+ and K^+ -dependent Cl^- cotransporter (NKCC1) and K^+ -dependent Cl^- cotransporter (KCC2) in several brain regions, in regulating $[Cl^-]_i$ has been reported (Rivera et al., 1999; Sung et al., 2000). To correlate depolarizing and hyperpolarizing glycine activity with an age-dependent gene expression of KCC2 and NKCC1, RT-PCR analysis of several brain regions including the brainstem at P3 (depolarizing age) and P12 (hyperpolarizing age) were performed.

3.2.1 Multiplex RT-PCR expression analysis of NKCC1 and KCC2 in several brain regions

Developmental changes of KCC2 and NKCC1 was explored in the following rat brain regions, cerebellum, cortex, brainstem and auditory brainstem slice at P3 and P12. Multiplex RT-PCR was carried out to identify gene transcripts of NKCC1 (Fig. 3.5)

and KCC2 (Fig. 3.6) along with β -actin as a control. At P3, NKCC1 and β -actin expression was observed in cerebellum, cortex and brainstem. Surprisingly, NKCC1 expression was hard to detect in the auditory brainstem slice at the level of the SOC, which indicates a negative stance on the role of NKCC1. The discrepancy in NKCC1 expression, between brainstem and auditory brainstem slice at the level of SOC, could be due to expression of NKCC1 in other brainstem nuclei. At P12, NKCC1 expression was comparatively higher than β -actin in all regions analyzed.

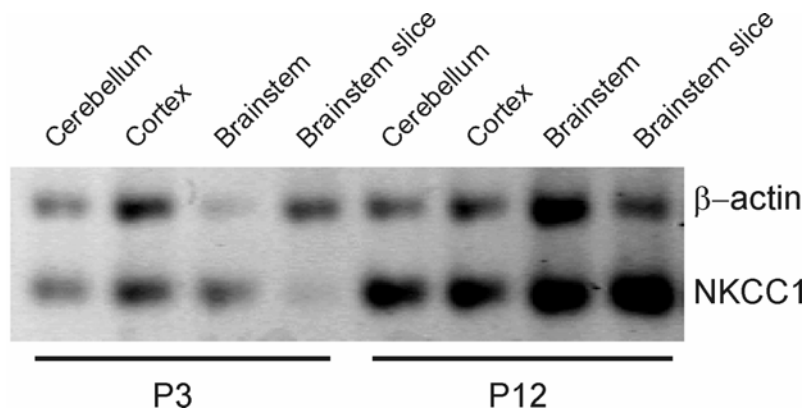


Fig. 3.5: Expression analysis of NKCC1 mRNA by multiplex RT-PCR assay. Expression of NKCC1 was analysed in cerebellum, cortex, brainstem and auditory brainstem slice at P3 and P12. At P3, no NKCC1 signal was detected in the auditory brainstem slice but β -actin (positive control) was detected. In the cerebellum and cortex, uniform NKCC1 and β -actin signals were detected, whereas in the brainstem NKCC1 signal was more prominent than β -actin. At P12, NKCC1 and β -actin expression was detected in every brain region analysed. Compared to NKCC1 signals, β -actin signals were low in every brain region analyzed.

β -actin (positive control) was detected. In the cerebellum and cortex, uniform NKCC1 and β -actin signals were detected, whereas in the brainstem NKCC1 signal was more prominent than β -actin. At P12, NKCC1 and β -actin expression was detected in every brain region analysed. Compared to NKCC1 signals, β -actin signals were low in every brain region analyzed.

As for NKCC1, KCC2 was coamplified with β -actin. KCC2 transcripts were found in all brain regions analyzed, irrespective of the age. This result implicates that functional KCC2 dominance upon development is not only due to up-regulation of the expression. In order to study the gene expression at high resolution, single cell RT-PCR was performed.

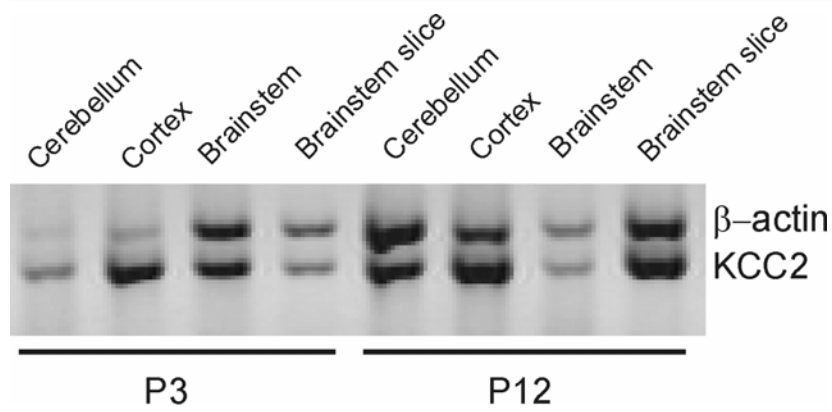


Fig. 3.6: Expression analysis of KCC2 mRNA by multiplex RT-PCR assay. Expression of KCC2 was analysed in cerebellum, cortex, brainstem and auditory brainstem slice at P3 and P12. KCC2 mRNA expression was observed irrespective of age in all

tissues analyzed. At P3, KCC2 expression was higher than β -actin in cerebellum and cortex, whereas uniform in brainstem and auditory brainstem slice. At P12, KCC2 and β -actin expression was similar in all tissues tested.

3.2.2 Single-cell RT-PCR confirms the presence of KCC2 mRNA at P3 and P12 and the absence of NKCC1 mRNA at P3

To determine whether there is a correlation between depolarizing and hyperpolarizing glycine activity and the gene expression of NKCC1 and KCC2, respectively, in individual LSO neurons, single-cell RT-PCR experiments were performed (Geiger et al., 1995). The mRNA expression profile of KCC2 and NKCC1 was compared with the glycine reversal potential (E_{Gly}). Both NKCC1 and KCC2 were probed for 20 neurons, 10 neurons each at P3 and P12. To do so, bipolar LSO neurons in the core region of the nucleus, most likely representing principal neurons (Rietzel and Friauf, 1998), were selected under visual control using DIC-infrared microscopy (see methods). After determining E_{Gly} , as mentioned in the above section, the cell content was carefully harvested while watching the gradual collapse of the soma (Fig. 2.1D), and a nested RT-PCR was performed. In the amplifications with the cotransporter specific primers, the obtained amplicons had the expected sizes of 323 bp and 464 bp for KCC2 and NKCC1, respectively.

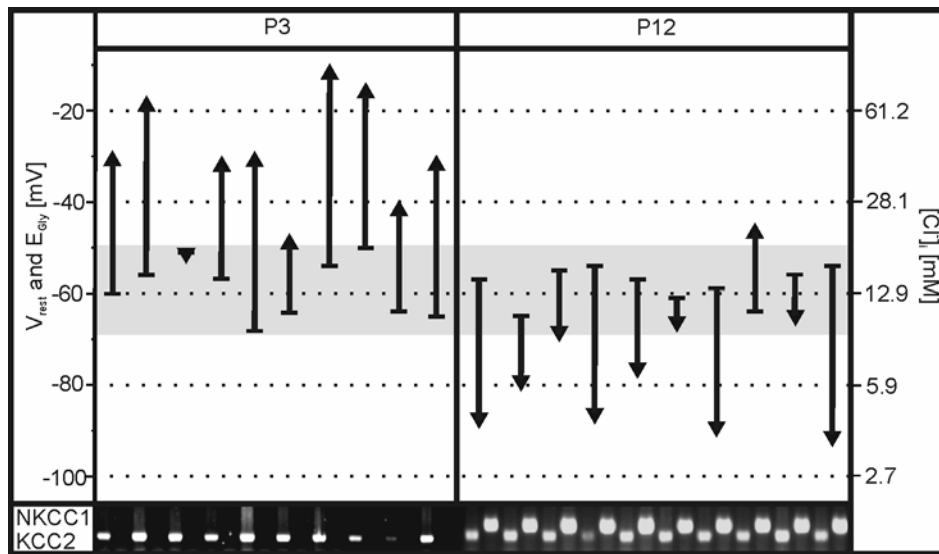


Fig. 3.7: Relationship between E_{Gly} and the presence of KCC2 and NKCC1 transcripts in individual LSO neurons at P3 and P12. Each arrow illustrates the difference between the V_{rest} (base of arrow) and E_{Gly} (tip of arrow) of 20 individual neurons. At P3, in 9 of 10 neurons E_{Gly} was more positive than V_{rest} (upward arrows). At P12, in 9 out of 10 neurons E_{Gly} was more negative than V_{rest} (downward arrows). Values for $[\text{Cl}]_i$ were calculated with the Nernst equation from the measured E_{Gly} values and are shown on the right Y-axis. The gray band illustrates the range for V_{rest} (-50 to -68 mV). V_{rest} averaged -59 ± 2 mV at P3 (mean \pm SEM) and did not significantly differ from V_{rest} at P12 (-58 ± 1 mV; $p > 0.05$). In contrast, E_{Gly} at P3 (mean: -32 ± 4 mV; range: -12 to -52 mV) became significantly more negative until P12 (mean: -76 ± 4 mV; range: -47 to -92 mV; $p < 0.001$). In line with this, $[\text{Cl}]_i$ averaged 44 ± 7 mM at P3 which was significantly higher than 8 ± 2 mM ($p < 0.001$). The results from the single cell RT-PCR experiments are depicted in the lower part of the figure. Every neuron analyzed was positive for KCC2 mRNA, regardless of age. In contrast, no NKCC1 transcript was detected in the P3 group, whereas it was present in every neuron at P12.

KCC2 was found in every single LSO neuron analyzed ($n = 20$), regardless of age or whether E_{Gly} was more negative or less negative than V_{rest} (Fig. 3.7). In contrast, NKCC1 mRNA was detected only in the P12 group ($n = 10$), which comprised 9 neurons whose E_{Gly} was more negative than V_{rest} (Fig. 3.7). As no NKCC1 transcripts were seen at P3, when 9 of 10 neurons showed depolarizing responses to glycine, it is very likely that NKCC1 is not the inward-directed Cl^- transporter during the depolarizing phase in the LSO. Together, the single-cell RT-PCR data show that KCC2 and NKCC1 transcripts can exist in the same LSO neuron, but

coexpression is not obligatory. Most importantly, however, they confirm that KCC2 expression does not correlate with hyperpolarizing glycine activity, and, likewise, NKCC1 expression does not correlate with depolarizing glycine activity in the LSO. The data imply that KCC2 activity may be regulated at the posttranslational level in the LSO, and they also raise the question concerning the nature of the inward-transporting chloride transporter during early ontogeny.

3.3 Characterization of Cl⁻ homeostasis in KCC2 knockout mice

Expression analyses demonstrate the existence of KCC2 mRNA in LSO at P3 and P12 (Fig. 3.7). To determine the functional role of KCC2 in LSO neurons, experiments with KCC2 knockout (-/-) mice were performed. KCC2 -/- mice, in which the KCC2 gene is disrupted and more than 95% reduction of protein expression is achieved, were chosen (as determined by Western blots; Woo et al., 2002). It was shown that homozygous offsprings (KCC2 -/-) exhibit frequent and generalized seizures during the first postnatal week and die between P10 and P16, while heterozygous animals (KCC2 +/-) are indistinguishable from wildtype (+/+) mice during that period (Woo et al., 2002). In the present study, E_{Gly} of KCC2 -/- animals were measured and compared with that from KCC2 +/+.

3.3.1 LSO neurons of P3 KCC2 -/- mice display normal E_{Gly}

As shown before (3.1.3), in LSO neurons of +/+ mice, the switch from depolarizing to hyperpolarizing glycine action takes place at P8 (Fig. 3.4). Consequently, P3 and P12 represent ages at which $E_{\text{Gly}} > V_{\text{rest}}$ and $E_{\text{Gly}} < V_{\text{rest}}$, respectively, and therefore KCC2 -/- mice were investigated at these ages. Current-clamp recordings from LSO neurons of KCC2 -/- mice at P3 consistently showed depolarizing responses with a

mean peak amplitude of 7 ± 1 mV ($n = 4$), which was not significantly different to that seen in KCC2 $+/+$ mice (7 ± 1 mV, $n = 5$; $p > 0.05$; Fig. 3.8A). The I-V relationship of glycine-induced responses in KCC2 $-/-$ mice was indistinguishable from that of KCC2 $+/+$ mice (Fig. 3.8B). The average E_{Gly} in KCC2 $-/-$ mice was -32 ± 7 mV ($n = 4$) and did not significantly differ ($p > 0.05$) from the value found in KCC2 $+/+$ mice (-38 ± 9 mV; $n = 5$). These results provide evidence that KCC2 is not an active Cl⁻ transporter in P3 LSO neurons.

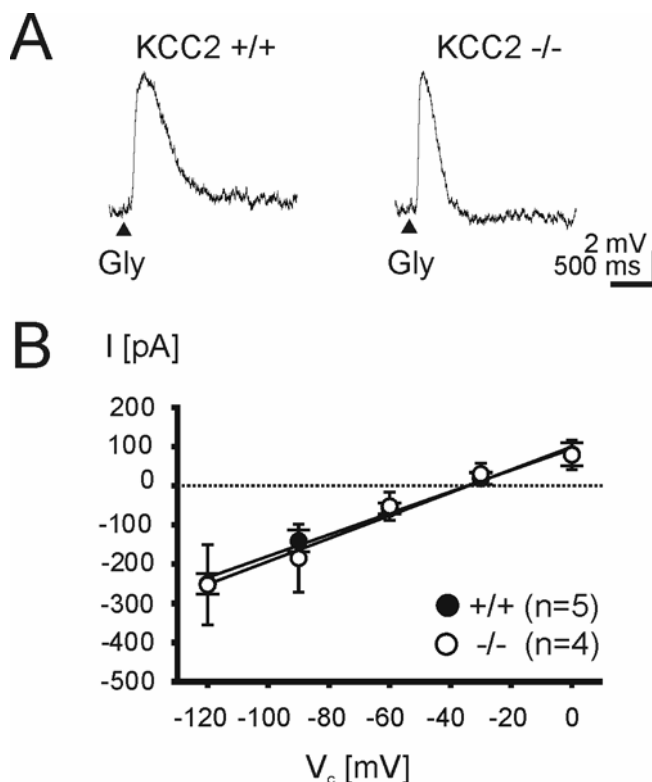


Fig. 3.8: Characterization of glycine-induced responses in P3 LSO neurons of KCC2 knockout ($-/-$) mice. (A) At V_{rest} of -58 mV and -60 mV, LSO neurons from wildtype ($+/+$) mice and $-/-$ mice, show glycine-induced depolarizations. Triangles indicate glycine application. (B) I-V relationships of glycine-induced responses in $-/-$ and $+/+$ mice in comparison. No considerable difference in E_{Gly} between $+/+$ (-38 ± 9 mV) and $-/-$ (-32 ± 7 mV) mice was found ($p > 0.05$). Error bars illustrate SEM (long horizontal endings apply for $+/+$, short endings for $-/-$ mice).

3.3.2 LSO neurons of P12 KCC2 $-/-$ mice display abnormal E_{Gly}

In contrast to the unaffected E_{Gly} seen at P3 in LSO neurons of KCC2 $-/-$ mice, $[\text{Cl}^-]_i$ regulation was obviously disturbed in P12 LSO neurons of these KCC2 $-/-$ mice. This was evidenced by depolarizing glycine-induced responses ($n = 6$), while LSO neurons in KCC2 $+/+$ mice ($n = 6$) showed hyperpolarizing responses (Fig. 3.9A).

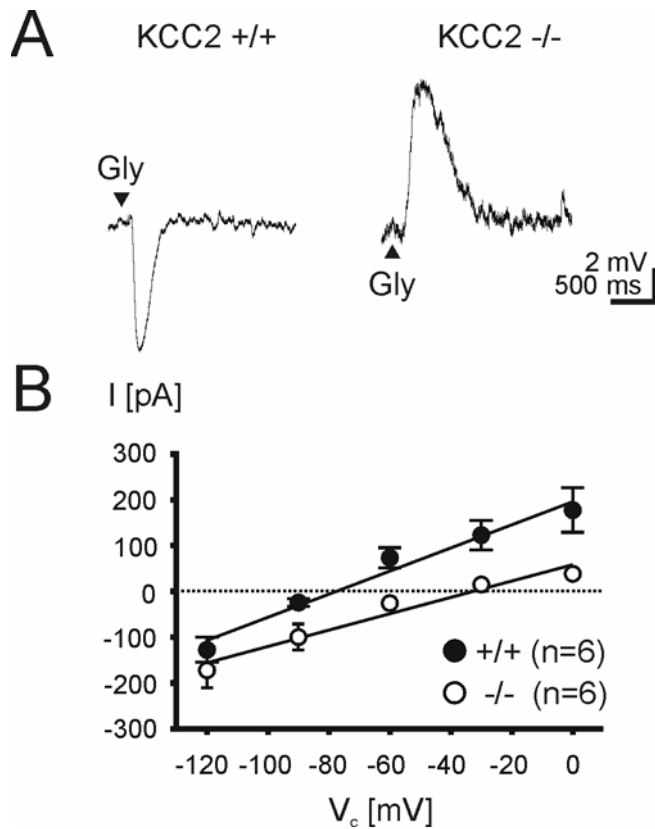


Fig. 3.9: Characterization of glycine-induced responses in P12 LSO neurons of KCC2 $-/-$ mice. (A) At V_{rest} of -58 mV and -62 mV, LSO neurons from $+/+$ mice show glycine-induced hyperpolarization and in contrast $-/-$ mice show depolarization. Triangles indicate glycine application. (B) I-V relationships of glycine-induced responses in $-/-$ and $+/+$ mice in comparison. Significant difference in E_{Gly} between $+/+$ (-75 ± 3 mV) and $-/-$ (-33 ± 3 mV) mice was found ($p < 0.001$). Error bars illustrate SEM (long horizontal endings apply for $+/+$, short endings for $-/-$ mice).

The I-V relationships were clearly shifted towards more positive membrane potentials and exhibited a slightly shallower slope in the KCC2 $-/-$ group (Fig. 3.9B). In KCC2 $-/-$ mice, E_{Gly} was significantly different ($p < 0.001$) from the value obtained for KCC2 $+/+$ mice (-33 ± 3 mV versus -75 ± 3 mV). Interestingly, E_{Gly} in KCC2 $-/-$ mice at P12 did not differ from E_{Gly} in KCC2 $+/+$ mice at P3 ($p > 0.05$), indicating that the genetic-knockout leaves the LSO neurons in an immature state concerning Cl^- regulation. Moreover, there is no significant difference in the resting membrane potential of the neurons among the groups ($p > 0.05$), implying that KCC2 activity does not contribute to V_{rest} (P3 $+/+$: -58 ± 2 mV, $n = 5$; P3 $-/-$: -59 ± 3 mV, $n = 4$; P12 $+/+$: -61 ± 3 mV, $n = 6$; P12 $-/-$: -63 ± 2 mV, $n = 6$). The data obtained from the KCC2 $-/-$ mice strongly corroborate the idea that KCC2 transporter is active at P12. Thus, KCC2 achieves E_{Gly} values that are more negative than V_{rest} by extruding Cl^- from

mature neurons, thus generating a low $[Cl^-]_i$ and relatively negative values for E_{Cl} ($\approx E_{Gly}$) which ultimately result in hyperpolarizing glycine activity.

3.4 Pharmacological characterization of the role of NKCC1 in Cl^- homeostasis

In order to compare the results of NKCC1 expression analysis, showing no NKCC1 transcripts at P3, but at P12, with a possible functional role, pharmacological studies were done with a specific blocker of NKCC1. Bumetanide at low concentration (10–30 μ M) has been shown to perturb chloride inward transport mechanisms in immature neurons by blocking NKCC1 specifically (Isenring et al., 1998; Sung et al., 2000; Hannaert et al., 2002; Payne et al., 2003). Bumetanide at high concentration have been described to elicit non-specific inhibition among the cation chloride cotransporters. NKCC1 and KCC2 strongly differ in their sensitivity to bumetanide, i.e., IC_{50} of bumetanide to NKCC1 and KCC2 is 0.1 vs. 55 μ M, respectively (Cabantchik and Greger, 1992; Lauf, 1984; Russell, 2000).

3.4.1 At low (NKCC1-specific) concentration, bumetanide does not influence E_{Gly} of P3-5 and P12 LSO neurons

To pharmacologically characterize the role of NKCC1 in chloride homeostasis of P3-5 LSO neurons, 30 μ M bumetanide was bath applied. As a control, E_{Gly} was determined before the application of bumetanide and amounted to -35 ± 3 mV, $n = 5$. Subsequently to the bath application of bumetanide, the effect on E_{Gly} was monitored (Fig. 3.10). No significant change in the E_{Gly} (-37 ± 3 mV, $n = 5$) was observed in P3-5 LSO neurons upon bumetanide application ($p > 0.05$). This result is likely to exclude the possibility of the role of NKCC1 in the accumulation of chloride in P3-5 LSO neurons.

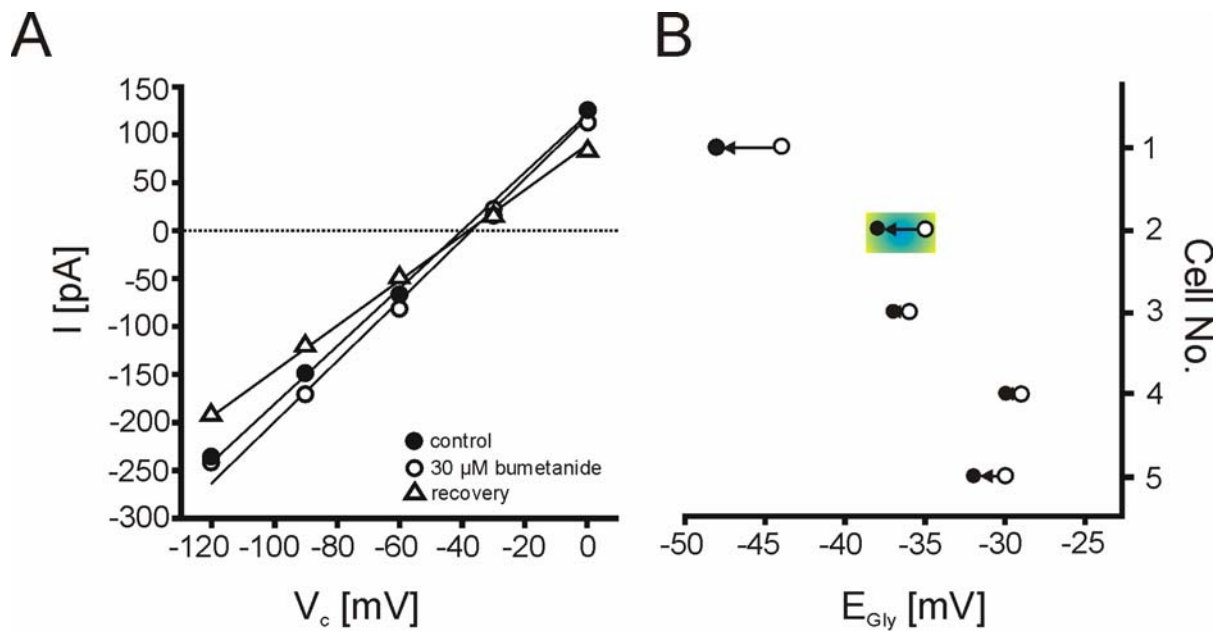


Fig. 3.10: Treatment with low concentration of bumetanide reflects no role of NKCC1 in $[Cl]_i$ regulation in P3 LSO neurons. (A) I-V relations of a P3 LSO neuron under control conditions (open circles), in the presence of 30 μ M bumetanide (closed circles) and after the washout of bumetanide (triangles). (B) Summary of bumetanide effects obtained from five different neurons: the values of E_{Gly} upon control conditions (open circles) are compared with those upon bumetanide treatment (closed circles). The arrows illustrate the direction and magnitude of bumetanide-induced shift in E_{Gly} which was not significant ($p > 0.05$). Color-marked cell represents the example shown in A.

As described above, P12 LSO neurons were challenged with 30 μ M bumetanide in order to find a functional correlate to the expression of NKCC1 mRNA at this age (Fig. 3.7). Under control conditions, E_{Gly} amounted to -79 ± 4 mV ($n = 5$). No significant change in E_{Gly} (-79 ± 5 mV, $n = 5$) was observed upon bumetanide bath application (Fig. 3.11, $p > 0.05$). The data rule out the possibility of the functional involvement of NKCC1 in chloride regulation during the hyperpolarizing phase even though NKCC1 transcripts were observed by expression analysis at this age.

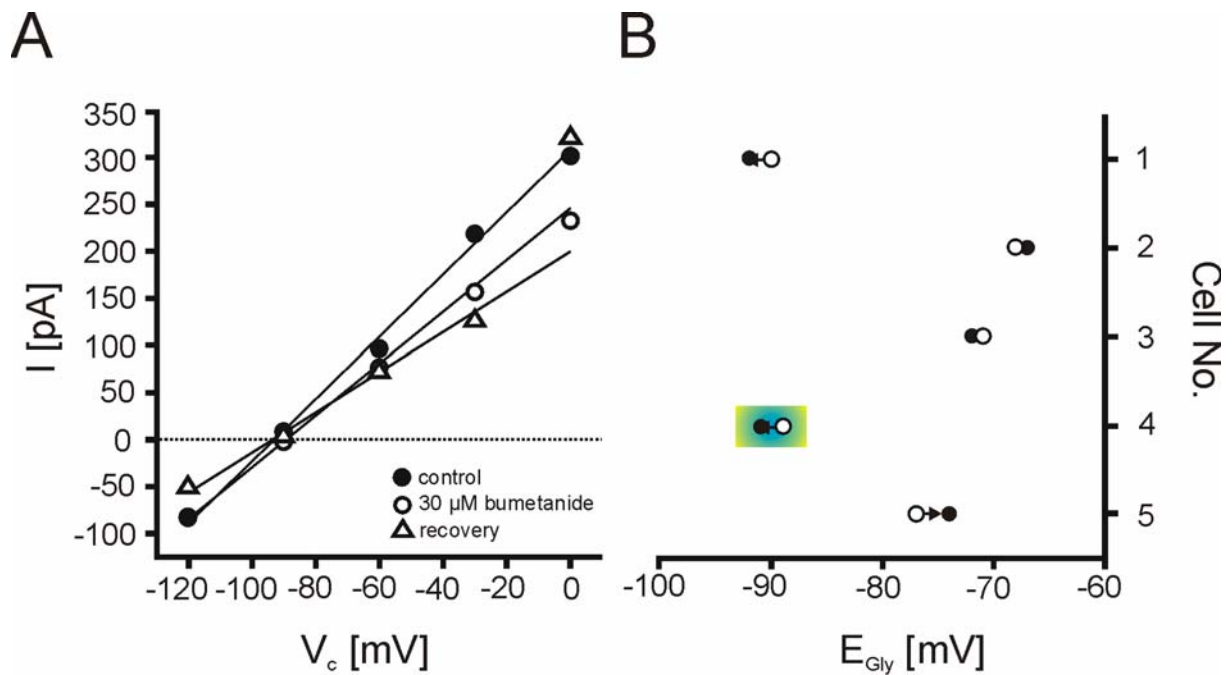


Fig. 3.11: Treatment with low concentration of bumetanide reflects no role of NKCC1 in $[Cl^-]_i$ regulation in P12 LSO neurons. (A) I-V relations of a P12 LSO neuron under control conditions (open circles), in the presence of 30 μ M bumetanide (closed circles) and after the washout of bumetanide (triangles). (B) Summary of bumetanide effects obtained from five different neurons: the values of E_{Gly} upon control conditions (open circles) are compared with those upon bumetanide treatment (closed circles). The arrows illustrate the direction and magnitude of bumetanide-induced shift in E_{Gly} which was not significant ($p > 0.05$). Color-marked cell represents the example shown in A.

3.4.2 At low (NKCC1-specific) concentration, bumetanide influences E_{GABA} in P3-5 pyramidal LSO neurons

In cultured hippocampal pyramidal neurons, NKCC1 was reported to play a role in setting the $[Cl^-]_i$, evidenced by the effects of bumetanide treatment (Hara et al., 1992). Thus, pyramidal neurons served as a positive control to the above experiments with low concentrations of bumetanide. I-V relationships were made after focal application of 500 μ M GABA, and the reversal potentials of GABA induced currents (E_{GABA}) were determined as E_{Gly} , described above. Under control conditions E_{GABA} of P3-5 pyramidal neurons amounted to -37 ± 6 mV ($n = 6$). In the presence of 30 μ M bumetanide E_{GABA} significantly shifted towards more negative potential amounted to -53 ± 8 mV ($n = 6$; $p < 0.01$). The effect of 30 μ M bumetanide on E_{GABA}

was reversible (Fig. 3.12A). The slope of the I-V relationships were reduced after bumetanide application.

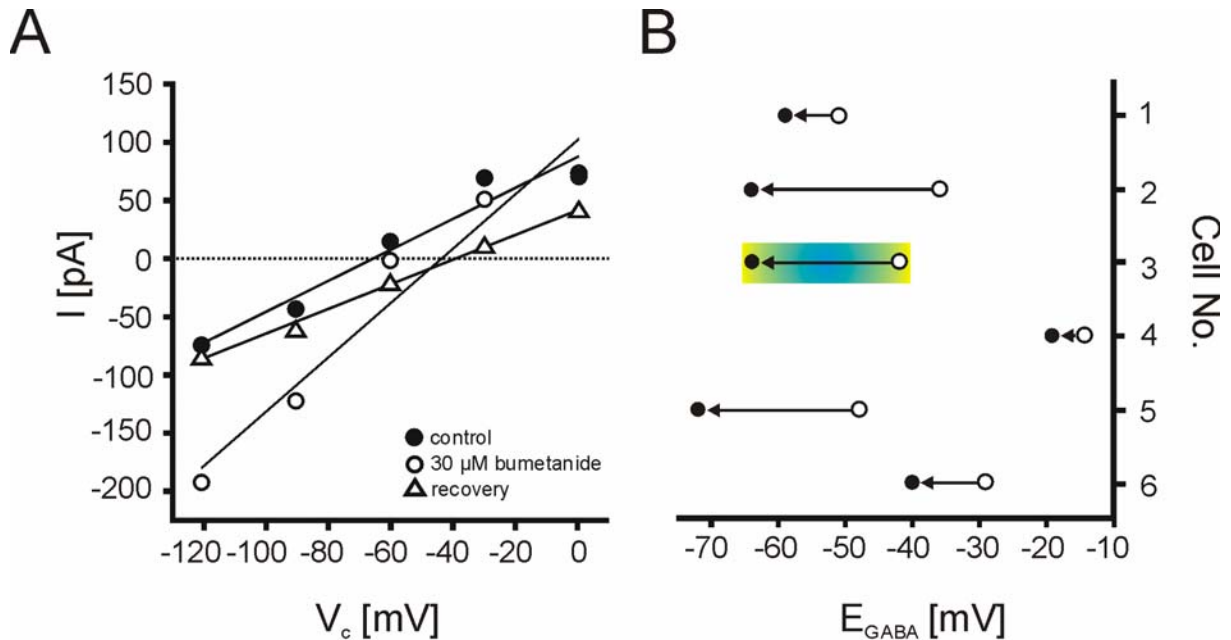


Fig. 3.12: Treatment with low concentration of bumetanide reflects the role of NKCC1 in $[Cl]_i$ in P3 pyramidal neurons of hippocampal CA1 layer. (A) I-V relations of a P3 pyramidal neuron under control conditions (open circles), in the presence of 30 μ M bumetanide (closed circles) and after the washout of bumetanide (triangles). (B) Summary of bumetanide effects obtained from five different neurons: the values of E_{GABA} upon control conditions (open circles) are compared with those upon bumetanide treatment (closed circles). The arrows illustrate the direction and magnitude of bumetanide-induced shift in E_{GABA} which was significant ($p < 0.01$). Color-marked cell represents the example shown in A.

3.4.3 At high (non-specific) concentration, bumetanide influences E_{Gly} of P12 LSO neurons

At P12, under control conditions, E_{Gly} amounted to -78 ± 5 mV, $n = 5$. In the presence of 100 μ M bumetanide, a change in E_{Gly} was monitored namely a significant shift towards less negative value amounting to -64 ± 6 mV, $n = 5$ ($p < 0.01$, Fig. 3.13). This effect was reversible upon washout of the drug (Fig. 3.13A). This result is likely due to a non-specific blockade of functional KCC2, caused by the high bumetanide concentration.

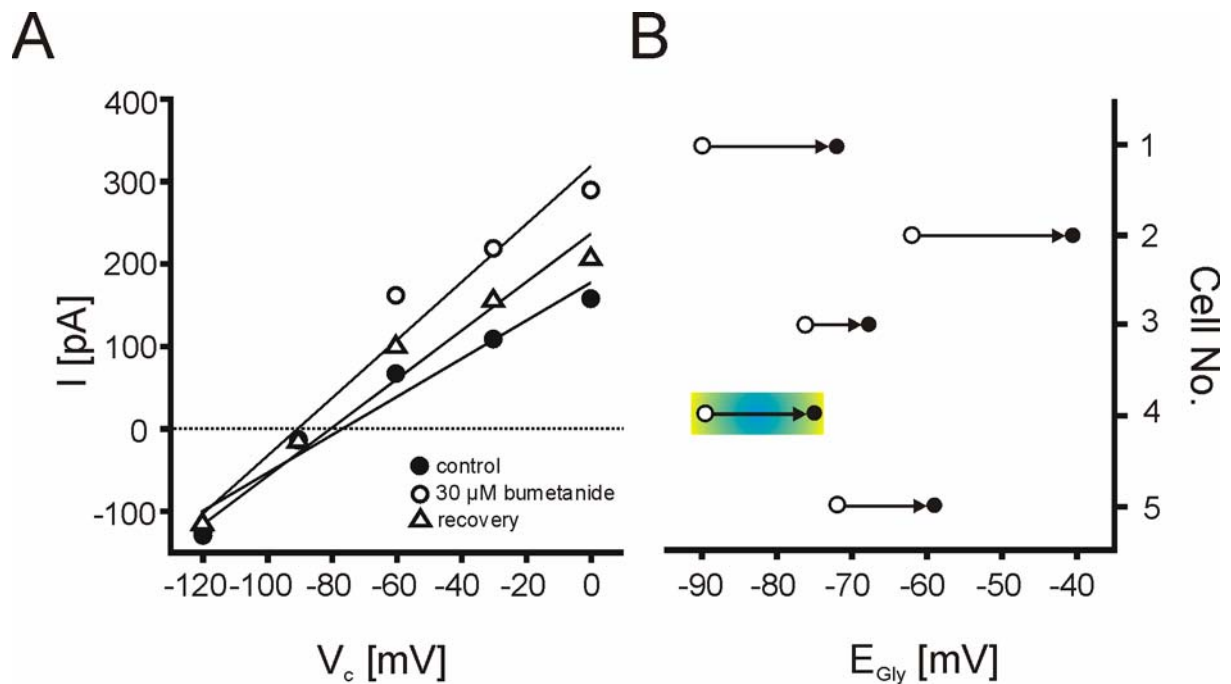


Fig. 3.13: Treatment with high concentration of bumetanide reflects a role of KCC2 in $[Cl^-]_i$ regulation in P12 LSO neurons. (A) Shown are the I-V relations of a P12 LSO neuron under control conditions (open circles), in the presence of 100 μ M bumetanide (closed circles) and after the washout of bumetanide (triangles). (B) Summary of bumetanide effects obtained from five different neurons: the values of E_{Gly} upon control conditions (open circles) are compared with those upon bumetanide treatment (closed circles). The arrows illustrate the direction and magnitude of bumetanide-induced shift in E_{Gly} which was significant ($p < 0.01$). Color-marked cell represents the example shown in A.

3.5 On the role of Na^+ involved in Cl^- homeostasis of LSO neurons

Several inward chloride cotransporters depend on Na^+ gradient for their functional activity (Fig. 1.2). To physiologically characterize if there is any Na^+ -dependent chloride homeostasis in LSO neurons, experiments manipulating the extracellular and intracellular Na^+ concentration ($[Na^+]_i$) were performed.

3.5.1 Lowering $[Na^+]_o$ has no effect on E_{Gly} in P3/4 LSO neurons, but shifts E_{GABA} towards negative in P3/4 pyramidal neurons

To study the effect of lowering $[Na^+]_o$ in chloride homeostasis, E_{Gly} was measured under different $[Na^+]_o$ in the extracellular solution (for composition see Table 2.1) as

shown in Fig. 3.14. Under normal $[\text{Na}^+]_o$, before application of Na^+ -reduced extracellular solution ($t = 0$ min), E_{Gly} amounted to -39 ± 2 mV ($n = 6$) and did not change significantly when $[\text{Na}^+]_o$ was reduced to 18% (-38 ± 2 mV; $n = 6$; $t = 20$ min; $p > 0.05$). Further experiments with LSO neurons were attempted to examine the effect of 100% replacement of $[\text{Na}^+]_o$. But these were unsuccessful, the seal broke down and whole-cell mode was attained.

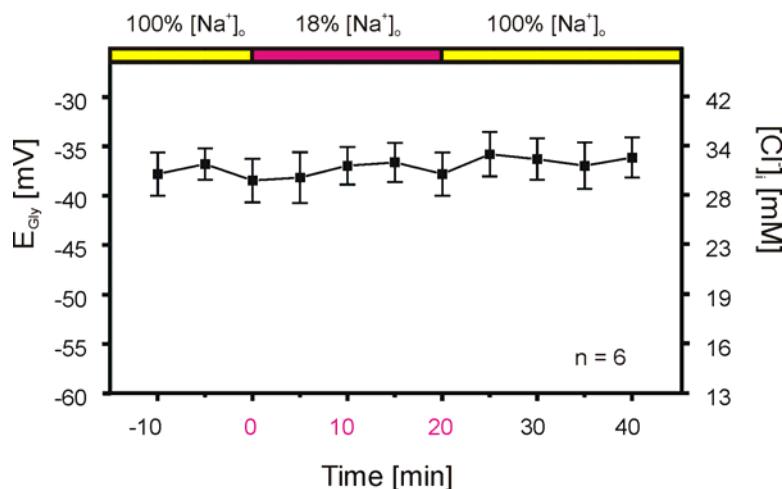


Fig. 3.14: Lowering extracellular Na^+ concentration ($[\text{Na}^+]_o$) has no effect on $[\text{Cl}^-]_i$ in P3 LSO neurons. Mean E_{Gly} values of 6 cells were plotted as a function of time, where $[\text{Na}^+]_o$ was lowered from 100% to 18% for 20 min. The E_{Gly} values at 0 and 20 min were statistically compared. The reduced $[\text{Na}^+]_o$ had no significant

effect on E_{Gly} ($p > 0.05$). Values for $[\text{Cl}^-]_i$ were calculated with the Nernst equation and are shown on the right Y-axis.

In addition to P3 LSO neurons, pyramidal neurons from the CA1 region of the hippocampus were analyzed with normal and low $[\text{Na}^+]_o$. E_{GABA} amounted to -38 ± 1 mV ($n = 4$; $t = 0$ min) with normal $[\text{Na}^+]_o$ and -45 ± 3 mV ($n = 4$; $t = 20$ min) with low $[\text{Na}^+]_o$ (Fig. 3.15). This shift of E_{GABA} towards more negative values was significant ($p < 0.05$), revealing a Na^+ dependent Cl^- accumulation in these hippocampal neurons.

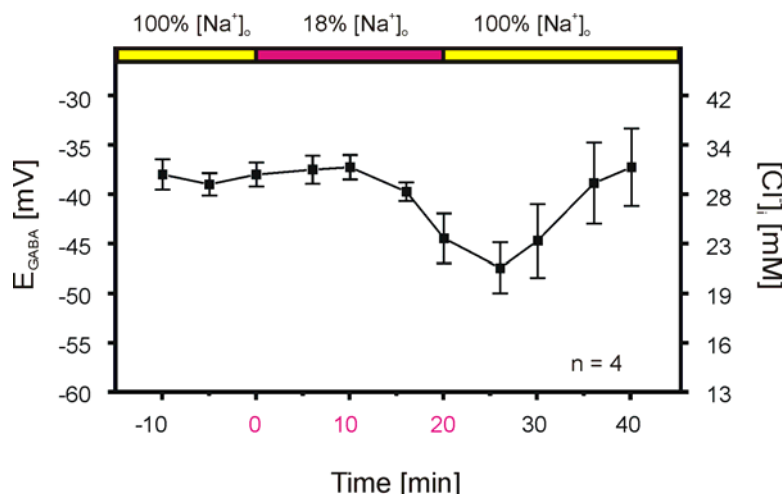


Fig. 3.15: Lowering $[\text{Na}^+]_o$ influences $[\text{Cl}^-]_i$ in P3 hippocampal CA1 pyramidal neurons. Mean E_{GABA} values of 4 cells were plotted as a function of time, where $[\text{Na}^+]_o$ was lowered from 100% to 18% for 20 min. The E_{Gly} values at 0 and 20 min were statistically compared. The

reduction of $[\text{Na}^+]_o$ significantly shifted E_{GABA} towards more negative ($p < 0.05$). Values for $[\text{Cl}^-]_i$ were calculated with the Nernst equation and are shown on the right Y-axis.

3.5.2 Effects of altering $[\text{Na}^+]_i$ on E_{Gly} of neonatal LSO neurons

In order to study the influence of $[\text{Na}^+]_i$ in chloride homeostasis at early postnatal ages, E_{Gly} was measured in P3/4 LSO neurons with two different pipette solutions, containing 4.6 and 24.6 mM Na^+ , respectively (solution 2 and 3; see Table 2.2). Since gramicidin pores are permeable to monovalent cations (Tajima et al., 1996), the cell interior is expected to be influenced by the pipette Na^+ concentration ($[\text{Na}^+]_p$). Experiments with $[\text{Na}^+]_p = 4.6$ mM resulted in an average E_{Gly} value of -40 ± 3 mV ($n = 7$; Fig. 3.16). In contrast, at $[\text{Na}^+]_p = 24.6$ mM, E_{Gly} amounted to -52 ± 5 mV ($n = 7$), which was significantly different ($p < 0.05$). These results indicate the presence of Na^+ -dependent chloride accumulation in LSO neurons, but contradict the experiments performed with low $[\text{Na}^+]_o$ (3.5.1). It can be reasoned that reduction to 18% $[\text{Na}^+]_o$ was not sufficient to interrupt the Na^+ -dependent chloride accumulation.

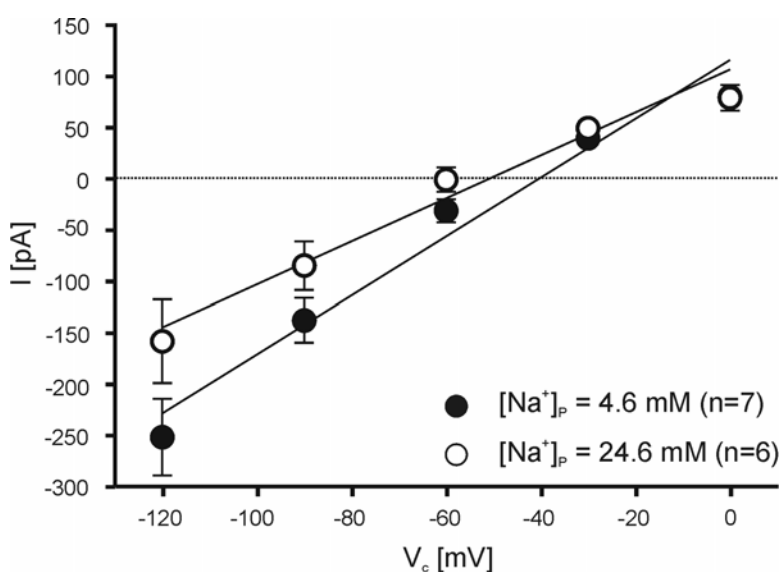


Fig. 3.16: Intracellular Na^+ concentration influences E_{Gly} in P3/4 LSO neurons. I-V relationships obtained from P3/4 LSO neurons under two different pipette Na^+ concentrations ($[\text{Na}^+]_p$). Neurons recorded with 4.6 mM $[\text{Na}^+]_p$ (filled circles) had a mean E_{Gly} of -40 ± 3 mV ($n = 7$), which was significantly different to that recorded with 24.6 mM $[\text{Na}^+]_p$ (-52 ± 5 mV, $n = 6$, $p < 0.05$).

3.6 Characterization of Cl⁻ homeostasis in NKCC1 knockout mice

From all the experiments done so far, the knowledge about KCC2 as an outward chloride cotransporter was conclusive, but the chloride inward transport mechanism remained puzzling. Gene expression and pharmacology excluded NKCC1 as a candidate, but there seemed to be some Na⁺-dependent mechanism involved in setting the [Cl⁻]_i. To finally test whether NKCC1 might play a role, NKCC1 ^{-/-} mice were analyzed like those of KCC2 ^{-/-} at P3 and P12.

3.6.1 LSO neurons of P3 NKCC1 ^{-/-} mice display normal E_{Gly}

The role of NKCC1 in chloride regulation was addressed with NKCC1 ^{-/-} mice at P3 and P12. Current-clamp recordings from LSO neurons obtained in brainstem slices of NKCC1 ^{-/-} mice at P3 consistently showed depolarizing responses, whose peak amplitudes were in the range of those seen in NKCC1 ^{+/+} mice (8 ± 2 mV; n = 4 and 5 ± 1 mV; n = 5, respectively, p > 0.05, Fig. 3.17A). The I-V relationship of glycine-induced responses in NKCC1 ^{-/-} mice was considerably similar to that in ^{+/+} mice (Fig. 3.17B). The average E_{Gly} in P3 ^{-/-} mice was -31 ± 6 mV (n = 4) and did not significantly differ (p > 0.05) from the value found in P3 ^{+/+} mice (-35 ± 3 mV; n = 5). These results provide evidence that NKCC1 plays no role in P3 LSO neurons, consistent with the above described expression analysis (Fig. 3.7), and the pharmacological findings (Fig. 3.10).

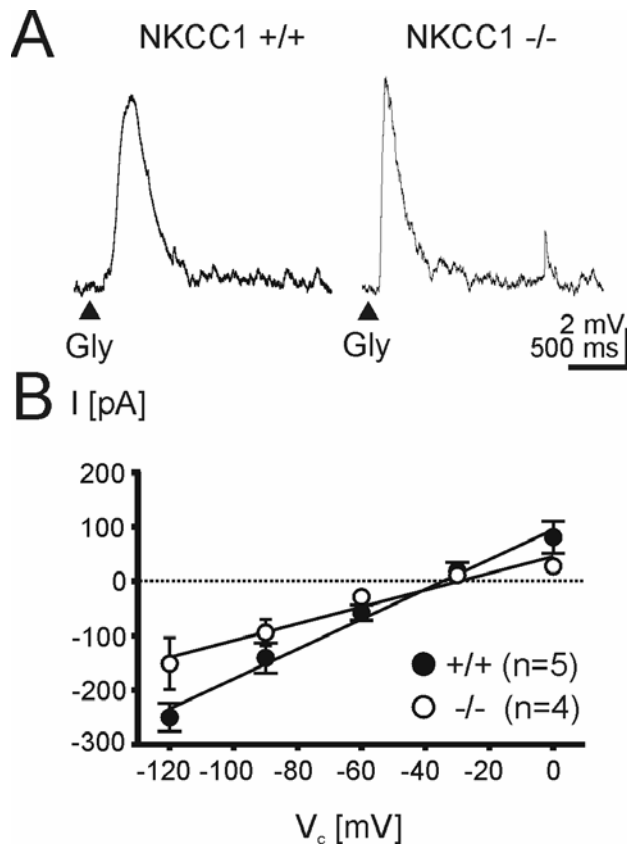


Fig. 3.17: Characterization of glycine-induced responses in P3 LSO neurons of NKCC1 $-/-$ mice. (A) At V_{rest} of -62 mV and -59 mV, LSO neurons from $+/+$ mice and $-/-$ mice, show glycine-induced depolarizations. Triangles indicate glycine application. (B) I-V relationships of glycine-induced responses in $-/-$ and $+/+$ mice in comparison. No considerable difference in E_{Gly} between $+/+$ (-35 ± 3 mV) and $-/-$ (-31 ± 6 mV) mice was found ($p > 0.05$). Error bars illustrate SEM (long horizontal endings apply for $+/+$, short endings for $-/-$ mice).

3.6.2 LSO neurons of P12 NKCC1 $-/-$ mice display normal E_{Gly}

Expression analyses demonstrated an upregulation of NKCC1 with age (Fig. 3.7). To unravel the role of NKCC1 at P12, NKCC1 $-/-$ mice were analyzed at the same age. Current-clamp recordings from LSO neurons obtained in brainstem slices of NKCC1 $-/-$ mice at P12 ($n = 4$) consistently showed hyperpolarizing responses with a mean peak amplitude of 7 ± 2 mV ($n = 5$), which was not significantly different to that seen in NKCC1 $+/+$ mice (6 ± 1 mV; $n = 6$; $p > 0.05$; Fig. 3.18A). The I-V relationship of glycine-induced responses in $-/-$ mice was compared with $+/+$ mice (Fig. 3.18B). The average E_{Gly} in NKCC1 $-/-$ mice was -74 ± 4 mV ($n = 5$) and did not significantly differ ($p > 0.05$) from the value found in NKCC1 $+/+$ mice (-78 ± 3 mV; $n = 6$). These results provide evidence that NKCC1 plays no role in P12 LSO neurons, consistent with the above described pharmacological findings (Fig. 3.11).

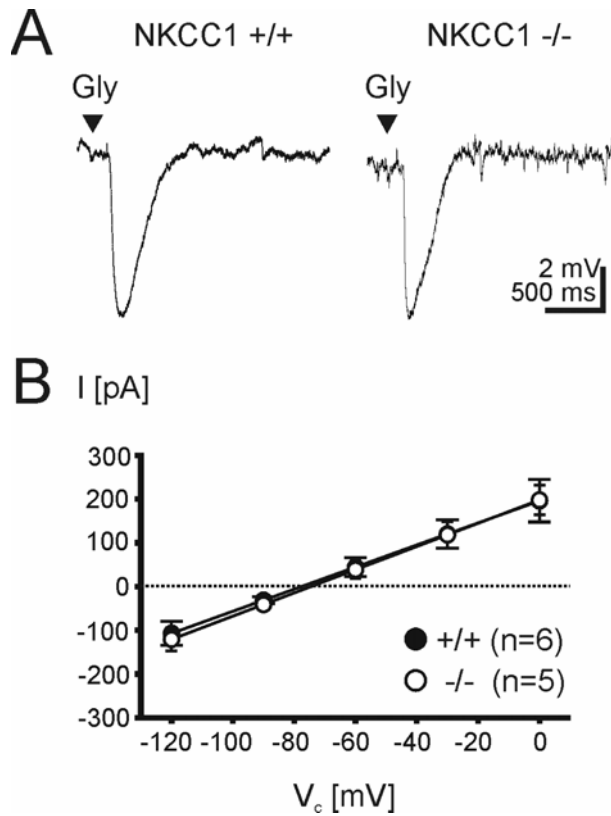


Fig. 3.18: Characterization of glycine-induced responses in P12 LSO neurons of NKCC1 $-/-$ mice. (A) At V_{rest} of -57 mV and -63 mV, LSO neurons from $+/+$ mice and $-/-$ mice, show glycine-induced depolarizations. Triangles indicate glycine application. (B) I-V relationships of glycine-induced responses in $-/-$ and $+/+$ mice in comparison. No considerable difference in E_{Gly} between $+/+$ (-78 ± 3 mV) and $-/-$ (-74 ± 4 mV) mice was found ($p > 0.05$). Error bars illustrate SEM (long horizontal endings apply for $+/+$, short endings for $-/-$ mice).

3.7 Voltage treatment modulates $[Cl^-]_i$ in young LSO neurons

Since the involvement of NKCC1 in chloride accumulation was ruled out by the above results, other possible candidates were investigated. The role of anion exchanger isoform 3 (AE3; Fig. 1.2) was reported to be negligible due to glycine-induced depolarization observed in the absence of HCO_3^- buffer (Kakazu et al., 1999). In order to further investigate the mechanism of chloride accumulation, I focus my studies on the possible involvement of electrogenic transporters like GABA (GAT) and glycine (GLYT) transporters (Fig. 1.2). In general, GAT and GLYT are primarily known as GABA and glycine transporters, respectively, which also cotransport Cl^- along with Na^+ (King and Tunnicliff, 1990; Kavanaugh et al., 1992; Kanner, 1994; Takahashi et al., 1995; Supplisson and Roux, 2002). To investigate the role of these electrogenic transporters in chloride homeostasis, experiments

employing different (depolarization and hyperpolarization) voltage treatments were performed in both P3 and P12 LSO neurons.

3.7.1 Hyperpolarizing voltage treatment induces the Cl⁻ influx in P3 LSO neurons

To check the influence of negative voltage treatment in chloride transport mechanism, E_{Gly} was determined before and after subjecting the neurons to a potential of -120 mV for 15 min (Fig. 3.19). Three consecutive E_{Gly} values, obtained with time interval of 5 min before voltage treatment was used to monitor the stability of E_{Gly} . The control E_{Gly} was determined before the voltage treatment (at 10 min), and amounted to -42 ± 6 mV, $n = 7$. The E_{Gly} was measured after the voltage treatment (at 25 min) amounted to -30 ± 7 mV, which was significantly different from the control ($p < 0.01$). This change corresponds to an increase in $[\text{Cl}^-]_i$ of about 16 mM and indicates that long lasting hyperpolarization increase chloride influx in LSO neurons.

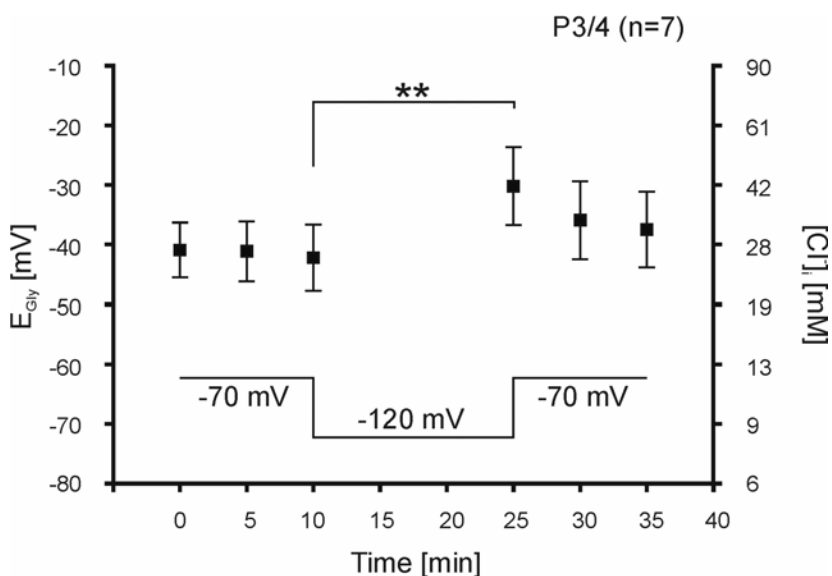


Fig. 3.19: Effect of long lasting hyperpolarization on E_{Gly} in P3/4 LSO neurons. Plot of average E_{Gly} observed in seven P3/4 LSO neurons, before and after the treatment with a 15 min lasting hyperpolarization of -120 mV. Values for $[\text{Cl}^-]_i$ were calculated from Nernst equation and are shown on the right Y-axis. At the last measurement before the

hyperpolarizing step (time = 10 min) the mean E_{Gly} amounted to -42 ± 6 mV ($\approx [\text{Cl}^-]_i = 26$ mM). At the first measurement after the hyperpolarizing step (time = 25 min), the mean E_{Gly} amounted to -30 ± 7 mV ($\approx [\text{Cl}^-]_i = 42$ mM), that is significantly less negative than before the voltage treatment ($p < 0.01$).

3.7.2 Depolarizing voltage treatment reduces the Cl⁻ influx in P3 LSO neurons

In line with the observed effect due to long lasting hyperpolarizations, long lasting depolarizations were expected to produce an opposite effect. To check the influence of long lasting depolarization in chloride transport mechanism, E_{Gly} was determined by I-V relationships of glycine-induced responses in LSO neurons before and after subjecting the neurons to a voltage potential of -40 mV for 15 min (Fig. 3.20). Three consecutive E_{Gly} values obtained with time interval of 5 min, before voltage treatment, were used to monitor the stability of E_{Gly} . The control E_{Gly} was determined before the voltage treatment (at 10 min), and amounted to -23 ± 2 mV, $n = 11$. The E_{Gly} measured after the treatment amounted to -34 ± 3 mV ($n = 11$), which was significantly different from the control ($p < 0.001$). This change corresponds to a decrease in $[\text{Cl}^-]_i$ of about 19 mM. Thus, long lasting depolarization, diminish the chloride influx in LSO neurons.

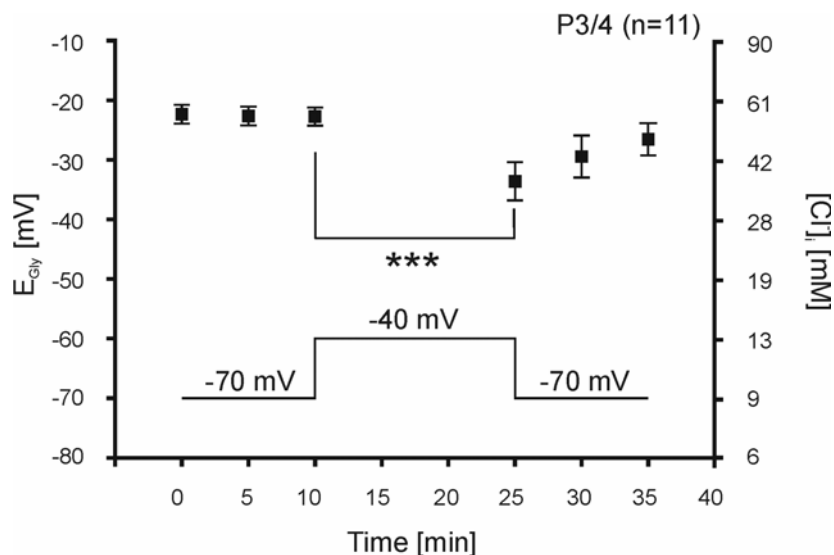


Fig. 3.20: Effect of long lasting depolarization on E_{Gly} in P3/4 LSO neurons. Plot of average E_{Gly} observed in eleven P3/4 LSO neurons, before and after the treatment with a 15 min lasting depolarization of -40 mV. Values for $[\text{Cl}^-]_i$ were calculated from Nernst equation and are shown on the right Y-axis. At the last

measurement before the depolarizing step (time = 10 min) the mean E_{Gly} amounted to -23 ± 2 mV ($\approx [\text{Cl}^-]_i = 55$ mM). At the first measurement after the depolarizing step (time = 25 min), the mean E_{Gly} amounted to -34 ± 3 mV ($\approx [\text{Cl}^-]_i = 36$ mM), that is significantly more negative than before the voltage treatment ($p < 0.001$).

3.7.3 Depolarizing voltage treatment causes no change in Cl⁻ regulation of P12 LSO neurons

The experiments with P3 LSO neurons indicate the presence of voltage dependent transport mechanism involved in Cl⁻ homeostasis. Existence of such mechanism at P12 was checked, by subjecting the neurons to long lasting depolarization as described above for the P3 neurons. Three consecutive E_{Gly} values obtained with time interval of 5 min, before voltage treatment, were used to monitor the stability of E_{Gly} (Fig 3.21). The control E_{Gly} which was determined before the depolarizing step at 10 min amounted to -67.8 ± 4.7 mV, $n = 5$. The E_{Gly} measured after the treatment (at 25 min) amounted to -68.2 ± 5.2 mV ($n = 5$), which was not significantly different from the control ($p > 0.05$). Thus, long lasting depolarization has no influence in the chloride homeostasis of P12 LSO neurons. Altogether, the experiments indicate the existence of electrogenic transporters playing a role in chloride accumulation in LSO neurons.

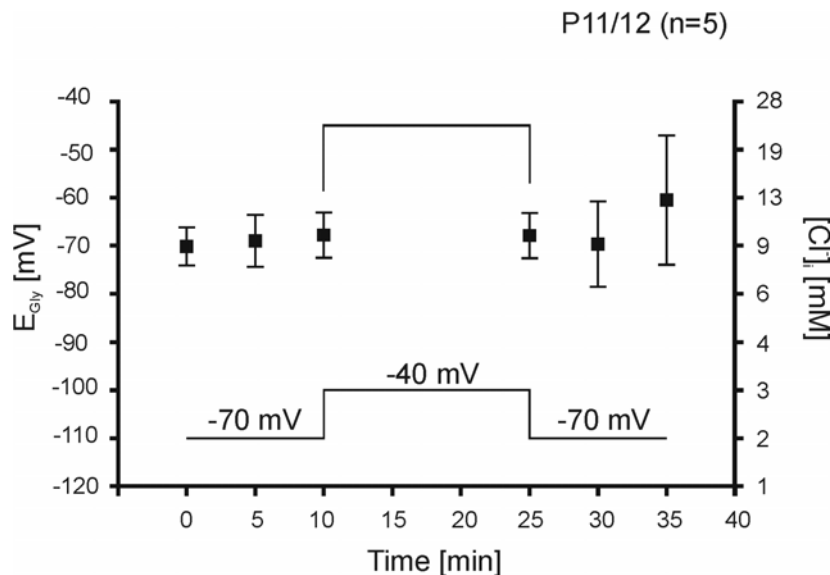


Fig. 3.21: Effect of long lasting depolarization on E_{Gly} in P11/12 LSO neurons. Plot of average E_{Gly} observed in five P11/12 LSO neurons, before and after the treatment with a 15 min lasting depolarization of -40 mV. Values for $[\text{Cl}^-]_i$ were calculated from Nernst equation and are shown on the right Y-axis. At the last measurement before

depolarizing step (time = 10 min), the mean E_{Gly} amounted to -68 ± 5 mV ($\approx [\text{Cl}^-]_i = 9$ mM). At the first measurement after the depolarizing step (time = 25 min), the mean E_{Gly} amounted to -68 ± 5 mV ($\approx [\text{Cl}^-]_i = 9$ mM) as well ($p > 0.05$).

3.8 Pharmacological revealing of GAT1 in Cl⁻ homeostasis

Voltage treatment experiments indicate a role of electrogenic transporters like GAT and/or GLYT. GAT1 is the predominant GABA transporter in the brain. To examine the role of GAT1 in [Cl⁻]_i regulation in LSO neurons, experiments with GAT1 specific inhibitor and activator were performed. SKF 89976A (SKF) was used as a specific blocker of GAT1 in several studies (Mager et al., 1993; Zuiderwijk et al., 1996; Loo et al., 2000) and nipecotic acid (NPA) as a transportable substrate of GAT1, i.e., NPA is transported in place of GABA (Takahashi et al., 1995; Bernstein and Quick, 1999).

3.8.1 GAT1 specific inhibitor influences the [Cl⁻]_i in LSO neurons at P3/4, but not at P11/12.

To examine the effect of GAT1 in [Cl⁻]_i regulation, E_{Gly} under control condition and during bath application of 100 μM SKF for 30 min was compared. E_{Gly} was measured at intervals of 5 min for up to 90 min as shown in Fig. 3.22. At P3/4, under control conditions (at 10 min), the mean E_{Gly} was -33 ± 3 mV (n = 6). In the presence of SKF (at 30 min), E_{Gly} significantly shifted towards more negative (-51 ± 6 mV; n = 6; p < 0.05). In contrast, at P11/12, the E_{Gly} amounted to -75 ± 4 mV (n = 7) under control conditions (at 10 min), which was not significantly different to E_{Gly} obtained in the presence of SKF (-78 ± 5 mV, n = 7; p > 0.05).

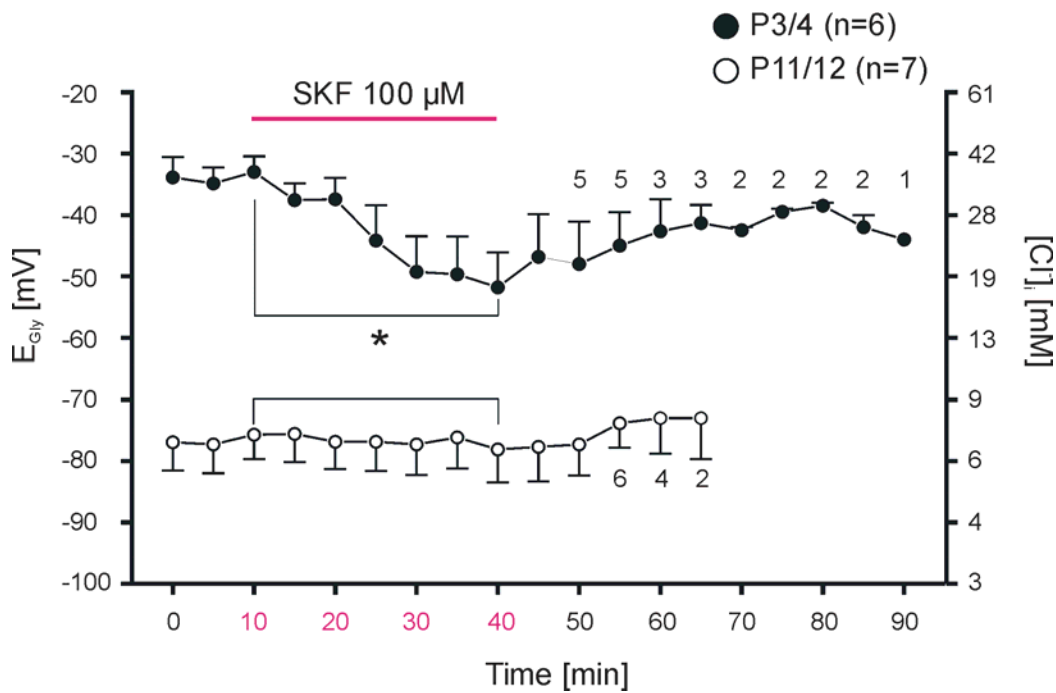


Fig. 3.22: The blockade of GABA transporter 1 (GAT1) influences $[Cl]_i$ in P3/4 but not in P11/12 LSO neurons. Plot of mean E_{Gly} values obtained from six P3/4 and seven P11/12 neurons, before, during and after 30 min application of the specific GAT inhibitor SKF 89976A (SKF). Values for $[Cl]_i$ were calculated with the Nernst equation and are shown on the right Y-axis. E_{Gly} was significantly reduced at P3/4 i.e., from -33 ± 3 mV at 10 min to -52 ± 6 mV at 40 min ($p < 0.05$), indicating the blockade of a net inward Cl^- transport mechanism. In contrast, at P12 SKF induced no significant shift in E_{Gly} (-76 ± 4 mV at 10 min, and -78 ± 5 mV at 40 min, $p > 0.05$), revealing no role of GAT1 in setting the $[Cl]_i$. The numbers adjacent to the symbols indicate individual n value of that mean.

3.8.2 GAT1 specific inhibitor influences $[Cl]_i$ in the presence of GABA receptors blockers.

SKF treatment is likely to increase the extracellular GABA concentration in the synaptic cleft, which may lead to activation of postsynaptic GABA receptors. To elucidate that the reduction of $[Cl]_i$ by SKF was not due to the activation of GABA receptors via an increased GABA concentration, experiments with antagonists against the three types of GABA receptors were performed (GABA_A : 30 μ M bicuculin, GABA_B : 10 μ M SCH 50911 and GABA_C : 10 μ M I4AA). In the presence of these GABA receptor antagonists, LSO neurons were challenged with SKF for 30 min as shown in Fig. 3.23. The E_{Gly} before this treatment amounted to -33 ± 5 mV (n

= 6). Upon SKF treatment, E_{Gly} amounted to -49 ± 6 mV ($n = 6$), which was significantly different to the control situation ($p < 0.05$). Furthermore, the time courses of the SKF treatment obtained from experiments with and without GABA receptor antagonists were very similar. Quantitatively, E_{Gly} under SKF (at 40 min, Fig. 3.23), in the presence and absence of GABA receptor antagonists amounted to -49 ± 6 mV and -52 ± 6 mV, respectively.

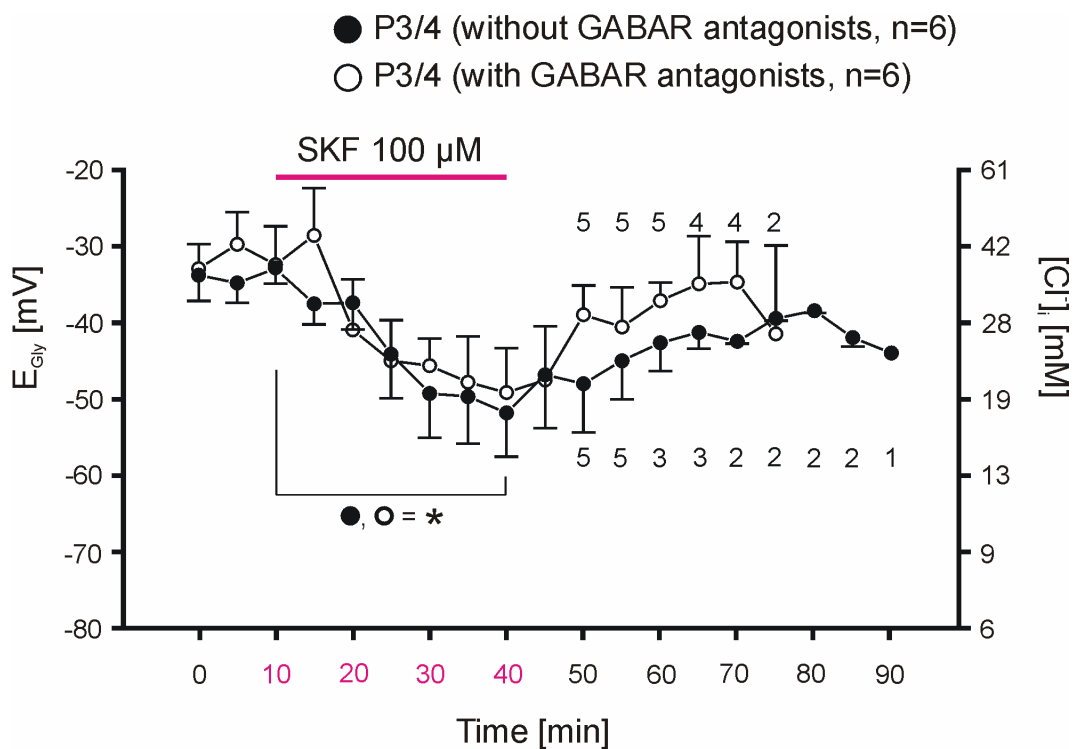


Fig. 3.23: Influence of GAT1 on $[Cl]_i$ is independent of GABA receptor activation in P3/4 LSO neurons. Plot of mean E_{Gly} values obtained from twelve P3/4 neurons, before, during and after, 30 min application of SKF. In one group (open circles, $n = 6$), the GABA receptor agonists were added to the extracellular solution. In the second group (filled circles, $n = 6$), the standard extracellular solution was used (same cells as in Fig. 3.22). Values for $[Cl]_i$ were calculated with the Nernst equation and are shown on the right Y-axis. Similar to the situation under standard conditions (filled circles, for details see 3.22), in the presence of GABA receptor antagonists, E_{Gly} (open circles) was significantly reduced i.e., from -33 ± 5 mV at 10 min to -49 ± 6 mV at 40 min ($p < 0.05$). The change in E_{Gly} upon SKF treatment, in the presence and absence of GABA receptor antagonists, display no significant difference ($p > 0.05$), indicating that the effect of GAT1 is independent of GABA receptor activation. The numbers adjacent to the symbols indicate individual n value of that mean.

3.8.3 GAT specific activator influences $[Cl^-]_i$ in LSO neurons at P3/4, but not at P11/12.

P3 and P12 LSO neurons were treated with 100 μ M NPA, usable as a substrate of GAT, for 30 min. By activating GAT, increase in the Cl^- accumulation was expected at P3/4, because it is necessary at early postnatal development (P3/4) and not at latter ages (P11/12). E_{Gly} was measured in an interval of 5 min up to 90 min as shown in Fig. 3.24. At P3/4, under control conditions (at 10 min), the mean E_{Gly} was -35 ± 1 mV ($n = 7$). In the presence of NPA (at 30 min), E_{Gly} significantly shifted towards more positive (-28 ± 2 mV; $n = 7$; $p < 0.01$). In contrast, at P12, the E_{Gly} amounted to -70 ± 5 mV ($n = 7$) under control conditions (at 10 min), which was not significantly different to E_{Gly} obtained in the presence of NPA (-67 ± 8 mV; $n = 7$; $p > 0.05$). These experiments hint a possible role of GAT1 in Cl^- accumulation in P3/4 LSO neurons.

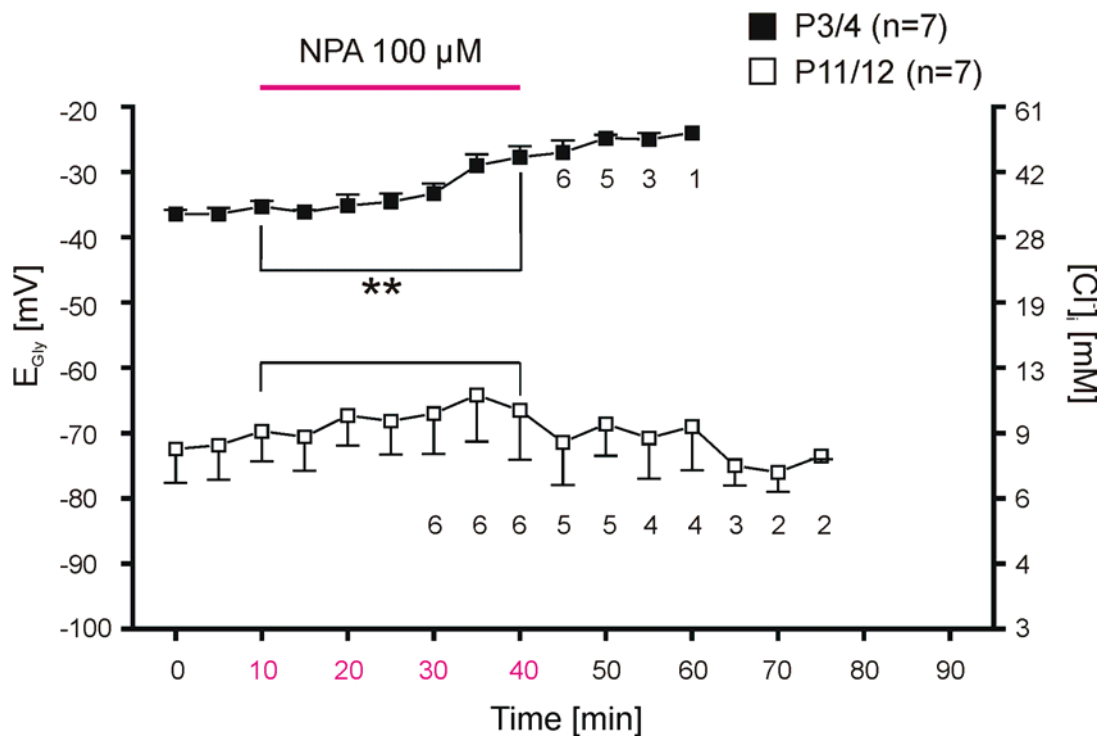


Fig. 3.24: The activation of GAT1 influences $[Cl^-]_i$ in P3/4 but not in P11/12 LSO neurons. Plot of mean E_{Gly} values obtained from seven P3/4 and seven P11/12 neurons, before, during and after, 30 min application of the specific GAT activator, nipecotic acid (NPA). Values for $[Cl^-]_i$ were calculated with the Nernst equation and are shown on the right Y-axis. At P3/4, E_{Gly} was significantly increased

from -35 ± 1 mV at 10 min to -28 ± 2 mV at 40 min ($p < 0.01$), indicative of the activation of a net inward Cl^- transport mechanism. At P12, NPA induce no significant (-70 ± 5 mV at 10 min and -67 ± 8 mV at 40 min, $p > 0.05$), revealing no role of GAT1 in setting the $[\text{Cl}^-]_i$. The numbers adjacent to the symbols indicate individual n value of that mean.

3.9 Characterization of Cl^- homeostasis in GLYT2 knockout mice

Like GABA transporters, glycine transporters (GLYT) also cotransport Cl^- inwardly (Supplisson and Roux, 2002). Among the two isoforms, GLYT1 and GLYT2, GLYT2 displays neuronal expression (Zafra et al., 1995; Friauf et al., 1999). To unravel any possible role of glycine transporter in Cl^- regulation in LSO neurons, E_{Gly} from GLYT2 $-/-$ mice (Gomez et al., 2003) were compared with that from GLYT2 $+/+$.

3.9.1 At P3/4, LSO neurons of GLYT2 $-/-$ mice display relatively negative E_{Gly} values

In current-clamp recordings at P3/4, LSO neurons of GLYT2 $-/-$ mice consistently showed depolarizing glycine responses with a mean peak amplitude of 8 ± 1 mV ($n = 8$). The wildtype (GLYT2 $+/+$) and heterozygous (GLYT2 $+/-$) littermates showed 7 ± 1 mV ($n = 8$) and 7 ± 1 mV ($n = 20$), respectively (Fig. 3.25A).

In voltage-clamp mode, the I-V relationships of glycine-induced responses in GLYT2 $-/-$ mice were compared to that in GLYT2 $+/+$ mice (Fig. 3.25B). The average E_{Gly} in GLYT2 $-/-$ mice was -52 ± 3 mV ($n=8$) and significantly different ($p < 0.001$) from the value found in P3 GLYT2 $+/+$ mice (-29 ± 4 mV; $n = 8$). Furthermore, the latter and GLYT2 $+/-$ (-37 ± 2 mV; $n = 20$) mice differed by reaching significance ($p = 0.0498$). This result indicates the involvement of GLYT2 in chloride homeostasis of LSO neurons which needs further pharmacological investigation.

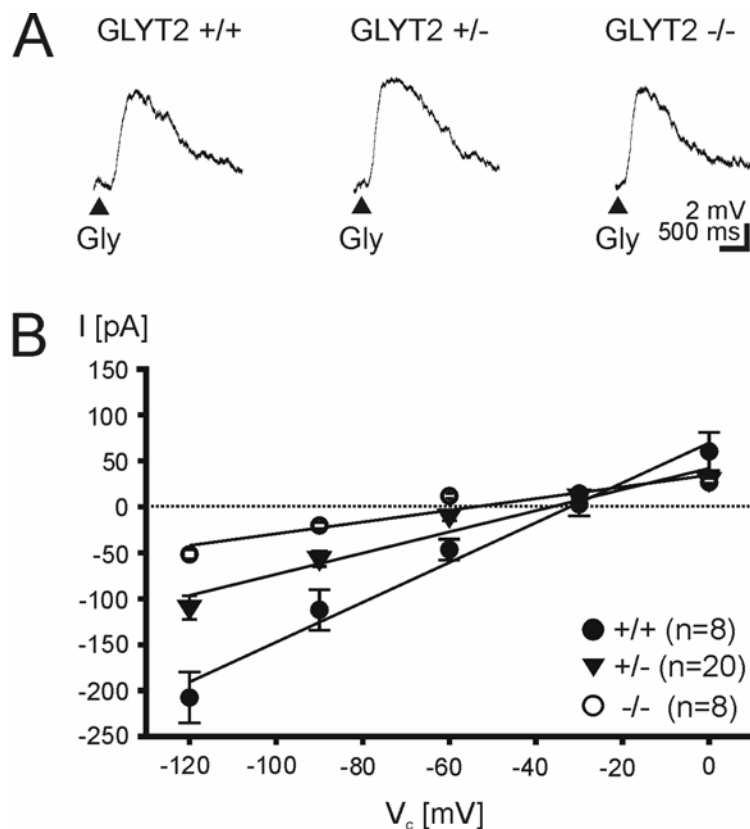


Fig. 3.25: Characterization of glycine-induced responses in P3/4 LSO neurons of GLYT2 $-/-$ mice.

(A) Examples of glycine-induced depolarizations, obtained from LSO neurons of three different genotypes, i.e., GLYT2 $+/+$, GLYT2 heterozygous ($+/-$) and GLYT2 $-/-$ at V_{rest} of -68 mV, -62 mV and -64 mV respectively. Triangles indicate glycine application. (B) I-V relationships of glycine-induced responses from $-/-$, $+/-$ and $+/+$ mice. Their E_{Gly} values amounted to -52 ± 3 mV ($-/-$), -37 ± 2 mV ($+/-$) and -29 ± 4 mV ($+/+$), whereas those from $-/-$ and $+/+$, as well as those from $+/-$ and $+/+$, were significantly different ($p < 0.001$ and

$p < 0.05$, respectively). Error bars illustrate SEM (long horizontal endings apply for $+/+$, medium endings $+/-$ and short endings for $-/-$ mice).

3.10 Influence of phosphorylation in the regulation of $[Cl^-]_i$

The phosphorylation status of proteins plays a pivotal role in determining the function in almost every conceivable way (Cohen, 2000). Several transport systems were reported to be dynamically regulated via phosphorylation mechanisms. For example, tyrosine phosphorylation has been implicated in the regulation of K-Cl transport (Sachs and Martin, 1993; Flatman et al., 1996); regulation of the dopamine transporter includes direct phosphorylation effects (Page et al., 2001; Mortensen and Amara, 2003); Protein kinase A phosphorylation of AMPA receptor controls synaptic trafficking (Esteban et al., 2003). To test whether the phosphorylation status of transporters influences the Cl^- regulation, LSO neurons were treated with protein

phosphatase inhibitor calyculin A which was aimed to increase the phosphorylation of proteins in general (Ishihara et al., 1989).

3.10.1 In P3 LSO neurons treated with calyculin A, $[Cl^-]_i$ is reduced

P3 rat SOC slices were treated with 100 μ M calyculin A for 1 hr. E_{Gly} was determined from a population of neurons from treated and untreated slices and statistically compared. E_{Gly} in LSO neurons treated or untreated with calyculin A, demonstrated the influence of phosphorylation status in Cl^- regulation (Fig. 3.26). Under control conditions, E_{Gly} was measured from ten P3 neurons and amounted on average to -32 ± 4 mV. A total of 9 cells with calyculin A treatment showed a mean E_{Gly} of -51 ± 3 mV, which was significantly more negative than the value obtained from the control group ($p < 0.01$). The resting membrane potential of these two groups displayed no considerable difference (untreated = -59 ± 2 mV and calyculin A treated = -58 ± 2 mV; $p > 0.05$).

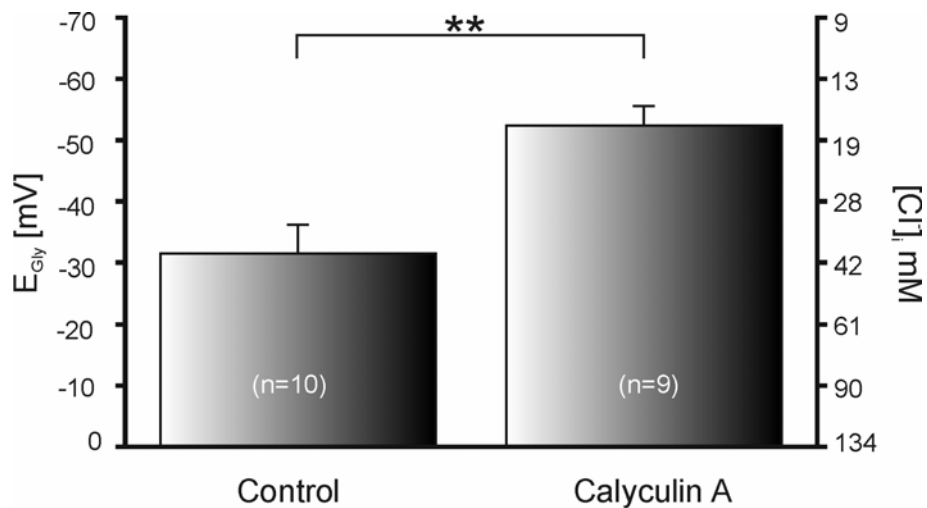


Fig. 3.26: The phosphorylation status of proteins influences $[Cl^-]_i$. P3 LSO neurons treated with 100 μ M calyculin A, a protein phosphatase inhibitor, showed significantly ($p < 0.01$) more negative mean E_{Gly} (-51 ± 3 mV, $n = 9$) compared to that from untreated controls (-32 ± 4 mV, $n = 10$).

3.11 Influence of thyroid hormone in the regulation of $[Cl^-]_i$

Thyroid hormone (TH) plays an important role in brain development (Thompson and Potter, 2000; Konig et al., 2002; Bernal et al., 2003). For example, TH deficiency before the onset of hearing causes irreversible damage of peripheral and central auditory systems (Knipper et al., 2000). Moreover, TH regulates brain-derived neurotrophic factor (BDNF), neurotrophin-3 (NT3) and nerve growth factor (NGF) which are thought to play a role in chloride homeostasis (Giordano et al., 1992; Koibuchi et al., 1999; Neveu and Arenas, 1996). In the present study, the possible role of TH in the developmental regulation of chloride homeostasis was examined, by determining the developmental switch in E_{Gly} in hypothyroid animals.

3.11.1 Hypothyroid rats lack a developmental shift in E_{Gly} between P5 and P12

In LSO neurons from normal rats and mice, the age-dependent negative shift in E_{Gly} occurs between P5-8 (Ehrlich et al., 1999; chapter 3.1.3 of present study). In order to elucidate the possible role of TH in chloride homeostasis, E_{Gly} was determined from 25 LSO neurons of hypothyroid rats aged P5-12 (open black symbols in Fig. 3.27). The V_{rest} of these neurons amounted to -64 ± 1 mV ($n = 25$) and showed no considerable change with age (filled red symbols in Fig. 3.27). The majority of the hypothyroid LSO neurons ($n = 21/25$) displayed depolarizations irrespective of the postnatal ages. Thus, abnormal chloride homeostasis in the LSO neurons of hypothyroid rats indicates the role of thyroid hormone in the development of inhibitory synapses.

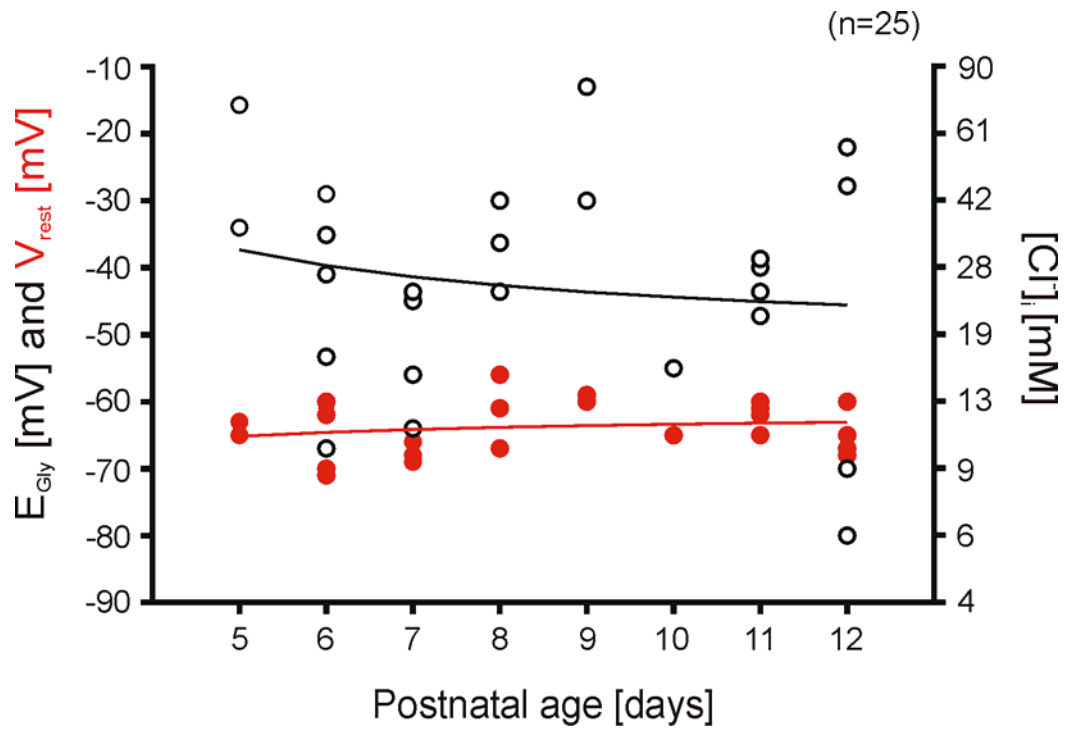


Fig. 3.27: Thyroid hormone signalling is involved in $[Cl]_i$ regulation in rat LSO neurons. The E_{Gly} (open black circles) and V_{rest} (closed red circles) values from LSO neurons of hypothyroid animals ($n = 25$) were plotted against their postnatal age (P5-12). Within this period, they displayed no shift in E_{Gly} , which is in contrast to LSO neurons from normal animals (cf. Fig. 3.4C). Note, that like in normal animals, V_{rest} remained considerably the same throughout the developmental period analyzed.

4 DISCUSSION

Six major results concerning the Cl⁻ regulation in LSO neurons were obtained in this study: (1) In mice, glycinergic responses shift from depolarizing to hyperpolarizing at P8, similar to the situation in rats. (2) As an outward Cl⁻ transporter, KCC2 renders glycine hyperpolarizing. (3) NKCC1 plays no role in setting a high [Cl⁻]_i; therefore, it is not involved in depolarization. (4) Cl⁻ accumulation during the early depolarizing phase is achieved by the neurotransmitter transporters GAT1 and GLYT2. (5) The phosphorylation status of proteins influences Cl⁻ regulation, indicating the involvement of posttranslational mechanisms in Cl⁻ homeostasis. (6) Hypothyroid rats display no developmental shift in the glycine response at a time when normal rats do so (i.e., P6-8). Thus, thyroid hormone is reasoned to play a role in the maturation of inhibitory synapses through influencing Cl⁻ homeostasis of LSO neurons.

4.1 Developmental changes in glycine-induced responses in mice LSO neurons

GABA-induced and glycine-induced responses undergo a developmental shift from depolarization to hyperpolarization. Such a shift has been reported in several systems during their early postnatal life, e.g., hippocampus (Mueller et al., 1984; Janigro and Schwartzkroin, 1988; Ben-Ari et al., 1989; Cherubini et al., 1990; Zhang et al., 1990), cerebral cortex (Luhmann and Prince, 1991; Yuste and Katz, 1991; Lo Turco et al., 1995; Owens et al., 1996), hypothalamus (Chen et al., 1996), spinal cord (Wu et al., 1992; Reichling et al., 1994; Rohrbough and Spitzer, 1996) and retina (Huang and Redburn, 1996; Billups and Attwell, 2002). Gramicidin perforated patch-clamp recordings performed in rat LSO neurons demonstrate such an age-

dependent depolarization at P3 and hyperpolarization at P12, which is due to high and low $[Cl^-]_i$, respectively. At P3, the E_{Gly} is more positive than V_{rest} , whereas it is more negative at P12 (Ehrlich et al., 1999; Kakazu et al., 1999).

In the present thesis, the developmental shift of E_{Gly} was also studied in mice LSO neurons (strain: C57BL/6J). The earliest hyperpolarization was observed at P5 and the day of developmental shift in E_{Gly} was denoted as P8. But Kullmann and Kandler (2001) report that the day of shift is at around P5 in mice LSO neurons. This discrepancy can be explained by a recent finding in rat LSO neurons, demonstrating regional differences in the timing of glycine response shift (Srinivasan et al., 2004). Remarkably, the high frequency region displays an early shift. Such regional differences in the developmental shift may also be present in mice.

4.2 KCC2 renders glycine hyperpolarizing by setting $E_{Gly} < V_{rest}$

The results from multiplex and single cell RT-PCR analyses provided firm evidence that there is no simple causality between the presence of KCC2 mRNA and hyperpolarizing glycine activity in LSO neurons. KCC2 mRNA was found in the brainstem throughout the first two postnatal weeks, showing no sign of up regulation. Similar results were observed in spinal cord motoneurons and hippocampal pyramidal cells, i.e., phosphorylated KCC2 protein was already present early in development even when the switch in GABA activity had not yet occurred (Stein et al., 2004). However, in other reports on rat hippocampus, it was shown that the amount of both KCC2 mRNA and protein gradually increased between P0 and P9, thereby rendering GABAergic activity hyperpolarizing (Rivera et al., 1999; Ganguly et al., 2001; Gulyás et al., 2001). An age-dependent increase of KCC2 expression was also reported for the rat neocortex (after P7, Clayton et al., 1998; between P3 and P25, DeFazio et al., 2000), and the rat retina (between P1 and P14, Vu et al.,

2000). Lu et al. (1999) investigated the rat brain by Northern and Western blot analysis and found a low expression of KCC2 at birth and a significant increase until P28. Unfortunately, in this study, the brainstem was not specifically investigated. It is possible that the developmental regulation of KCC2 activity differs in regional aspects of the CNS, e.g. along a caudal to rostral axis. Spinal cord neurons and cranial motor neurons, which also display a developmental switch of glycine activity from depolarization to hyperpolarization (Wu et al., 1992; Reichling et al., 1994; Serafini et al., 1995; Singer and Berger, 2000), need to be investigated regarding their KCC2 expression to understand its nature in caudal brain regions.

Posttranslational modifications that activate an initially inactive form of the KCC2 protein were described in cultured hippocampal neurons (Kelsch et al., 2001). The activation involves a phosphorylation step via the action of insulin-like growth factor 1 and a protein tyrosine kinase, and it propels the switch of GABAergic responses. The authors concluded that the onset of transporter activity does not correlate with the amount of mRNA or with the mere presence of KCC2 protein. Immunohistochemical staining data from our group displayed an early diffuse pattern and later a crisply and densely outlined fashion (Balakrishnan et al., 2003), corroborating the activation upon phosphorylation and showing that such changes can also occur *in vivo*. The age-related integration of the KCC2 protein into the plasma membrane of LSO neurons per se does not necessarily imply the onset of function, since posttranslational modifications may well occur after the integration step (Balakrishnan et al., 2003). Nonetheless, the integration step is a necessity for functionality. In the rat hippocampus, a diffuse KCC2 immunolabeling and an association with membranes of transport vesicles was described at P0-P2 by electron microscopy, whereas at P4, most of the reaction products were observed in the plasma membrane (Gulyás et al., 2001). In these neurons, the change from

depolarizing to hyperpolarizing GABAergic activity occurs at the end of the first postnatal week (Cherubini et al., 1991), indicating that functionality is not merely determined by the incorporation of the protein into the plasma membrane.

In line with the above arguments, experiments performed with KCC2 *-/-* mice revealed that KCC2 renders hyperpolarization at older ages and plays no role in accumulating Cl⁻ at early ages (Fig. 4.1). Thus, KCC2 can be ruled out to operate in reverse and accumulate intracellular Cl⁻ under conditions of an elevated [K⁺]_o (Payne, 1997; Jarolimek et al., 1999; Kakazu et al., 2000). In summary, KCC2 is concluded to be a common Cl⁻ outward transporter for both the forebrain and the hindbrain (Rivera et al., 1999; Hübner et al., 2001; Balakrishnan et al., 2003).

4.3 NKCC1 is not involved in setting $E_{\text{Gly}} > V_{\text{rest}}$ in immature LSO neurons

In search of the inward Cl⁻ transporter, literature points to NKCC1 as the most favored candidate (for review, see Russell, 2000). Two different isoforms of NKCC namely, NKCC1, and NKCC2 have been identified. NKCC1 is found in nearly all cell types, whether epithelial or not, but NKCC2 is found exclusively in kidney. NKCC1 in CNS neurons catalyzes Cl⁻ uptake (Kaila, 1994; Haas and Forbush, 1998; Misgeld et al., 1986; Rohrbough and Spitzer, 1996; Plotkin et al., 1997; Clayton et al., 1998; Li et al., 2002). The cotransport process of NKCC1 is electroneutral, with a stoichiometry of 1Na⁺:1K⁺:2Cl⁻ (Russell, 1984; Alvarez-Leefmans et al., 1988) and sensitive to loop diuretics (Hannaert et al., 2002). Ion translocation by NKCC requires the simultaneous presence of all three ions (Na⁺, K⁺, and Cl⁻) at both sides of the membrane (Russell, 2000). The transporter can work in forward and backward mode; that is, net transport may occur into or out of the cells, the magnitude and direction of this transport being determined by the sum of the chemical gradients of the transported ions (Lytle et al., 1998).

In the present study, three different approaches were undertaken to investigate the role of NKCC1 in Cl^- accumulation in LSO neurons, namely RT-PCR analyses, pharmacological studies and experiments with NKCC1 $-/-$ mice. None of them led to the conclusion that NKCC1 is involved in setting the high $[\text{Cl}^-]_i$ during the depolarizing phase of glycine activity.

First, at P3, NKCC1 mRNA expression was missing in auditory brainstem slice and LSO neurons, as demonstrated by multiplex RT-PCR and single cell RT-PCR, respectively. These results contradict previous findings in the forebrain (Plotkin et al., 1997; Sun and Murali 1999), but are in accordance with observations from the spinal cord (Hübner et al., 2001). In E12.5 spinal cord, NKCC1 transcripts appeared to be concentrated and had almost disappeared by E18.5. Hence, the authors concluded that NKCC1 may not be the major transporter leading to an excitatory GABA response in the embryonic spinal cord (Hübner et al., 2001). In different forebrain regions, like hippocampus and cortex, the amount of NKCC1 mRNA expression is high during the early depolarizing phase and gradually declines thereafter, thereby rendering GABAergic activity depolarizing (Plotkin et al., 1997; Sun and Murali 1999). Moreover, in hippocampal pyramidal cells, there is a developmental shift in the NKCC1 localization from a predominantly somatic to a predominantly dendritic location at the end of the first postnatal week (Marty et al., 2002).

Second, pharmacological studies, with NKCC1-specific bumetanide treatment, had no effect on the $[\text{Cl}^-]_i$ of LSO neurons, whereas bumetanide induced a significant reduction of $[\text{Cl}^-]_i$ in hippocampal pyramidal neurons. The latter results are consistent with previous studies, demonstrating a functional role of NKCC1 in hippocampal neurons (Hara et al., 1992). Furosemide inhibits cation Cl^- cotransporters (Alvarez-Leefmans, 2001) and it has been demonstrated to induce a shift of E_{Gly} in the

negative direction and reasoned to be a block on net inward Cl^- transport that was assumed to be mediated by NKCC1 by Ehrlich et al., (1999). This could be a non-specific effect of the high concentration of furosemide (1 mM), as this concentration was shown to inhibit several processes (Lerma and Martin del Rio, 1992; Tosco et al., 1993; McConnell and Aronson, 1994). But current studies demonstrate a lack of NKCC1 expression during the depolarizing age in LSO neurons (Balakrishnan et al., 2003), therefore the effect of furosemide observed by Ehrlich et al., (1999) is concluded as a non-specific action of furosemide. The results demonstrating the absence of NKCC1 during the depolarizing period of glycine responses, drawn in the present study, contradict those described by Kakazu and coworkers (1999) in the LSO, who replaced external Na^+ to affect Na^+ -dependent transport and found a shift of E_{Gly} towards more negative values in four P3 neurons. Kakazu and coworkers (1999) reasoned that a Na^+ -dependent transporter (NKCC or NCC) regulates E_{Gly} . But in a recent paper, the same group demonstrates that there is no K^+ -dependent mechanism for Cl^- accumulation in P0 LSO neurons (Shibata et al., 2004), consistent with the conclusion of the present study that NKCC1 does not act as an inward transporter. This implies that neither KCC2 nor NKCC1 play a role in accumulating Cl^- in LSO neurons. Since neither one of the NKCC isoforms nor NCC appears to be present in the neonatal LSO (present study and Becker et al., 2003), it is possible that the effect of Na^+ replacement on E_{Gly} may be due to some other Na^+ -dependent mechanisms, involved in intracellular Cl^- regulation.

Third, the experiments with NKCC1 $-/-$ mice revealed a normal Cl^- homeostasis, like that observed in wild type mice, which leads me to conclude that NKCC1 plays no role in Cl^- accumulation in LSO neurons during the depolarizing age. However, this result contradicts the decrease in Cl^- accumulation observed in dorsal root ganglion

neurons of NKCC1 *-/-* mice (Sung et al., 2000). The difference may be due to a regional difference.

4.4 GAT1 and GLYT2 – a focus on their role on Cl⁻ accumulation

GAT1 and GLYT2 are known as electrogenic, Na⁺-dependent transporters of inhibitory amino acids rather than as Cl⁻ cotransporters (Jursky et al., 1994; Nelson, 1998). Apart from presynaptic and glial cell mediated uptake of synaptically released neurotransmitters, amino acid transporters play a dynamic role in synaptic activity. For example, inhibitory amino acid transporters control brain excitability by modulating the level of tonic inhibition in response to neuronal activity (Richerson and Wu, 2003). GAT1 is the predominant GABA transporter in the brain, exhibiting high expression levels in neocortex, hippocampus, cerebellum, basal ganglia, brainstem, spinal cord, olfactory bulb, and retina (Guastella et al., 1990; Nelson et al., 1990). It co-localizes with markers for GABAergic neurons, specifically along axons and presynaptic nerve terminals. Interestingly, GAT1 mRNA is expressed not only in GABAergic neurons, but also in non-GABAergic neurons and/or glial cells which are not involved in GABAergic neurotransmission (Yasumi et al., 1997; Fletcher et al., 2002).

Results from three different experiments focusing on GAT1, namely voltage treatment experiments, Na⁺ dependency experiments, and experiments with both a GAT1 agonist and antagonist, suggest its involvement in Cl⁻ homeostasis during the depolarizing phase of glycine responses. First, upon voltage treatment, P3 LSO neurons demonstrated accumulation or depletion of [Cl⁻]_i due to a prolonged hyperpolarization and depolarization stimulus, respectively. This indicates the involvement of an electrogenic mechanism in Cl⁻ regulation. Second, increasing

$[\text{Na}^+]_i$ reduced the accumulation of Cl^- in the LSO neurons, depicting the Na^+ dependency of the transport mechanism. Third, during the depolarizing period of glycine responses, a GAT1-specific antagonist (SKF 89967A) reduced the Cl^- accumulation, whereas a GAT1 agonist (nipecotic acid) increased it. Overall, I conclude that GAT1 is involved in Cl^- homeostasis of LSO neurons during the depolarizing period of glycine response. In line with these results, a recent finding that demonstrates the developmental switch from GABA to glycine release in single central synaptic terminals during the second postnatal week of the rat MNTB-LSO connection is reported (Nabekura et al., 2004). Such a shift was also demonstrated in gerbils (Kotak et al., 1998). On the other side, the presence of neurotransmitter transporters in the presynaptic side of the neurons was highlighted in several studies (Itouji et al., 1996; Jursky and Nelson 1996; Chiu et al., 2002). Only very few studies discuss their postsynaptic localization (Snow et al., 1992; Hu et al., 1999). To address the postsynaptic localization of neurotransmitter transporters, immuno-gold electron microscopic studies are needed.

Like GAT1, GLYT2 is also a potential candidate that can accumulate chloride in LSO neurons. This neuronal isoform of the glycine transporter has been shown to be expressed in the LSO during development and it was speculated that GLYT2 participates in the process of early synapse maturation (Friauf et al, 1999). In the present study I investigated the role of glycine transporter in chloride homeostasis in GLYT2 $-/-$ mice. The results show that besides GAT1, GLYT2 also plays a role in chloride accumulation (Fig. 4.1). In order to confirm that the effect observed with GLYT2 $-/-$ mice is due to a direct effect of the lack of GLYT2, pharmacological experiment employing highly specific drugs against GLYT2 are needed.

The brain-specific anion exchanger (AE3) is another possible candidate for Cl^- accumulation. It is expressed in LSO neurons (Becker et al., 2003). AE3 is an

antiporter, which exchanges one Cl^- in and one HCO_3^- out (Kopito et al., 1989). In the present study, it was not considered as a possible inward Cl^- transporter in neonatal LSO neurons, because glycine-induced depolarizations were demonstrated in the absence of HCO_3^- buffer, that is in the presence of HEPES-buffered extracellular solution. Therefore, in case of LSO neurons, AE3 has no role in setting a high $[\text{Cl}^-]_i$.

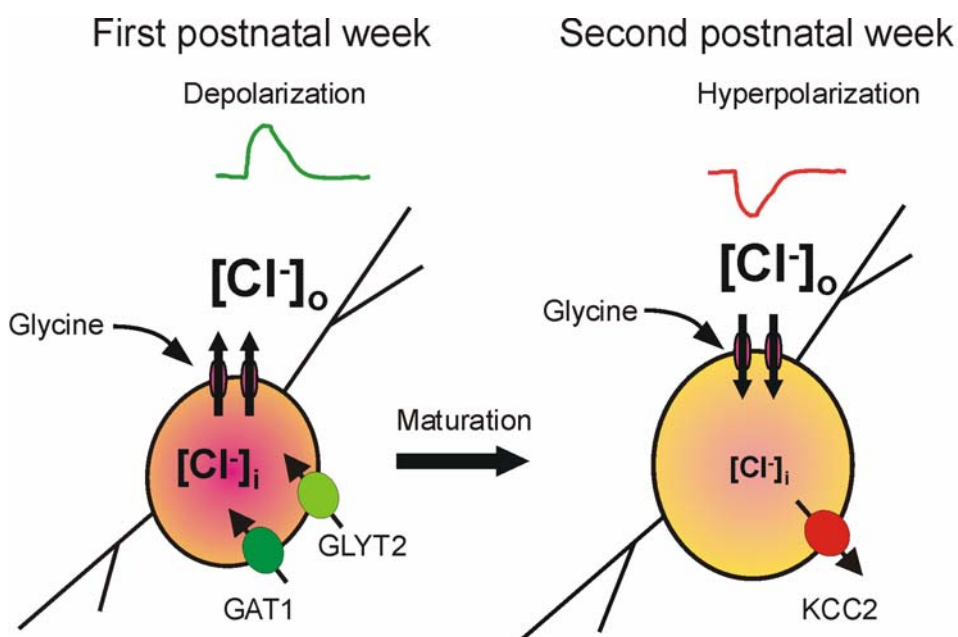


Fig. 4.1: Transporters involved in chloride regulation during LSO development. During the first postnatal week, GAT1 and GLYT2 are transporting Cl^- in to the neurons, maintaining a high $[\text{Cl}^-]_i$. From the second postnatal week, KCC2 is transporting Cl^- out of the neurons, maintaining a low $[\text{Cl}^-]_i$.

4.5 Inhibitory circuits in SOC develop through excitation

The MNTB-LSO projection develops through excitatory GABAergic and glycinergic synapses, rather than relying on inhibitory interactions to drive the development and refinement. The time course of anatomical refinement follows the development of inhibition in the MNTB-LSO projection (Kim and Kandler, 2003). As shown for the development of inhibitory neurons in other CNS regions, such as cortex (Owens and

Kriegstein, 2002), in the LSO, E_{Gly} is more positive than V_{rest} which results in depolarization during the first postnatal week (Ehrlich et al., 1999). The early appearance of GABA release mechanisms as well as the early appearance of spontaneous GABA- and glycine- mediated synaptic events well before development of synaptic inhibition supports the notion that GABA and glycine have a functional role in nervous system development. GABA even may have an influence on the key processes of proliferation (Fizman et al., 1999), migration (Behar et al., 1996; Barker et al., 1998) and differentiation (Barbin et al., 1993; Davis et al., 2000; Tapia et al., 2001; Varja et al., 2002). However, recent reports contradict the role of GABA in trophic support, i.e., inhibitory synapses mature without GABAergic neurotransmission (Titz et al., 2003; Ludwig et al., 2003).

During early development, glycinergic and GABAergic inputs depolarize the postsynaptic cell (Ben-Ari, 2002). Depolarization results in an increase of the postsynaptic Ca^{2+} concentration through voltage-dependent calcium channels (VDCC) and NMDA channels (Yuste and Katz, 1991; Lin et al., 1994; LoTurco et al., 1995; Takebayashi et al., 1996; Leinekugel et al., 1997; Obrietan and van den Pol, 1997; Flint et al., 1998) and can also result in action potentials (Kullmann et al., 2002). Calcium entry via VDCC has been shown to upregulate brain-derived neurotrophic factor (BDNF) expression in immature hippocampal neurons (Berninger et al., 1995). BDNF is involved in the maturation of inhibitory synapses via determining the functional expression of KCC2 (Aguado et al., 2003). Thus, GABA may act as a trophic factor in early development by depolarizing cells, activating VDCCs, and regulating gene expression through the activation of Ca^{2+} -dependent second messenger pathways (Ben-Ari et al., 1994; Lauder et al., 1998; Ganguly et al., 2001; Kriegstein and Owens, 2001).

4.6 Possible induction factors underlying the developmental shift in E_{Gly}

The $[Cl^-]_i$ determines the polarity of glycinergic/GABAergic responses in LSO neurons (Ehrlich et al., 1999). From the present study and several others (Delpire 2000; Hübner et al., 2001; Woo et al., 2002), it is clear that the crucial maintenance of Cl^- homeostasis is achieved by functional Cl^- cotransporters. Recent studies support the idea that the maturation of inhibitory synapses follows several steps, triggering e.g. posttranslational modifications of inward or outward transporters, resulting in changes of the phosphorylation (Bize et al., 2000) and/or glycosylation (Hiki et al., 1999) status. What triggers the change in the functional expression of the transporters that regulate the Cl^- homeostasis? In the present thesis, LSO neurons treated with calyculin A demonstrated a decline in the $[Cl^-]_i$ which indicates a possible role of phosphorylation in the process of inhibitory synapse maturation. Recent studies pinpoint the involvement of BDNF action via TrkB receptors with the functional expression of KCC2 (Rivera et al., 2002; Aguado et al., 2003) or inhibitory neurotransmission (Frerking et al., 1998). Moreover, an activity- and Ca^{2+} -dependent modulation of TrkB was demonstrated in hippocampal neurons (Du et al., 2003).

In the present study, the role of thyroid hormone in the maturation of inhibitory synapses was tested. It was found that hypothyroid rats display an abnormality in the shift from depolarization to hyperpolarization. The shift did not occur during the usual time frame, i.e., between P6-8. It is well documented that thyroid hormone plays a critical role in brain development and plasticity (Chan and Kilby, 2000; Anderson et al., 2003; Vara et al., 2003). Neurotrophins like BDNF and neurotrophin 3 (NT3) are regulated by thyroid hormone (Koibuchi et al., 1999; 2001). Several studies hint that there is a correlation between thyroid hormone deficiency and deafness (Forrest et al., 1996; 2002; Flamant and Samarut, 2003). For example,

hypothyroidism before hearing onset is reported to cause irreversible damage to auditory systems, i.e., within a critical period between the onset of fetal thyroid gland function and the onset of hearing at P12, any postponement in the rise of thyroid hormone-plasma levels, as can be brought about by treating lactating mothers with methimazole, leads to permanent hearing defects of the adult offsprings (Knipper et al., 2000). This leads to the hypothesis that thyroid hormone can also influence Cl^- homeostasis by which it can play a role in the maturation of inhibitory synapses. Indeed, my results imply a role of thyroid hormone in the development of inhibitory synapses in the auditory brainstem, i.e., it may act as a possible induction factor in the developmental switch of the polarity of glycine/GABA responses.

4.7 Outlook:

The present study leaves several open questions:

1. Through what cascade does calcium influx support the maturation of inhibitory synapses?
2. What factors lead to the activation of KCC2 function at the end of the first postnatal week?
3. Does chloride regulation guide the refinement of inhibitory synapses?
4. Is the somatic $[\text{Cl}^-]_i$ different from the dendritic $[\text{Cl}^-]_i$?
5. Is there any cooperation between the molecular mechanisms that govern the maturation of inhibitory and excitatory synapses?

Addressing these questions may shed further light on our understanding of the function and maturation of inhibitory synapses.

5 SUMMARY

Compared to our knowledge of the development of neuronal excitation, little is known about the development of *inhibitory* circuits. Recent studies showed that inhibitory circuits develop in a way similar to that of excitatory circuits. One such similarity is the development of inhibitory circuits through a transient period of excitation. The neurotransmission from the medial nucleus of the trapezoid body (MNTB) to the lateral superior olive (LSO) starts at embryonic day (E) 18 and is depolarizing until the end of the first postnatal week, after which it becomes hyperpolarizing. The depolarizing effect of glycine is due to a high intracellular chloride concentration ($[Cl^-]_i$), whereas hyperpolarization is due to a low $[Cl^-]_i$. Active regulation of $[Cl^-]_i$ is achieved by cation Cl^- cotransporters, such as the Na^+ -, K^+ -dependent Cl^- cotransporter (NKCC1; a Cl^- inward transporter) and the K^+ -dependent Cl^- cotransporter (KCC2; a Cl^- outward transporter).

Here, I used the inhibitory MNTB-LSO projection as a model system to unravel some mechanisms governing the development of inhibitory synapses. The focus was laid on the molecular mechanism behind the Cl^- homeostasis in LSO neurons. To assess whether the shift in glycine action correlates with changes in the molecular repertoire of Cl^- cotransporters, I combined gramicidin perforated patch-clamp recordings and single cell RT-PCR in LSO neurons of acute brainstem slices from postnatal day (P)3 and P12 rats. The impermeability of gramicidin pores for anions allows recordings of glycine-induced currents under native $[Cl^-]_i$. The reversal potential of glycine (E_{Gly}), which is equivalent to the reversal potential of Cl^- (E_{Cl}), was determined and thereby $[Cl^-]_i$ was calculated. In P3 and P12 neurons, the $[Cl^-]_i$ amounted to 44 ± 7 mM and 8 ± 2 mM, respectively. If Cl^- were passively

distributed, then E_{Gly} would equal the resting membrane potential (V_{rest}). With $V_{\text{rest}} \approx -60$ mV, $[\text{Cl}^-]_i$ would then approximately be 13 mM. The deviating values are indicative of an active Cl^- inward transport at P3, and an active Cl^- outward transport at P12. Surprisingly, the expression analysis resulted in a paradox. The mRNA of the Cl^- inward transporter NKCC1 was not observed during the early depolarizing phase but seen during hyperpolarizing phase. The mRNA of the Cl^- outward transporter KCC2 appeared throughout development.

To unravel the function of KCC2, experiments were performed with KCC2 knockout mice (-/-), and results were compared with those from wild type mice (+/+). At P3, $[\text{Cl}^-]_i$ of KCC2 +/+ and -/- were not significantly different, confirming no role of KCC2 in chloride accumulation during the depolarizing phase. In contrast, at P12 a significant difference in $[\text{Cl}^-]_i$ was observed between KCC2 +/+ and -/- KCC2 -/- mice displayed depolarizations at P12 due to the high $[\text{Cl}^-]_i$, and the $[\text{Cl}^-]_i$ at P12 was indistinguishable from that in P3 KCC2 +/+. This demonstrates that the genetic-knockout leaves the LSO neurons in an immature state concerning Cl^- regulation. Taken together, I conclude that KCC2 renders glycine hyperpolarizing in LSO neurons at P12.

To focus on the role of NKCC1, LSO neurons were challenged with bumetanide, a specific NKCC1 blocker at low concentration. Both at P3 and at P12, LSO neurons displayed no change in $[\text{Cl}^-]_i$ upon bumetanide treatment (30 μM), demonstrating that NKCC1 has no function. In contrast, in P3 hippocampal pyramidal neurons, E_{GABA} showed a negative shift at this concentration, demonstrating that NKCC1 is a Cl^- inward transporter in these neurons. When P12 LSO neurons were challenged with a higher bumetanide concentration (100 μM), they displayed an increase in $[\text{Cl}^-]_i$,

most probably due to the blockade of KCC2 function. To confirm the negative pharmacological results on the role of NKCC1, NKCC1 $-/-$ mice were compared with $+/+$ mice for any change in the $[Cl^-]_i$. In accordance with the pharmacological results, no significant difference was observed between the two groups. Therefore, it is clear that NKCC1 plays no role in establishing a high $[Cl^-]_i$ in young LSO neurons.

In search for alternative transporter candidates that elevate the $[Cl^-]_i$ in immature LSO neurons, several experiments were performed. To check whether a Na^+ -dependent chloride regulatory mechanism exists, experiments employing different $[Na^+]_i$ were performed. In P3 LSO neurons, an effect of $[Na^+]_i$ on $[Cl^-]_i$ was observed: increasing $[Na^+]_i$ led to a decline in $[Cl^-]_i$. Next, voltage dependency of Cl^- regulation was analyzed by subjecting LSO neurons to different voltage potentials ($-40\text{ mV} > V_{rest}$; $-120\text{ mV} < V_{rest}$). Interestingly, voltage-dependent Cl^- regulation was observed at P3, yet not at P12: the positive voltage treatment decreased the $[Cl^-]_i$, whereas the negative voltage treatment increased the $[Cl^-]_i$. The two criteria described above (Na^+ dependency and voltage dependency) are fulfilled by amino acid transporters which play a major role in the reuptake of amino acids (e.g. glycine, GABA, glutamate) from the synaptic cleft. Moreover, amino acid transporters are Cl^- cotransporters. The focus was laid on GABA transporters, since early LSO neurons were reported to receive mainly GABAergic inputs aside from their glycinergic inputs. As a predominantly neuronal expression was reported for the GABA transporter 1 (GAT1), I concentrated on this isoform. Addressing GAT1, pharmacological studies with the specific inhibitor SKF 89976A were done. SKF 89976A significantly reduced the Cl^- inward transport in LSO neurons at P3, but not at P12. In line with this, nipecotic acid, an activator of GAT1, promoted Cl^- uptake, which confirms the role of GAT1 in neonatal LSO neurons. In a further set of experiments, the involvement of

the glycine transporter isoform 2 (GLYT2) in Cl^- regulation was analyzed. Experiments with GLYT2 $-/-$ mice revealed a significant role of this transporter in chloride regulation. These results led to the conclusion that both GAT1 and GLYT2 play important roles in the uptake of chloride ions during the early depolarizing phase in LSO neurons.

After having identified the inward and outward chloride transporters, the trigger for the age-dependent shift in E_{Gly} was analyzed. Reports on the correlation of the phosphorylation status and function of Cl^- transporters, provoked me to study such a possible mechanism. P3 LSO neurons were treated with the protein phosphatase inhibitor calyculin A to modulate the phosphorylation status. $[\text{Cl}^-]_i$ significantly declined upon calyculin A treatment, revealing a possible role of phosphorylation mechanisms behind the Cl^- regulation in LSO neurons. Furthermore, the role of thyroid hormones, well known to play a pivotal role in the development of the auditory system, was studied with hypothyroid rats. In contrast to normal rats, hypothyroid rats (P5-12) showed no shift in E_{Gly} values in the expected time window (P6-8).

In conclusion, this study has accumulated considerable evidence for the nature of the transporters involved in chloride homeostasis in the auditory brainstem. It also sheds some light on the molecular mechanisms underlying the maturation of inhibitory synapses.

6 BIBLIOGRAPHY

- Aguado F, Carmona MA, Pozas E, Aguiló A, Martínez-Guijarro, FJ, Alcantara S, Borrell V, Yuste R, Ibañez CF, Soriano E (2003) BDNF regulates spontaneous correlated activity at early developmental stages by increasing synaptogenesis and expression of the K⁺/Cl⁻ co-transporter KCC2. *Development* 130: 1267-1280.
- Alvarez-Leefmans FJ, Gamino SM, Giraldez F, Nogueron I (1988) Intracellular chloride regulation in amphibian dorsal root ganglion neurones studied with ion-selective microelectrodes. *J Physiol (Lond)* 406: 225-246.
- Alvarez-Leefmans FJ (2001) Intracellular chloride regulation. In: *Cell physiology sourcebook: A molecular approach* (Sperelakis N, ed), pp 301-318. San Diego: Academic Press.
- Anderson GW, Schoonover CM, Jones SA (2003) Control of thyroid hormone action in the developing rat brain. *Thyroid* 13: 1039-1056.
- Backus KH, Deitmer JW, Friauf E (1998) Glycine-activated currents are changed by coincident membrane depolarization in developing rat auditory brainstem neurones. *J Physiol (Lond)* 507: 783-794.
- Balakrishnan V, Becker M, Lohrke S, Nothwang HG, Guresir E, Friauf E (2003) Expression and function of chloride transporters during development of inhibitory neurotransmission in the auditory brainstem. *J Neurosci* 23: 4134-4145.
- Barbin G, Pollard H, Gaiarsa JL, Ben Ari Y (1993) Involvement of GABA_A receptors in the outgrowth of cultured hippocampal neurons. *Neurosci Lett* 152: 150-154.
- Barker JL, Behar T, Li YX, Liu QY, Ma W, Maric D, Maric I, Schaffner AE, Serafini R, Smith SV, Somogyi R, Vautrin JY, Wen XL, Xian H (1998) GABAergic cells and signals in CNS development. *Perspect Dev Neurobiol* 5: 305-322.
- Barmack NH, Guo H, Kim HJ, Qian H, Qian Z (1999) Neuronally modulated transcription of a glycine transporter in rat dorsal cochlear nucleus and nucleus of the medial trapezoid body. *J Comp Neurol* 415: 175-188.
- Basavappa S, Ellory JC (1996) The role of swelling-induced anion channels during neuronal volume regulation. *Mol Neurobiol* 13: 137-153.
- Becker M, Nothwang HG, Friauf E (2003) Differential expression pattern of chloride transporters NCC, NKCC2, KCC1, KCC3, KCC4, and AE3 in the developing rat auditory brainstem. *Cell Tissue Res* 312: 155-165.
- Behar TN, Li YX, Tran HT, Ma W, Dunlap V, Scott C, Barker JL (1996) GABA stimulates chemotaxis and chemokinesis of embryonic cortical neurons via calcium-dependent mechanisms. *J Neurosci* 16: 1808-1818.

-
- Ben Ari Y, Cherubini E, Corradetti R, Gaiarsa JL (1989) Giant synaptic potentials in immature rat CA3 hippocampal neurones. *J Physiol (Lond)* 416: 303-325.
- Ben Ari Y, Tseeb V, Ragozzino D, Khazipov R, Gaiarsa JL (1994) gamma-aminobutyric acid (GABA): a fast excitatory transmitter which may regulate the development of hippocampal neurones in early postnatal life. *Prog Brain Res* 102: 261-273.
- Ben Ari Y (2002) Excitatory actions of gaba during development: the nature of the nurture. *Nat Rev Neurosci* 3: 728-739.
- Bernal J, Guadano-Ferraz A, Morte B (2003) Perspectives in the study of thyroid hormone action on brain development and function. *Thyroid* 13: 1005-1012.
- Berninger B, Marty S, Zafra F, da Penha BM, Thoenen H, Lindholm D (1995) GABAergic stimulation switches from enhancing to repressing BDNF expression in rat hippocampal neurons during maturation in vitro. *Development* 121: 2327-2335.
- Bernstein EM, Quick MW (1999) Regulation of gamma-aminobutyric acid (GABA) transporters by extracellular GABA. *J Biol Chem* 274: 889-895.
- Billups D, Attwell D (2002) Control of intracellular chloride concentration and GABA response polarity in rat retinal ON bipolar cells. *J Physiol (Lond)* 545: 183-198.
- Bize I, Guvenc B, Buchbinder G, Brugnara C (2000) Stimulation of human erythrocyte K-Cl cotransport and protein phosphatase type 2A by n-ethylmaleimide: role of intracellular Mg²⁺. *J Membr Biol* 177: 159-168.
- Brand A, Behrend O, Marquardt T, Mcalpine D, Grothe B (2002) Precise inhibition is essential for microsecond interaural time difference coding. *Nature* 417: 543-547.
- Cabantchik ZI, Greger R (1992) Chemical probes for anion transporters of mammalian cell membranes. *Am J Physiol* 262: 803-827.
- Cant NB (1991) Projections to the lateral and medial superior olivary nuclei from the spherical and globular bushy cells of the anteroventral cochlear nucleus. In: *Neurobiology of Hearing: The Central Auditory System* (Altschuler RA, Bobbin RP, Clopton BM, Hoffman DW, eds), pp 99-119. New York: Raven Press, Ltd.
- Cant NB, Casseday JH (1986) Projections from the anteroventral cochlear nucleus to the lateral and medial superior olivary nuclei. *J Comp Neurol* 247: 457-476.
- Chan S, Kilby MD (2000) Thyroid hormone and central nervous system development. *J Endocrinol* 165: 1-8.
- Chen G, Trombley PQ, van den Pol AN (1996) Excitatory actions of GABA in developing rat hypothalamic neurones. *J Physiol (Lond)* 494: 451-464.

- Cherubini E, Rovira C, Gaiarsa JL, Corradetti R, Ben-Ari Y (1990) GABA mediated excitation in immature rat CA3 hippocampal neurons. *Int J Dev Neurosci* 8: 481-490.
- Cherubini E, Gaiarsa JL, Ben-Ari Y (1991) GABA: an excitatory transmitter in early postnatal life. *Trends Neurosci* 14: 515-519.
- Chiu CS, Jensen K, Sokolova I, Wang D, Li M, Deshpande P, Davidson N, Mody I, Quick MW, Quake SR, Lester HA (2002) Number, density, and surface/cytoplasmic distribution of GABA transporters at presynaptic structures of knock-in mice carrying GABA transporter subtype 1-green fluorescent protein fusions. *J Neurosci* 22: 10251-10266.
- Clayton GH, Owens GC, Wolf JS, Smith RL (1998) Ontogeny of cation-Cl⁻ cotransporter expression in rat neocortex. *Dev Brain Res* 109: 281-292.
- Cohen P (2000) The regulation of protein function by multisite phosphorylation - a 25 year update. *Trends Biochem Sci* 25: 596-601.
- Davis AM, Grattan DR, McCarthy MM (2000) Decreasing GAD neonatally attenuates steroid-induced sexual differentiation of the rat brain. *Behav Neurosci* 114: 923-933.
- DeFazio RA, Keros S, Quick MW, Hablitz JJ. (2000) Potassium-coupled chloride cotransport controls intracellular chloride in rat neocortical pyramidal neurons. *J Neurosci* 20: 8069-8076.
- Delpire E (2000) Cation-chloride cotransporters in neuronal communication. *News Physiol Sci* 15: 309-312.
- Du J, Feng L, Zaitsev E, Je HS, Liu XW, Lu B (2003) Regulation of TrkB receptor tyrosine kinase and its internalization by neuronal activity and Ca²⁺ influx. *J Cell Biol* 163: 385-395.
- Ebihara S, Shirato K, Harata N, Akaike N (1995) Gramicidin-perforated patch recording: GABA response in mammalian neurones with intact intracellular chloride. *J Physiol (Lond)* 484: 77-86.
- Ehrlich I, Löhrke S, Friauf E (1999) Shift from depolarizing to hyperpolarizing glycine action in rat auditory neurons is due to age-dependent Cl⁻ regulation. *J Physiol (Lond)* 520: 121-137.
- Esteban JA, Shi SH, Wilson C, Nuriya M, Haganir RL, Malinow R (2003) PKA phosphorylation of AMPA receptor subunits controls synaptic trafficking underlying plasticity. *Nat Neurosci* 6: 136-143.
- Fizman ML, Borodinsky LN, Neale JH (1999) GABA induces proliferation of immature cerebellar granule cells grown in vitro. *Dev Brain Res* 115: 1-8.
- Flamant F, Samarut J (2003) Thyroid hormone receptors: lessons from knockout and knock-in mutant mice. *Trends Endocrinol Metab* 14: 85-90.

-
- Flatman PW, Adragna NC, Lauf PK (1996) Role of protein kinases in regulating sheep erythrocyte K-Cl cotransport. *Am J Physiol* 271: C255-C263.
- Fletcher EL, Clark MJ, Furness JB (2002) Neuronal and glial localization of GABA transporter immunoreactivity in the myenteric plexus. *Cell Tissue Res* 308: 339-346.
- Flint AC, Liu X, Kriegstein AR (1998) Nonsynaptic glycine receptor activation during early neocortical development. *Neuron* 20: 43-53.
- Forrest D, Erway LC, Ng L, Altschuler R, Curran T (1996) Thyroid hormone receptor beta is essential for development of auditory function. *Nat Genet* 13: 354-357.
- Forrest D, Reh TA, Rusch A (2002) Neurodevelopmental control by thyroid hormone receptors. *Curr Opin Neurobiol* 12: 49-56.
- Frahm C, Engel D, Draguhn A (2001) Efficacy of background GABA uptake in rat hippocampal slices. *Neuroreport* 12: 1593-1596.
- Frerking M, Malenka RC, Nicoll RA (1998) Brain-derived neurotrophic factor (BDNF) modulates inhibitory, but not excitatory, transmission in the CA1 region of the hippocampus. *J Neurophysiol* 80: 3383-3386.
- Friauf E, Ostwald J (1988) Divergent projections of physiologically characterized rat ventral cochlear nucleus neurons as shown by intraaxonal injection of horseradish peroxidase. *Exp Brain Res* 73: 263-284.
- Friauf E, Aragón C, Löhcke S, Westenfelder B, Zafra F (1999) Developmental expression of the glycine transporter GLYT2 in the auditory system of rats suggests involvement in synapse maturation. *J Comp Neurol* 412: 17-37.
- Friauf E, Lohmann C (1999) Development of auditory brainstem circuitry: activity-dependent and activity-independent processes. *Cell Tissue Res* 297: 187-195.
- Ganguly K, Schinder AF, Wong ST, and Poo M-m (2001) GABA itself promotes the developmental switch of neuronal GABAergic responses from excitation to inhibition. *Cell* 105: 521-532.
- Geiger JR, Melcher T, Koh DS, Sakmann B, Seeburg PH, Jonas P, Monyer H (1995) Relative abundance of subunit mRNAs determines gating and Ca²⁺ permeability of AMPA receptors in principal neurons and interneurons in rat CNS. *Neuron* 15: 193-204.
- Gerencser GA, Zhang J (2003) Existence and nature of the chloride pump. *Biochim Biophys Acta* 1618: 133-139.
- Giordano T, Pan JB, Casuto D, Watanabe S, Arneric SP (1992) Thyroid hormone regulation of NGF, NT-3 and BDNF RNA in the adult rat brain. *Mol Brain Res* 16: 239-245.

-
- Goldberg JM, Brown PB (1969) Response of binaural neurons of dog superior olivary complex to dichotic tonal stimuli: some physiological mechanisms of sound localization. *J Neurophysiol* 32: 613-636.
- Gomez J, Ohno K, Hulsmann S, Armsen W, Eulenburg V, Richter DW, Laube B, Betz H (2003) Deletion of the mouse glycine transporter 2 results in a hyperekplexia phenotype and postnatal lethality. *Neuron* 40: 797-806.
- Grothe B, Park TJ (1998) Sensitivity to interaural time differences in the medial superior olive of a small mammal, the Mexican free-tailed bat. *J Neurosci* 18: 6608-6622.
- Guastella J, Nelson N, Nelson H, Czyzyk L, Keynan S, Miedel M, Davidson N, Lester HA, Kanner BI (1990) Cloning and expression of a rat brain GABA transporter. *Science* 249: 1303-1306.
- Gulyás AI, Sík A, Payne JA, Kaila K, Freund TF (2001) The KCl cotransporter, KCC2, is highly expressed in the vicinity of excitatory synapses in the rat hippocampus. *Eur J Neurosci* 13: 2205-2217.
- Haas M, Forbush B (1998) The Na-K-Cl cotransporters. *J Bioenerg Biomembr* 30: 161-172.
- Hannaert P, Alvarez-Guerra M, Pirot D, Nazaret C, Garay RP (2002) Rat NKCC2/NKCC1 cotransporter selectivity for loop diuretic drugs. *Naunyn Schmied Arch Pharmacol* 365: 193-199.
- Hara M, Inoue M, Yasakura T, Ohnishi S, Mikami Y, Inagaki C (1992) Uneven distribution of intracellular Cl⁻ in rat hippocampal neurons. *Neurosci Lett* 143: 135-138.
- Helfert RH, Snead CR, Altschuler RA (1991) The Ascending Auditory Pathways. In: *Neurobiology of Hearing: The Central Auditory System* (Altschuler RA, Bobbin RP, Clopton BM, Hoffman DW, eds), pp 1-25. New York: Raven Press, Ltd.
- Hiki K, D'Andrea RJ, Furze J, Crawford J, Woollatt E, Sutherland GR, Vadas MA, Gamble JR (1999) Cloning, characterization, and chromosomal location of a novel human K⁺-Cl⁻ cotransporter. *J Biol Chem* 274: 10661-10667.
- Hoffmann EK (1986) Anion transport systems in the plasma membrane of vertebrate cells. *Biochim Biophys Acta* 864: 1-31.
- Hu M, Bruun A, Ehinger B (1999) Expression of GABA transporter subtypes (GAT1, GAT3) in the adult rabbit retina. *Acta Ophthalmologica Scandinavica* 77: 255-260.
- Huang BO, Redburn DA (1996) GABA-induced increases in [Ca²⁺]_i in retinal neurons of postnatal rabbits. *Vis Neurosci* 13: 441-447.
- Huang EJ, Reichardt LF (2003) Trk receptors: roles in neuronal signal transduction. *Annu Rev Biochem* 72: 609-642.

-
- Hübner CA, Stein V, Hermans-Borgmeyer I, Meyer T, Ballanyi K, Jentsch TJ (2001) Disruption of KCC2 reveals an essential role of K-Cl cotransport already in early synaptic inhibition. *Neuron* 30: 515-524.
- Irvine RF (1986) Calcium transients: mobilization of intracellular Ca^{2+} . *Br Med Bull* 42: 369-374.
- Irving R, Harrison JM (1967) The superior olivary complex and audition: a comparative study. *J Comp Neurol* 130: 77-86.
- Isenring P, Jacoby SC, Payne JA, Forbush B (1998) Comparison of Na-K-Cl cotransporters - NKCC1, NKCC2, and the HEK cell Na-K-Cl cotransporter. *J Biol Chem* 273: 11295-11301.
- Ishihara H, Ozaki H, Sato K, Hori M, Karaki H, Watabe S, Kato Y, Fusetani N, Hashimoto K, Uemura D (1989) Calcium-independent activation of contractile apparatus in smooth muscle by calyculin-A. *J Pharmacol Exp Ther* 250: 388-396.
- Itouji A, Sakai N, Tanaka C, Saito N (1996) Neuronal and glial localization of two GABA transporters (GAT1 and GAT3) in the rat cerebellum. *Mol Brain Res* 37: 309-316.
- Jang IS, Jeong HJ, Akaike N (2001) Contribution of the Na-K-Cl cotransporter on GABA(A) receptor-mediated presynaptic depolarization in excitatory nerve terminals. *J Neurosci* 21: 5962-5972.
- Janigro D, Schwartzkroin PA (1988) Effects of GABA and baclofen on pyramidal cells in the developing rabbit hippocampus: an '*in vitro*' study. *Brain Res* 469: 171-184.
- Jarolimek W, Lewen A, Misgeld U (1999) A furosemide-sensitive K^+ - Cl^- cotransporter counteracts intracellular Cl^- accumulation and depletion in cultured rat midbrain neurons. *J Neurosci* 19: 4695-4704.
- Jensen K, Chiu CS, Sokolova I, Lester HA, Mody I (2003) GABA transporter-1 (GAT1)-deficient mice: differential tonic activation of GABAA versus GABAB receptors in the hippocampus. *J Neurophysiol* 90: 2690-2701.
- Jentsch TJ, Gunther W (1997) Chloride channels: An emerging molecular picture. *Bioessays* 19: 117-126.
- Jursky F, Tamura S, Tamura A, Mandiyan S, Nelson H, Nelson N (1994) Structure, function and brain localization of neurotransmitter transporters. *J Exp Biol* 196:283-295.
- Jursky F, Nelson N (1996) Developmental expression of GABA transporters GAT1 and GAT4 suggests involvement in brain maturation. *J Neurochem* 67: 857-867.
- Kaila K (1994) Ionic basis of GABA_A receptor channel function in the nervous system. *Prog Neurobiol* 42: 489-537.

-
- Kakazu Y, Akaike N, Komiyama S, Nabekura J (1999) Regulation of intracellular chloride by cotransporters in developing lateral superior olive neurons. *J Neurosci* 19: 2843-2851.
- Kakazu Y, Uchida S, Nakagawa H, Akaike N, Nabekura J (2000) Reversibility and cation selectivity of the K^+ - Cl^- cotransport in rat central neurons. *J Neurophysiol* 84: 281-288.
- Kandler K, Friauf E (1995) Development of glycinergic and glutamatergic synaptic transmission in the auditory brainstem of perinatal rats. *J Neurosci* 15: 6890- 6904.
- Kandler K, Kullmann PHM, Ene FA, Kim G (2002) Excitatory action of an immature glycinergic/GABAergic sound localization pathway. *Physiol Behav* 77: 583-587.
- Kanner BI (1994) Sodium-coupled neurotransmitter transport: structure, function and regulation. *J Exp Biol* 196: 237-249.
- Kavanaugh MP, Arriza JL, North RA, Amara SG (1992) Electrogenic uptake of gamma-aminobutyric acid by a cloned transporter expressed in *Xenopus* oocytes. *J Biol Chem* 267: 22007-22009.
- Kelsch W, Hormuzdi S, Straube E, Lewen A, Monyer H, Misgeld U (2001) Insulin-like growth factor 1 and a cytosolic tyrosine kinase activate chloride outward transport during maturation of hippocampal neurons. *J Neurosci* 21: 8339-8347.
- Kim G, Kandler K (2003) Elimination and strengthening of glycinergic/GABAergic connections during tonotopic map formation. *Nat Neurosci* 6: 282-290.
- King SM, Tunnick G (1990) Na^+ - and Cl^- -dependent [3H]GABA binding to catfish brain particles. *Biochem Int* 20: 821-831.
- Knipper M, Zinn C, Maier H, Praetorius M, Rohbock K, Kopschall I, Zimmermann U (2000) Thyroid hormone deficiency before the onset of hearing causes irreversible damage to peripheral and central auditory systems. *J Neurophysiol* 83: 3101-3112.
- Koibuchi N, Fukuda H, Chin WW (1999) Promoter-specific regulation of the brain-derived neurotrophic factor gene by thyroid hormone in the developing rat cerebellum. *Endocrinology* 140: 3955-3961.
- Koibuchi N, Yamaoka S, Chin WW (2001) Effect of altered thyroid status on neurotrophin gene expression during postnatal development of the mouse cerebellum. *Thyroid* 11: 205-210.
- Konig S, Moura N, V (2002) Thyroid hormone actions on neural cells. *Cell Mol Neurobiol* 22: 517-544.
- Kopito RR, Lee BS, Simmons DS, Lindsey AE, Morgans CW, Schneider K (1989) Regulation of intracellular pH by a neuronal homolog of the erythrocyte anion exchanger. *Cell* 59: 927-937.

- Kotak VC, Korada S, Schwartz IR, Sanes DH (1998) A developmental shift from GABAergic to glycinergic transmission in the central auditory system. *J Neurosci* 18: 4646-4655.
- Kriegstein AR, Owens DF (2001) GABA may act as a self-limiting trophic factor at developing synapses. *Sci STKE* 2001: E1.
- Kullmann PH, Kandler K (2001) Glycinergic/GABAergic synapses in the lateral superior olive are excitatory in neonatal C57Bl/6J mice. *Brain Res Dev Brain Res* 131: 143-147.
- Kullmann PHM, Ene FA, Kandler K (2002) Glycinergic and GABAergic calcium responses in the developing lateral superior olive. *Eur J Neurosci* 15: 1093-1104.
- Kyrozis A, Reichling DB (1995) Perforated-patch recording with gramicidin avoids artifactual changes in intracellular chloride concentration. *J Neurosci Methods* 57: 27-35.
- Lauder JM, Liu J, Devaud L, Morrow AL (1998) GABA as a trophic factor for developing monoamine neurons. *Perspect Dev Neurobiol* 5: 247-259.
- Lauf PK (1984) Thiol-dependent passive K/Cl transport in sheep red cells: IV. Furosemide inhibition as a function of external Rb^+ , Na^+ , and Cl^- . *J Membr Biol* 77: 57-62.
- Leinekugel X, Tseeb V, Ben Ari Y, Bregestovski P (1995) Synaptic GABA_A activation induces Ca^{2+} rise in pyramidal cells and interneurons from rat neonatal hippocampal slices. *J Physiol (Lond)* 487: 319-329.
- Lerma J, Martin dR (1992) Chloride transport blockers prevent N-methyl-D-aspartate receptor-channel complex activation. *Mol Pharmacol* 41: 217-222.
- Li H, Tornberg J, Kaila K, Airaksinen MS, Rivera C (2002) Patterns of cation-chloride cotransporter expression during embryonic rodent CNS development. *Eur J Neurosci* 16: 2358-2370.
- Lin MH, Takahashi MP, Takahashi Y, Tsumoto T (1994) Intracellular calcium increase induced by GABA in visual cortex of fetal and neonatal rats and its disappearance with development. *Neurosci Res* 20: 85-94.
- Lo Turco JJ, Owens DF, Heath MJS, Davis MBE, Kriegstein AR (1995) GABA and glutamate depolarize cortical progenitor cells and inhibit DNA synthesis. *Neuron* 15: 1287-1298.
- Lohmann C, Ilic V, Friauf E (1998) Development of a topographically organized auditory network in slice culture is calcium dependent. *J Neurobiol* 34: 97-112.
- Loo DD, Eskandari S, Boorer KJ, Sarkar HK, Wright EM (2000) Role of Cl^- in electrogenic Na^+ -coupled cotransporters GAT1 and SGLT1. *J Biol Chem* 275: 37414-37422.

-
- Lu J, Karadsheh M, Delpire E (1999) Developmental regulation of the neuronal-specific isoform of K-Cl cotransporter KCC2 in postnatal rat brains. *J Neurobiol* 39: 558-568.
- Ludwig A, Li H, Saarma M, Kaila K, Rivera C (2003) Developmental up-regulation of KCC2 in the absence of GABAergic and glutamatergic transmission. *Eur J Neurosci* 18: 3199-3206.
- Luhmann HJ, Prince DA (1991) Postnatal maturation of the GABAergic system in rat neocortex. *J Neurophysiol* 65: 247-263.
- Lytle C, McManus TJ, Haas M (1998) A model of Na-K-2Cl cotransport based on ordered ion binding and glide symmetry. *Am J Physiol* 43: 299-309.
- Mager S, Naeve J, Quick M, Labarca C, Davidson N, Lester HA (1993) Steady states, charge movements, and rates for a cloned GABA transporter expressed in *Xenopus* oocytes. *Neuron* 10: 177-188.
- Marty S, Wehrle R, Alvarez-Leefmans FJ, Gasnier B, Sotelo C (2002) Postnatal maturation of Na⁺, K⁺, 2Cl⁻ cotransporter expression and inhibitory synaptogenesis in the rat hippocampus: an immunocytochemical analysis. *Eur J Neurosci* 15: 233-245.
- McConnell KR, Aronson PS (1994) Effects of inhibitors on anion exchangers in rabbit renal brush border membrane vesicles. *J Biol Chem* 269: 21489-21494.
- Misgeld U, Deisz RA, Dodt HU, Lux HD (1986) The role of chloride transport in postsynaptic inhibition of hippocampal neurons. *Science* 232: 1413-1415.
- Mortensen OV, Amara SG (2003) Dynamic regulation of the dopamine transporter. *Eur J Pharmacol* 479: 159-170.
- Mount DB, Gamba G (2001) Renal potassium-chloride cotransporters. *Curr Opin Nephrol Hypertens* 10: 685-691.
- Mueller AL, Taube JS, Schwartzkroin PA (1984) Development of hyperpolarizing inhibitory postsynaptic potentials and hyperpolarizing response to gamma-aminobutyric acid in rabbit hippocampus studied in vitro. *J Neurosci* 4: 860-867.
- Muller M (2000) Effects of chloride transport inhibition and chloride substitution on neuron function and on hypoxic spreading-depression-like depolarization in rat hippocampal slices. *Neuroscience* 97: 33-45.
- Nabekura J, Katsurabayashi S, Kakazu Y, Shibata S, Matsubara A, Jinno S, Mizoguchi Y, Sasaki A, Ishibashi H (2004) Developmental switch from GABA to glycine release in single central synaptic terminals. *Nat Neurosci* 7: 17-23.
- Nelson H, Mandiyan S, Nelson N (1990) Cloning of the human brain GABA transporter. *FEBS Lett* 269: 181-184.

-
- Nelson N (1998) The family of Na⁺/Cl⁻ neurotransmitter transporters. *J Neurochem* 71: 1785-1803.
- Neveu I, Arenas E (1996) Neurotrophins promote the survival and development of neurons in the cerebellum of hypothyroid rats in vivo. *J Cell Biol* 133: 631-646.
- Obrietan K, van den Pol AN (1995) GABA neurotransmission in the hypothalamus: developmental reversal from Ca²⁺ elevating to depressing. *J Neurosci* 15: 5065-5077.
- Obrietan K, van den Pol A (1999) GABA(B) receptor-mediated regulation of glutamate-activated calcium transients in hypothalamic and cortical neuron development. *J Neurophysiol* 82: 94-102.
- Owens DF, Boyce LH, Davis MB, Kriegstein AR (1996) Excitatory GABA responses in embryonic and neonatal cortical slices demonstrated by gramicidin perforated-patch recordings and calcium imaging. *J Neurosci* 16: 6414-6423.
- Owens DF, Kriegstein AR (2002) Is there more to GABA than synaptic inhibition? *Nat Rev Neurosci* 3: 715-727.
- Page G, Peeters M, Najimi M, Maloteaux JM, Hermans E (2001) Modulation of the neuronal dopamine transporter activity by the metabotropic glutamate receptor mGluR5 in rat striatal synaptosomes through phosphorylation mediated processes. *J Neurochem* 76: 1282-1290.
- Park TJ, Grothe B, Pollak GD, Schuller G, Koch U (1996) Neural delays shape selectivity to interaural intensity differences in the lateral superior olive. *J Neurosci* 16: 6554-6566.
- Payne JA (1997) Functional characterization of the neuronal-specific K-Cl cotransporter: implications for [K⁺]_o regulation. *Am J Physiol* 273: 1515-1525.
- Payne JA, Rivera C, Voipio J, Kaila K (2003) Cation-chloride co-transporters in neuronal communication, development and trauma. *Trends Neurosci* 26: 199-206.
- Plotkin MD, Snyder EY, Hebert SC, Delpire E (1997) Expression of the Na-K-2Cl cotransporter is developmentally regulated in postnatal rat brains: A possible mechanism underlying GABA's excitatory role in immature brain. *J Neurobiol* 33: 781-795.
- Reichling DB, Kyrozis A, Wang J, Mac Dermott AB (1994) Mechanisms of GABA and glycine depolarization-induced calcium transients in rat dorsal horn neurons. *J Physiol (Lond)* 476: 411-421.
- Reimer RJ, Fremeau RT, Jr., Bellocchio EE, Edwards RH (2001) The essence of excitation. *Curr Opin Cell Biol* 13: 417-421.

-
- Richerson GB, Wu YM (2003) Dynamic equilibrium of neurotransmitter transporters: not just for reuptake anymore. *J Neurophysiol* 90: 1363-1374.
- Rietzel H-J, Friauf E (1998) Neuron types in the rat lateral superior olive and developmental changes in the complexity of their dendritic arbors. *J Comp Neurol* 390: 20-40.
- Rivera C, Voipio J, Payne JA, Ruusuvuori E, Lahtinen H, Lamsa K, Pirvola U, Saarma M, Kaila K (1999) The K^+/Cl^- co-transporter KCC2 renders GABA hyperpolarizing during neuronal maturation. *Nature* 397: 251-255.
- Rivera C, Li H, Thomas-Crusells J, Lahtinen H, Vilkmann V, Nanobashvili A, Kokaia Z, Airaksinen MS, Voipio J, Kaila K, Saarma M (2002) BDNF-induced TrkB activation down-regulates the K^+-Cl^- cotransporter KCC2 and impairs neuronal Cl^- extrusion. *J Cell Biol* 159: 747-752.
- Rohrbough J, Spitzer NC (1996) Regulation of intracellular Cl^- levels by Na^+ -dependent Cl^- cotransport distinguishes depolarizing from hyperpolarizing GABA_A receptor-mediated responses in spinal neurons. *J Neurosci* 16: 82-91.
- Russell JM, Boron WF (1976) Role of chloride transport in regulation of intracellular pH. *Nature* 264: 73-74.
- Russell JM (2000) Sodium-potassium-chloride cotransport. *Physiol Rev* 80: 211-276.
- Sachs JR, Martin DW (1993) The role of ATP in swelling-stimulated K^+-Cl^- cotransport in human red cell ghosts. Phosphorylation-dephosphorylation events are not in the signal transduction pathway. *J Gen Physiol* 102: 551-573.
- Sanes DH, Goldstein NA, Ostad M, Hillman DE (1990) Dendritic morphology of central auditory neurons correlates with their tonotopic position. *J Comp Neurol* 294: 443-454.
- Sanes DH (1993) The development of synaptic function and integration in the central auditory system. *J Neurosci* 13: 2627-2637.
- Sanes DH, Friauf E (2000) Development and influence of inhibition in the lateral superior olivary nucleus. *Hearing Res* 147: 46-58.
- Schwarz DW (1992) Sound delay lines in the nucleus laminaris of the chicken. *J Otolaryngol* 21: 202-208.
- Serafini R, Valeyev AY, Barker JL, Poulter MO (1995) Depolarizing GABA-activated Cl^- channels in embryonic rat spinal and olfactory bulb cells. *J Physiol (Lond)* 488: 371-386.
- Shibata S, Kakazu Y, Okabe A, Fukuda A, Nabekura J (2004) Experience-dependent changes in intracellular Cl^- regulation in developing auditory neurons. *Neurosci Res* 48: 211-220.

-
- Singer JH, Talley EM, Bayliss DA, Berger AJ (1998) Development of glycinergic synaptic transmission to rat brain stem motoneurons. *J Neurophysiol* 80: 2608-2620.
- Singer JH, Berger AJ (2000) Development of inhibitory synaptic transmission to motoneurons. *Brain Res Bull* 53: 553-560.
- Snow H, Lowrie MB, Bennett JP (1992) A postsynaptic GABA transporter in rat spinal motor neurons. *Neurosci Lett* 143: 119-122.
- Srinivasan G, Friauf E, Löhrike (2004) Differential timing of the development of inhibition within the superior olivary complex (SOC) revealed by optical imaging. ARO mid winter research meeting, Florida.
- Stein V, Hermans-Borgmeyer I, Jentsch TJ, Hubner CA (2004) Expression of the KC1 cotransporter KCC2 parallels neuronal maturation and the emergence of low intracellular chloride. *J Comp Neurol* 468: 57-64.
- Sun D, Murali SG (1999) Na⁺ -K⁺ -2Cl⁻ cotransporter in immature cortical neurons: a role in intracellular Cl⁻ regulation. *J Neurophysiol* 81: 1939-1948.
- Suneja SK, Benson CG, Gross J, Potashner SJ (1995) Evidence for glutamatergic projections from the cochlear nucleus to the superior olive and the ventral nucleus of the lateral lemniscus. *J Neurochem* 64: 161-171.
- Sung KW, Kirby M, McDonald MP, Lovinger DM, Delpire E (2000) Abnormal GABA(A) receptor-mediated currents in dorsal root ganglion neurons isolated from Na-K-2Cl cotransporter null mice. *J Neurosci* 20: 7531-7538.
- Supplisson S, Roux MJ (2002) Why glycine transporters have different stoichiometries. *FEBS Lett* 529: 93-101.
- Tajima Y, Ono K, Akaike N (1996) Perforated patch-clamp recording in cardiac myocytes using cation-selective ionophore gramicidin. *Am J Physiol* 271: C524-C532.
- Takahashi K, Miyoshi S, Kaneko A (1995) GABA-induced chloride current in catfish horizontal cells mediated by non-GABAA receptor channels. *Jpn J Physiol* 45: 437-456.
- Takebayashi M, Kagaya A, Hayashi T, Motohashi N, Yamawaki S (1996) gamma-aminobutyric acid increases intracellular Ca²⁺ concentration in cultured cortical neurons: role of Cl⁻ transport. *Eur J Pharmacol* 297: 137-143.
- Thompson CC, Potter GB (2000) Thyroid hormone action in neural development. *Cereb Cortex* 10: 939-945.
- Titz S, Hans M, Kelsch W, Lewen A, Swandulla D, and Misgeld U (2003) Hyperpolarizing inhibition develops without trophic support by GABA in cultured rat midbrain neurons. *J Physiol (Lond)* 550: 719-730.

-
- Tolbert LP, Morest DK, Yurgelun-Todd DA (1982) The neuronal architecture of the anteroventral cochlear nucleus of the cat in the region of the cochlear nerve root: horseradish peroxidase labelling of identified cell types. *Neuroscience* 7: 3031-3052.
- Tollin DJ, Yin TCT (2002) The coding of spatial location by single units in the lateral superior olive of the cat. II. The determinants of spatial receptive fields in azimuth. *J Neurosci* 22: 1468-1479.
- Tosco M, Orsenigo MN, Faelli A (1993) Basolateral Cl/HCO₃ exchange in rat jejunum: the effect of sodium. *J Membr Biol* 135: 129-135.
- Vale C, Schoorlemmer J, Sanes DH (2003) Deafness disrupts chloride transporter function and inhibitory synaptic transmission. *J Neurosci* 23: 7516-7524.
- Valverde MA, Hardy SP, Sepulveda FV (1995) Chloride channels: a state of flux. *FASEB J* 9: 509-515.
- Vara H, Munoz-Cuevas J, Colino A (2003) Age-dependent alterations of long-term synaptic plasticity in thyroid-deficient rats. *Hippocampus* 13: 816-825.
- Vardi N, Zhang LL, Payne JA, Sterling P (2000) Evidence that different cation chloride cotransporters in retinal neurons allow opposite responses to GABA. *J Neurosci* 20: 7657-7663.
- Varja P, Katarova Z, Madarasz E, Szabo G (2002) Sequential induction of embryonic and adult forms of glutamic acid decarboxylase during in vitro-induced neurogenesis in cloned neuroectodermal cell-line, NE-7C2. *J Neurochem* 80: 605-615.
- Vater M (1995) Ultrastructural and immunocytochemical observations on the superior olivary complex of the mustached bat. *J Comp Neurol* 358: 155-180.
- Vu TQ, Payne JA, Copenhagen DR (2000) Localization and developmental expression patterns of the neuronal K-Cl cotransporter (KCC2) in the rat retina. *J Neurosci* 20: 1414-1423.
- Warr WB (1972) Fiber degeneration following lesions in the multipolar and globular cell areas in the ventral cochlear nucleus of the cat. *Brain Res* 40: 247-270.
- Wenthold RJ (1991) Neurotransmitters of brainstem auditory nuclei. In: *Neurobiology of Hearing: The Central Auditory System* (Altschuler RA, Bobbin RP, Clopton BM, Hoffman DW, eds), pp 121-139. New York: Raven Press.
- Woo NS, Lu JM, England R, McClellan R, Dufour S, Mount DB, Deutch AY, Lovinger DM, Delpire E (2002) Hyperexcitability and epilepsy associated with disruption of the mouse neuronal-specific K-Cl cotransporter gene. *Hippocampus* 12: 258-268.

-
- Wu SH, Kelly JB (1991) Physiological properties of neurons in the mouse superior olive: membrane characteristics and postsynaptic responses studied in vitro. *J Neurophysiol* 65: 230-246.
- Wu SH, Kelly JB (1992a) Binaural interaction in the lateral superior olive - time difference sensitivity studied in mouse brain slice. *J Neurophysiol* 68: 1151-1159.
- Wu SH, Kelly JB (1992b) Synaptic pharmacology of the superior olivary complex studied in mouse brain slice. *J Neurosci* 12: 3084-3097.
- Wu WL, Ziskind-Conhaim L, Sweet MA (1992) Early development of glycine- and GABA-mediated synapses in rat spinal cord. *J Neurosci* 12: 3935-3945.
- Yasumi M, Sato K, Shimada S, Nishimura M, Tohyama M (1997) Regional distribution of GABA transporter 1 (GAT1) mRNA in the rat brain: comparison with glutamic acid decarboxylase67 (GAD67) mRNA localization. *Mol Brain Res* 44: 205-218.
- Yuste R, Katz LC (1991) Control of postsynaptic Ca^{2+} influx in developing neocortex by excitatory and inhibitory neurotransmitters. *Neuron* 6: 333-344.
- Zafra F, Gomeza J, Olivares L, Aragon C, Gimenez C (1995) Regional distribution and developmental variation of the glycine transporters GLYT1 and GLYT2 in the rat CNS. *Eur J Neurosci* 7: 1342-1352.
- Zhang L, Spigelman I, Carlen PL (1990) Whole-cell patch study of GABAergic inhibition in CA1 neurons of immature rat hippocampal slices. *Brain Res Dev Brain Res* 56: 127-130.
- Zuiderwijk M, Veenstra E, Lopes da Silva FH, Ghijsen WE (1996) Effects of uptake carrier blockers SK & F 89976-A and L-trans-PDC on in vivo release of amino acids in rat hippocampus. *Eur J Pharmacol* 307: 275-282.

8 APPENDIX

Abbreviations

| | |
|------------|---|
| +/+ mice | Wild type mice |
| -/- mice | Knockout mice |
| +/- mice | Heterozygous mice |
| $[Cl^-]_i$ | Intracellular chloride concentration |
| $[Cl^-]_o$ | Extracellular chloride concentration |
| $[Cl^-]_p$ | Pipette chloride concentration |
| [Na] | Sodium concentration |
| $[Na]_i$ | Intracellular sodium concentration |
| $[Na]_o$ | Extracellular sodium concentration |
| $[Na]_p$ | Pipette sodium concentration |
| AE | Anion exchanger |
| AE3 | Anion exchanger isoform 3 |
| bp | Base pair |
| BDNF | Brain derived neurotrophic factor |
| cDNA | Complimentary Deoxyribonucleic acid |
| CCD | Charge coupled device |
| CN | Cochlear nucleus |
| CNS | Central nervous system |
| DIC | Differential interference contrast |
| DIV | Days in vitro |
| DMSO | Dimethyl sulfoxide |
| DNA | Deoxyribonuclei acid |
| E | Embryonic day |
| E_{Cl} | Cl^- equilibrium potential |
| E_{GABA} | GABA reversal potential |
| E_{Gly} | Glycine reversal potential |
| EGTA | Ethylene glycol-bis(β -aminoethyl ether) |
| EPSC | Excitatory postsynaptic current |
| EPSP | Excitatory postsynaptic potential |
| F | Faraday's constant |
| GABA | γ -amino-butyrlic acid |

| | |
|---------------------|--|
| GABAR | γ -amino-butyric acid receptor |
| GABA _A R | γ -amino-butyric acid receptor type A |
| GABA _B R | γ -amino-butyric acid receptor type B |
| GABA _C R | γ -amino-butyric acid receptor type C |
| GAT | GABA transporter |
| GAT1 | GABA transporter isoform 1 |
| GLYT | Glycine transporter |
| GLYT2 | Glycine transporter isoform 2 |
| HEPES | N-(2-hydroxyethyl)piperazine-N'-(4-ethanesulfonic acid) |
| IC | Inferior colliculus |
| IC ₅₀ | Half-maximal inhibitory concentration |
| I-V | Current-voltage |
| KCC | Potassium chloride cotransporter |
| KCC2 | Potassium chloride cotransporter isoform 2 |
| LJP | Liquid junction potential |
| LSO | Lateral superior olive |
| MNTB | Medial nucleus of the trapezoid body |
| mRNA | Messenger ribonucleic acid |
| MSO | Medial superior olive |
| NA | Numerical aperture |
| NCC | Na ⁺ -dependent chloride cotransporter |
| NDAE | Na ⁺ -dependent anion exchanger |
| NGF | Nerve growth factor |
| NKCC | Na ⁺ -dependent potassium chloride cotransporter |
| NKCC1 | Na ⁺ -dependent, potassium chloride cotransporter isoform 1 |
| NMDA | N-methyl-D-aspartate |
| NPA | Nipecotic acid |
| NT3 | Neurotrophin -3 |
| P | Postnatal day |
| PCR | Polymerase chain reaction |
| PON | Periolivary nucleus |
| R | Gas constant |
| RNA | Ribonuclei acid |

| | |
|------------|---|
| RT-PCR | Reverse transcription – polymerase chain reaction |
| SEM | Standard error of mean |
| SKF | SKF 89976A (GAT1 inhibitor) |
| SOC | Superior olivary complex |
| SPN | Superior paraolivary nucleus |
| tRNA | transfer ribonucleic acid |
| T | Absolute temperature |
| TrkB | Tyrosine kinase receptor B |
| TTX | Tetrodotoxin |
| TH | Thyroid hormone |
| VDCC | Voltage-dependent calcium channels |
| V_C | Command potential |
| V_H | Holding potential |
| V_{rest} | Resting membrane potential |

Curriculum vitae

Veeramuthu Balakrishnan

born 30th May 1977, Karambakudy, Tamilnadu, India

- 2000-present Ph.D student in the sensory and developmental neurobiology lab of Prof. Eckhard Friauf, University of Kaiserslautern, Germany
Thesis: The role of plasma membrane transporters in chloride homeostasis of developing auditory brainstem neurons
- 1999-2000 Research assistant in the biophysical chemistry lab of Prof. Ding-Kwo Chang, Inst. of Chemistry, Academia Sinica, Taiwan
- 1997 Winter school on Atomic force microscopy, CSIO, Chandigarh, India
- 1997 Summer training and project, Indian Institute of Chemical Biology, Calcutta, India
Project: Comparative genome analysis of *Shigella* spp. using PFGE
- 1994-1999 M.Sc., Life sciences (specialization in microbiology) - 5yrs integrated course, Bharathidasan University, Tiruchirappalli, India
Thesis: Molecular characterization of marine cyanobacteria using 16S rRNA gene sequencing
- 1992-1994 Vivekananda higher secondary school, Thiruvedakam, Madurai
- 1990-1992 Vivekananda Matriculation school, Pannaikadu, Kodaikanal Hills
- 1989-1990 John Dewey matriculation school, Panruti
- 1988-1989 Anderson higher secondary school, Kancheepuram
- 1984-1988 Rosemary matric & higher secondary school, Palayamkottai

Acknowledgements

I am deeply indebted to Prof. Dr. Eckhard Friauf, who provided me an opportunity to learn neurobiology and for his constant support, guidance and fellowship to carry out this Ph.D thesis in his department, and also for helping me to have better perspective in my scientific thinking. Thanks to Prof. Dr. Joachim W. Dietmer for agreeing to review my thesis and for his constructive criticisms during the neurobiology seminar.

I am grateful to Dr. Stefan Löhre, for teaching me patch-clamp technique, and for his critical advices and guidance at each step. I thank Dr. Hansgerd Nothwang, for his support and for guiding me in several molecular biology projects. I would like to personally thank Dr. Karl Kandler for his kind support.

Thanks to Dr. Harald Vitten for his help and to Dr. Ingrid Ehrlich for her comments and kind support. I would like to thank Michael and Obi for their collaboration and for rendering me personal help. I wish to thank Sascha, for his excellent technical assistance and for his help. Many thanks to Petra for her help in several aspects. Thanks to my colleagues Kornelia, Katia, Peter, Nicole, Isa, Alex, Jens, and Anne for the good times in the lab. Thanks to Dennis Daniel for his help in solving the computer problems.

Thanks to my friends (Ajoy, Kitcha, Susmith, Ajay, Sara, and Poongo) for providing me with literatures whenever I requested, and for chats which helped me to pace myself during my research process. Thanks to Venk, Karthi, Rajan, and Dany for the good times in K-town.

I would like to thank Dr. S. Karuthapandian and Dr. N. Thajuddin for their encouragement. Thanks to my family members for their sacrifice and support throughout the whole course of my studies. I am very grateful to my fiancée, Gee for her support and patience.